Water-Based Fine-Grained Detectors for the T2K Experiment

by

Jérôme Coulombe

B.A.Sc., Université Laval, 2004

A THESIS SUBMITTED IN PARTIAL FULFILMENT OF
THE REQUIREMENTS FOR THE DEGREE OF

Master of Science

in

The Faculty of Graduate Studies

(Physics)

The University of British Columbia

August 2006

Abstract

T2K is a next-generation neutrino oscillation experiment that will use an off-axis beamline, produced at J-PARC and directed towards the Super-Kamiokande detector, to precisely measure muon neutrino disappearance as well as electron neutrino appearance in a ν_μ beam. A near detector, built 280 m downstream of the proton target, is needed in order to monitor the beam as well as to measure neutrino interaction cross-sections. As part of the near detector, two fine-grained detectors (FGDs) combined with three time-projection chambers (TPCs) will form the target mass for neutrino interaction. One FGD will consist of plastic scintillator while the other will contain a significant admixture of water in order to estimate nuclear effects as well as to match Super-K's target material. The liquid fraction of the water-rich FGD will either consist of pure water (passive configuration) or be made of an active water/liquid scintillator cocktail. This thesis presents the latest design and construction developments relating to the water FGD, looking specifically at important physics issues that need to be solved, such as the mechanical design of the structure, fluid sealing, light yield and stability of aged materials. Extruded sheets of polypropylene with a hollow profile have been considered as a structural element to contain the liquid due to their mechanical strength and low cost. In the active configuration, the individual cells of such an extrusion will become readout channels once threaded with wavelength shifting fibers. Fluid sealing has been studied for both the case of a passive as well as an active water detector, and successful seal prototypes have been built: a simple epoxy seal for the passive water case and a more elaborate two-piece thermal welded endcap for the active detector option. Single-cell prototypes have been filled with the scintillator cocktail, and light yield tests have been performed using a 400-MeV/c proton beam. More specifically, the attenuation length of the fiber has been measured and long term stability of the liquid mixture has been investigated. Results of aging for all considered materials when put in contact with the chemically reactive liquid scintillator are also presented.

Table of Contents

List of Tables

List of Figures

Acknowledgements

Many thanks to Prof. Scott Oser and Prof. Stanley Yen for their support and assistance throughout my Master's degree; your continued advice and constructive feedback are major reasons for this thesis to be completed. Also, I would like to express my gratitude to the following people for all the weekly helpful comments, new ideas and computing advice: Robert Henderson, Peter Kitching, Andy Miller, Peter Vincent, Akira Konaka, Juergen Wendland and Pierre-Luc Drouin.

Chapter 1

Introduction

1.1 Theoretical Foundation of Neutrino Oscillation Studies

Neutrinos are electrically neutral elementary particles belonging to the lepton family. These chargeless, colourless and spin $\hbar/2$ fermions are characterized by an extremely small mass as well as by the fact that they only interact with matter through the weak force and gravity. Because cross-sections of weak nuclear interactions are very small, neutrinos may pass through a large amount of matter without being hampered. Detecting these particles is consequently a challenging task and massive detectors and/or high intensity neutrino beams are required. These particles come in three different flavors, each of them associated with its corresponding charged lepton: ν_e, ν_μ, ν_τ. Technically, we define a neutrino's flavor eigenstate as the state that will produce a charged lepton of a specific flavor when interacting with a W-boson. The neutrino was initially postulated by Pauli in 1931 in order to ensure energy and angular momentum conservation in β-decay. [1] The first experimental detection of such particle had to wait nearly 25 years, and since then all flavors have been observed. What makes neutrinos most interesting, however, is the fact that their properties seem to change as they propagate, that is, they oscillate. Neutrino oscillation is the peculiar quantum mechanical phenomenon by which the probability of measuring a particular neutrino flavor changes periodically as the particle propagates with a velocity close to the speed of light.

This phenomenon is directly related to the concept of a mass eigenstate. A mass eigenstate for some arbitrary massive particle is a state that obeys Einstein's relativistic energy-momentum equation:

$$E = \sqrt{|\vec{p}|^2 c^2 + m^2 c^4}. \tag{1.1}$$

When such a particle propagates, its wavefunction acquires a phase that can be written as: $\phi(\vec{x}, t) = e^{-i(\vec{p}\cdot\vec{x} - Et)/\hbar}$. Therefore, mass eigenstates with dif-

ferent masses have different energies and frequencies for a given momentum. Consequently, even though mass eigenstate particles propagate without any change in their properties, a particle that is a linear combination of different mass eigenstates would show interference patterns due to the various component frequencies and therefore behave differently as it propagates. This is exactly what happens in the case of neutrinos. Nothing *a priori* implies that mass eigenstates correspond to flavor eigenstates and recent studies led to the quite radical conclusion that neutrinos actually are linear combinations of three neutrino mass eigenstates, that is:

$$|\nu_\alpha\rangle = \sum_{j=1}^{3} a_j \, |\nu_j\rangle \qquad |\nu_\alpha\rangle = \{|\nu_e\rangle \, ; |\nu_\mu\rangle \, ; |\nu_\tau\rangle\} \tag{1.2}$$

with a_j being the weight of each mass eigenstate component.

From the preceding equations, one can see that neutrino oscillation is a concept implying non-zero masses for the particles. This particular point is of extreme importance considering the original Standard Model did not allow for massive neutrinos.[†] A revised version of the theory, with even more free parameters, may accomodate this new fact, but the Model certainly does not predict it. The zero mass of neutrinos in the Model is a direct consequence of the absence of a right-handed neutrino field ψ_R in the theory. Without such a field, the term in the Lagrangian responsible for generating the mass goes to zero, unlike the case of all other fermions: that is, $-m\psi\overline{\psi} = -m(\overline{\psi}_L\psi_R + \overline{\psi}_R\psi_L) = 0$. [2] In other words, according to the Standard Model, all neutrinos are left-handed, having their spin orientation antiparallel to their momentum. One of the current greatest puzzles for particle physics corresponds to finding a way to alter the Model in order to account for neutrino masses. An obvious solution could be to add a right-handed field term to the Lagrangian, but such a term – called a Dirac mass term – raises two major concerns: firstly, ν_R would have to be a sterile field, not coupling to any of the vector gauge bosons and it would therefore be very different from all other fermions. Secondly, because the mass is so small, it would imply an anomalously small coupling between ν_R and ν_L through the Higgs field. These are a few reasons why physicists try to find

[†]It is largely accepted now that the Standard Model is the best theory yet developed that tries to explain all of the physics related to the strong, the weak and the electromagnetic forces. Even if the theory has given a significant number of accurate predictions (QED for instance), it is commonly believed to be incomplete and immature, being often considered as a transition theory towards a Unified Theory.

new theoretical ways to generate massive neutrinos. In this sense, another possibility to add a mass term to the Lagrangian could be to combine a neutrino with an antineutrino, recognizing the fact that antineutrinos are right-handed particles. Such a coupling would be impossible for any other elementary particles due to a violation in charge conservation, but remains valid for chargeless neutrinos. If neutrinos are their own antiparticle, they will be called Majorana particles; only future experiments will answer the question as to whether neutrinos are Dirac or Majorana particles. The impact of massive neutrinos on all fields of physics are countless and not yet fully understood, but the key to understanding the mass generation process may lie within the hidden mass of neutrinos and the inherent oscillation process.

Let's now develop the formalism of neutrino oscillation. The phenomenon was first proposed in 1962 by three theorists who were inspired by the work done on the coupling between all quarks generations. [3] The Maki-Nakagawa-Sakata matrix, the equivalent of the CKM matrix for the case of quarks mixing, relates the flavor eigenstates to the mass eigenstates:

$$\begin{bmatrix} |\nu_e\rangle \\ |\nu_\mu\rangle \\ |\nu_\tau\rangle \end{bmatrix} = \begin{bmatrix} U_{e1} & U_{e2} & U_{e3} \\ U_{\mu 1} & U_{\mu 2} & U_{\mu 3} \\ U_{\tau 1} & U_{\tau 2} & U_{\tau 3} \end{bmatrix} \begin{bmatrix} |\nu_1\rangle \\ |\nu_2\rangle \\ |\nu_3\rangle \end{bmatrix} \tag{1.3}$$

Coefficients of the MNS matrix are non-trivial and most of today's neutrino research has to do with determining these matrix elements or at least improving an upper bound value. Defining $s_{ij} \equiv \sin(\theta_{ij})$ and $c_{ij} \equiv \cos(\theta_{ij})$, the matrix takes the form:

$$\begin{bmatrix} c_{12}c_{13} & s_{12}c_{13} & s_{13}e^{i\delta} \\ -s_{12}c_{23} - c_{12}s_{13}s_{23}e^{-i\delta} & c_{12}c_{23} - s_{12}s_{13}s_{23}e^{-i\delta} & c_{13}s_{23} \\ s_{12}s_{23} - c_{12}s_{13}c_{23}e^{-i\delta} & -c_{12}s_{23} - s_{12}s_{13}c_{23}e^{-i\delta} & c_{13}c_{23} \end{bmatrix} \tag{1.4}$$

with $\theta_{12} \simeq \pi/6, \theta_{23} \simeq \pi/4, \theta_{13} < \pi/20$ as mixing angles and δ as the Dirac CP phase. Mixing angle values are only approximations at this point and the CP phase value is still completely unknown.[†] Let's recall the values for the quarks mixing angles: $\theta_{12} \simeq \pi/14, \theta_{23} \simeq \pi/76, \theta_{13} \sim \pi/870$. A quick comparison between neutrino and quark mixing angles allows one to see how large the former are; it remains yet to be explained why that is.

[†]CP violation still has not been proven for the case of neutrinos and this is an issue the second phase of the T2K project plans to explore.

Let's explicitely calculate the probability of oscillation between two neutrino flavor eigenstates. [4] Defining the flavor eigenstates and the mass eigenstates respectively as $|\nu_\alpha\rangle = \{|\nu_e\rangle\,;|\nu_\mu\rangle\,;|\nu_\tau\rangle\}$ and $|\nu_j\rangle = \{|\nu_1\rangle\,;|\nu_2\rangle\,;|\nu_3\rangle\}$, we may express one in terms of the other as follows:

$$|\nu_\alpha\rangle = \sum_j U_{\alpha j}\,|\nu_j\rangle \tag{1.5}$$

$$|\nu_j\rangle = \sum_\alpha U^*_{\alpha j}\,|\nu_\alpha\rangle \tag{1.6}$$

with $U_{\alpha j}$ being the corresponding coefficients of the MNS matrix. Moreover, the propagation of a mass eigenstate may be described by the time-dependant Schroedinger equation,

$$i\hbar\frac{\partial\,|\nu_j(t)\rangle}{\partial t} = H\,|\nu_j(t)\rangle = E_j\,|\nu_j(t)\rangle\,, \tag{1.7}$$

the solution of which is of the form: $|\nu_j(t)\rangle = e^{-iE_jt/\hbar}\,|\nu_j\rangle$. We may then write the time-dependant flavor eigenstate as a function of the initial flavor state:[†]

$$|\nu_\alpha(t)\rangle = \sum_{\beta,\ j} U_{\alpha j}\ e^{-iE_jt/\hbar}\ U^*_{\beta j}\,|\nu_\beta\rangle \tag{1.8}$$

The square of the module of the projection on $\langle\nu_\beta|$ then gives the probability of oscillation between neutrino flavor eigenstates:

$$|\langle\nu_\beta|\nu_\alpha(t)\rangle|^2 = \sum_{j,\ k} U_{\alpha j}U^*_{\beta j}U^*_{\alpha k}U_{\beta k}\ e^{i(E_k-E_j)t/\hbar} \tag{1.9}$$

Now, if $E_j, E_k \gg m_j, m_k$, then:

$$E_k - E_j = \sqrt{m_k^2c^4 + p^2c^2} - \sqrt{m_j^2c^4 + p^2c^2} \approx \left(\frac{m_k^2 - m_j^2}{2p}\right)c^3 \tag{1.10}$$

Moreover, $\mathrm{p} \approx E/c$ and $t = L/c$:

$$|\langle\nu_\beta|\nu_\alpha(t)\rangle|^2 = \sum_{j,\ k} U_{\alpha j}U^*_{\beta j}U^*_{\alpha k}U_{\beta k}\ e^{(i\Delta m^2_{kj}c^3L/2\hbar E_\nu)} \tag{1.11}$$

with $\Delta m^2 = m_k^2 - m_j^2$, L being the distance over which the neutrino has propagated and E_ν being the neutrino's highly relativistic energy. This last

[†]In order to obtain such a result, one must assume the momentum to be the same for all mass eigenstates ($\mathrm{p}_1 = \mathrm{p}_2 = \mathrm{p}_3$).

equation is for the general case of a three-dimensional oscillation. In the special case where only two neutrinos and one mixing angle are considered, the oscillation probability simplifies to:

$$P(\nu_\alpha \to \nu_\beta) = \sin^2 2\theta \sin^2 \left(\frac{\Delta m^2 c^4 L}{4\hbar c E_\nu} \right) \tag{1.12}$$

One salient feature of this expression is the fact that it does not depend on the intrinsic neutrino masses, but only upon the difference of the squares of the two particle masses. This also means that any success in quantifying neutrino oscillation will only lead to finding the difference between masses values. On the other hand, the absolute mass scale of neutrinos is of crucial importance in generally understanding fermion masses and could possibly determine the scale of new physics. Although it may be possible to make an educated guess for the order of magnitude of the neutrino absolute masses from oscillation studies assuming either a normal or inverted hierarchy for the masses, it is more likely that cosmology will provide the best upper limit for such values. The current limits are such that for the normal hierarchy ($m_1 \ll m_2 \ll m_3$), $m_1 \approx 0$ eV, $m_2 \approx \sqrt{\Delta m^2_{21}} = 0.009$ eV and $m_3 \approx \sqrt{\Delta m^2_{32}} = 0.05$ eV. On the other hand, an inverted hierarchy would give $m_3 \approx 0$ eV and $m_1 \approx m_2 \approx 0.05$ eV. Finally, there is also a possibility for a degenerate case where $m_1 \approx m_2 \approx m_3 \approx 0.2$ eV, where cosmology limits $\sum_i m_i < 0.6$ eV. [5]

1.2 Experimental Evidence for Neutrino Oscillation

The first strong evidence for neutrino oscillation came in 1998, when the Super-Kamiokande collaboration found an asymmetry between the number of muon atmospheric neutrinos entering their detector from above and below. When high energy cosmic rays hit the Earth's atmosphere and interact with nuclei making up the air, they often create a spray of secondary particles, and some of these decay into neutrinos. Cosmic rays spectra have been extensively studied over the years and because the particles arrive at the Earth's atmosphere uniformly from all directions, they should be detected with the same uniformity. The atmospheric neutrinos seen by the Super-K detector are either coming from the atmosphere over the area of Japan, or else from the opposite side of the planet. Because neutrinos essentially don't interact with matter at all, these pass right through the Earth and the only

difference between the ones entering the bottom of the detector versus the ones entering the top is the total distance over which they have propagated. In the absence of neutrino oscillations, there would be an equal number of particles coming from both ends of the detector. This is not however what has been observed and it is believed that the missing particles have oscillated into ν_τ. [6]

The Super-K detector has been designed to study solar and atmospheric neutrinos as well as proton decay and neutrinos coming from possible supernova within the galaxy. It is a water Čerenkov detector made of 50 000 tons of pure water surrounded by 11 200 photomultiplier tubes and built underground in the Mozumi zinc mine located in the Japanese Alps. [7] Such a detector does not directly see the neutrinos, but rather detects the light produced by relativistic particles propagating in the water and resulting from the interaction between the original neutrino and electrons or nuclei in the water. Such a reaction often produces particles propagating faster than the speed of light in water and it is the shape of the light cone created through the Čerenkov effect that allows one to deduce the direction of propagation of the neutrino as well as to distinguish its flavor. The flavor may be distinguished from the sharpness of the edge of the cone: because the μ^- is a relatively heavy particle, it is not strongly deflected when travelling in the water and therefore forms a very sharp light cone. On the other hand, electrons are greatly deflected by Coulomb scattering which results in a fuzzier cone of light.

In order to study ν oscillation in a more detailed and controlled manner, the K2K (KEK to Kamioka) collaboration built, in 1999, the first long baseline neutrino oscillation experiment using the 12-GeV proton synchroton accelerator at the High Energy Accelerator Research Organization (KEK) in Tsukuba (Japan). The idea was to create a man-made muon neutrino beam at KEK pointing towards the Super-K detector in Kamioka, 250 km away. Front detectors near the beam source were used to measure precisely the flux of particles as well as a low degree of contamination by wrong flavors of neutrinos. By comparing the front detector measurements to what Super-K observed, it was therefore possible to look for effects of neutrino oscillation and, more specifically, ν_μ disappearance. The anatomy of the K2K beamline is relatively simple : over the first 300 m, the proton beam strikes an aluminum target, which interaction results in the formation of various secondary particles such as π^+ and K^+. Horns consisting of toroidal magnetic fields then focus these secondary particles into the 200-m long decay pipe

which ultimately decay into muon neutrinos. The neutrino beam formed is then pointed towards the far detector, Super-K. Over its years of operation, Super-K found that $\theta_{23} \simeq \pi/4$ and $\Delta m^2_{23} \simeq 2.5 \times 10^{-3}$ eV^2. [8][9]

Although Super-K brought the first strong evidence of neutrino oscillation, the concept was formulated way before the 1990s. Actually, it was first hypothesized when studying the solar neutrino problem, an issue that arose as early as the mid-1960s. Our understanding of the physics describing the Sun's interior, acting as a fusion reactor, was believed to be quite accurate at the time: four protons + two electrons are transformed into a helium nucleus, electron neutrinos, and energy. The energy is released as gamma rays as well as kinetic energy for all particles; the neutrinos then travel from the Sun's core to the Earth without any appreciable interaction. The problem was the number of electron neutrinos observed on Earth seemed to be only a fraction of what was believed to be produced by the Sun. The measurements were such that even if they were wrong by three standard deviations, they still would not be in agreement with theory. This implied that either the solar model or the Standard Model of elementary particles was wrong. As we now know, the answer lies in the fact that a large fraction of the neutrinos coming from the Sun are no longer of electron-type due to the oscillation process and may consequently not be accounted for when only ν_e are being detected. The solar neutrino problem could not be completely solved until 2001 when the Sudbury Neutrino Observatory collaboration published their results. The SNO detector, located in a nickel mine in Greater Sudbury (Ontario, Canada), consists of 1000 tons of heavy water designed to detect solar neutrinos through interactions with deuterium nuclei. The observatory has been able to study three types of reactions within the detector: [10]

Reaction		**Flavours Measured**
$\nu_e + d \rightarrow p + p + e^-$	(CC)	ϕ_e
$\nu_x + d \rightarrow p + n + \nu_x$	(NC)	ϕ_{all}
$\nu_x + e^- \rightarrow \nu_x + e^-$	(ES)	$\phi_e + \frac{1}{6}\phi_{\mu,\tau}$

The first reaction is called charged-current (CC) due to the fact that a charged W-boson is emitted in the process of the deuteron's neutron turning into a proton; such a process is only sensitive to electron-type neutrinos. On the other hand, the second equation, called neutral-current (NC)

because of the Z-boson exchange during the process, as well as the third equation, refering to the elastic scattering (ES) between a neutrino and an electron, are both sensitive to all types of neutrinos. Let's also add the fact that the elastic scattering process, although sensitive to all flavors, has a reduced sensitivity to ν_μ and ν_τ, unlike the neutral-current reaction which is equally sensitive to all flavor fluxes. Consequently, a discrepancy between the neutrino flux derived from the CC process ($\phi^{CC}(\nu_e)$) versus either the ES or NC process would allow one to quantify flavor transformation without any reference to the solar model. The very first result presented by the SNO collaboration was that the measurement of $\phi^{CC}(\nu_e)$ was significantly smaller than $\phi^{ES}(\nu_x)$, therefore implying the neutrinos detected were not only of electron-type, but did oscillate into other flavors. The subsequent results from the collaboration were even more conclusive about the reality of neutrino oscillation as direct evidence for flavor transformation has been observed from neutral-current interactions. [11] Yet another confirmation for neutrino oscillation came from a terrestrial Japanese experiment called KamLAND. KamLAND is a clever experiment counting the rate of $\overline{\nu}_e$ coming from nuclear reactors throughout Japan. The measured antineutrino flux turned out to be lower than what would be expected if there were no oscillation while being in good agreement with the neutrino oscillation hypothesis. [12] Finally, the MINOS experiment at Fermilab, conceptually quite similar to K2K but with a baseline 730 km long, also studies ν_μ oscillations; their latest and very recent results confirmed K2K's, with somewhat higher statistics: $\Delta m^2_{23} = 3.05^{+0.60}_{-0.55} \times 10^{-3}\text{eV}^2$ and $\sin^2 2\theta_{23} = 0.88^{+0.12}_{-0.15}$. [13]

At this point, one can safely say that the most recent results from SNO, Super-K, KamLAND and MINOS confirm the reality of neutrino oscillation, and the fact that flavor eigenstates correspond to a combination of mass eigenstates remains a peculiar but true property of nature. Furthermore, next-generation experiments will need to delve deeper than simple neutrino oscillation confirmation in order to quantify the phenomenon more precisely and get upper bounds on θ_{13} and δ as well as on neutrino masses values. This is specifically what T2K, a successor to the K2K experiment, plans to be doing.

1.3 The T2K Experiment

Tokai to Kamioka (T2K) is a next-generation long baseline neutrino oscillation experiment currently under construction in Japan. It will use an intense

off-axis neutrino beam produced at J-PARC and directed towards the Super-Kamiokande detector in order to study physics beyond the Standard Model. The experimental setup is quite similar to what has been used by the K2K collaboration, and in both cases Super-K is being used as the far detector. Although the experiments are similar in many ways, they ultimately pursue different objectives and therefore have different requirements. For instance, T2K will be using an off-axis beam, with a neutrino flux much larger than what has been used for K2K in order to increase statistics by a factor of about fifty.

1.3.1 T2K Specific Objectives

More specifically, the first phase of the T2K project aims at three main objectives: [14] firstly, searching for the muon to electron neutrino appearance in the far detector in order to greatly improve the sensitivity to θ_{13}. The oscillation probability is given by:

$$P(\nu_\mu \rightarrow \nu_e) = \sin^2(2\theta_{13}) \sin^2(\theta_{23}) \approx \frac{1}{2} \sin^2(2\theta_{13}). \tag{1.13}$$

Consequently, observation of a muon to electron neutrino appearance at Super-K would imply $\theta_{13} \neq 0$. In five years running with full operation of the detector, it is believed possible to improve by a factor of 20 the current upper limit. Secondly, the study of muon neutrino disappearance ($\nu_\mu \rightarrow \nu_x$) parameters as a function of energy will be performed, leading to measurements of θ_{23} and Δm^2_{23} with $\times 10$ the precision of the previous experiments. Lastly, T2K will be looking for a sterile component in ν_μ disappearance by studying neutral-current events. This will test if ν_μ ever oscillates into a sterile neutrino, a hypothetical particle that would not interact via any of the interactions described by the Standard Model. It will be possible to distinguish oscillation into sterile vs tau neutrinos by studying the production of neutral pions through NC events. Because active neutrinos all have the same NC interaction rates, a muon neutrino oscillating into a ν_τ over a distance of 295 km will not affect π^0 production at the far detector, unlike an oscillation into a sterile neutrino that would not create any neutral events. A deficit in the NC π^0 rate at Super-K will therefore indicate the existence of sterile neutrinos. Such a discovery would imply the necessity to update the fermion model in order to account for a 4^{th} neutrino. Needless to say news like this would be dramatic for some while exciting to others.

Moreover, assuming a successful achievement in the first stage of the project, an upgrade to the accelerator will be considered, and with a higher beam

power new experiments will be performed. This second phase of the project will aim at comparing ν_μ and $\overline{\nu}_\mu$ beams in order to search for CP violation in the lepton sector and get an estimate on the Dirac CP phase value δ. The second phase will also greatly improve $\nu_\mu \rightarrow \nu_e$ oscillation sensitivity as well as proton decay sensitivity (in case the Hyper-K project is undertaken [15]).

1.3.2 Off-Axis Beam Produced at J-PARC

The beam that will be used for the T2K experiment is currently still under construction at J-PARC, the Japan Proton Accelerator Research Complex located in Tokaimura. The Complex consists of 3 accelerators: a linear accelerator mostly used as an injector, a rapid cycle 3-GeV synchrotron, and a 50-GeV synchrotron. The secondary particles, such as muon neutrinos, are produced by bombarding a target with this intense proton beam fast-extracted from the main ring. The intensity of the synchrotron is 3.3×10^{14} protons/pulse, and with a pulse every 3.5 seconds, the resulting beam power is 0.75 MW. For a typical year of operation, $\sim$ 130 days, the number of protons on target will be of the order of 10^{21}. With a baseline 295 km in length, the neutrino energy will be tuned to between 0.4 and 1.0 GeV in order to correspond to $1.6 \times 10^{-3} < \Delta m^2_{23} < 4 \times 10^{-3} eV^2$, the range of masses differences the most likely to be measured according to the most recent Super-K, K2K and MINOS results. At these energies, the neutrinos mostly interact via the quasi-elastic charged-current reaction. At higher energies, however, the inelastic process becomes more important and problems arise in reconstructing the final energy due to a background that originates from not detecting π in inelastic interactions. Therefore, what is needed is a high intensity, low energy, nearly monoenergetic neutrino beam. This result may be obtained using an off-axis configuration, that is, a beam not pointing directly towards Super-K, but a few degrees off. For some finite decay angle, the characteristics of the Lorentz boost makes the neutrino energy almost independent of the pion's initial momentum (see figure 1.1), thus resulting in a narrow energy spectrum, the peak of which is accurately controlled by the off-axis angle. T2K's off-axis beamline is one of the main differences with the K2K experiment, which had an on-axis beam.

Just as it was the case for K2K, the secondary particles – mainly pions – will be produced by protons hitting the target. Magnetic horns will then focus the charged particles into the decay pipe where neutrinos will be produced via the reaction $\pi^+ \rightarrow \mu^+ + \nu_\mu$. Near detectors 280 m downstream of the proton target will be needed in order to monitor the beam as well as to

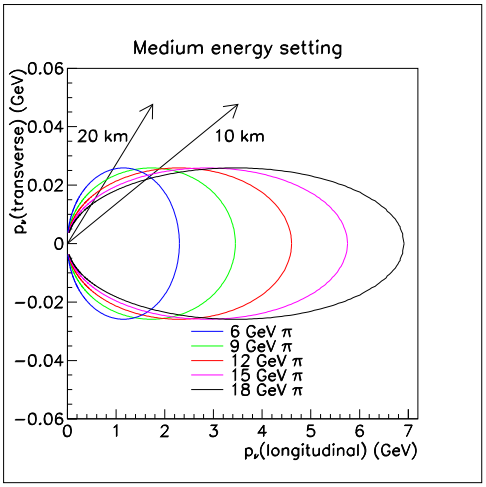

Figure 1.1: Plot showing pions of different energies giving ν's of the same energy when viewed off-axis. This idea has been developed at TRIUMF and will be used for the T2K experiment.

measure neutrino interaction cross-sections. It is essential to understand exactly the energy, direction and flavor composition of the beam in order to quantify the oscillation; this is the role played by the near detectors.

1.3.3 The ND280 Near Detector

Objectives and Their Implications

As previously discussed, the near detector will be located off-axis, 280 m downstream of the proton target. The approximate total size of the detector will be 3.5 m wide $\times$ 3.5 m high $\times$ 7 m deep. Its basic role consists of providing predictions of the expected neutrino flux and composition at Super-K. The detector will be able to identify many different types of charged-current as well as neutral-current events (see Appendix A for an exhaustive list). Undoubtedly, the most important mode is charged-current quasi-elastic (CCQE) as 65% of the total interactions forming a 1 ring muon-like event are expected to be of this sort according to Monte Carlo simulations when the ν energy is set to the oscillation maximum.[16] A few other important types of events are CC resonant single pion production (CCres) as well as CC multi-π production, CC coherent-π production (when the whole

nucleus recoils) and neutral-current π production (NC):

$$\nu_\mu + n \rightarrow \mu^- + p \qquad \text{(CCQE)} \tag{1.14}$$

$$\nu_\mu + p \rightarrow \Delta^{++} + \mu^- \rightarrow \mu^- + p + \pi^+ \qquad \text{(CCres)}^\dagger \tag{1.15}$$

$$\nu_\mu + N \rightarrow \nu_\mu + N + \pi^0 \qquad \text{(NC)} \tag{1.16}$$

As previously stated, most neutrinos will interact via the quasi-elastic interaction of the charged-current due to the beam energy and off-axis angle. In this process, a muon neutrino interacts with a neutron to produce a muon and a low energy proton which is easily detected; tagging the recoil proton is primarily used to confirm the occurence of a CCQE event. All the other interactions represent a background in the CCQE sample that could affect the ν_μ spectrum measurement at the near detector. The energy of the incoming neutrino is obtained from the energy, momentum and angle of the muon relative to the beam seen in a CCQE event (E_μ, p_μ, θ_μ):

$$E_\nu = \frac{m_N E_\mu - m_\mu^2/2}{m_N - E_\mu + p_\mu \cos\theta_\mu} \tag{1.17}$$

with m_N and m_μ being respectively the neutron and muon masses. The previous equation is obtained from energy and momentum conservation laws, solving for the energy of the initial particle. Let's note the fact that such a formula fails for non-quasi-elastic events.

In order for the energy reconstruction to be adequate, as well as for identifying pions coming from inelastic scattering events, the granularity of the detector must be sufficiently high and it should also have enough radiation lengths to allow a measurement of the energies and directions of π^0s coming from the neutral-current reactions. To answer these various requirements, the near detector will be an assembly of many smaller detectors such as electromagnetic calorimeters, a π^0 detector, time projection chambers and fine-grained detectors. All these separate parts form a whole that has to fit within a large magnet. Figure 1.2 shows a side view of the near detector and its components.

†There are other CC resonant interactions such as $\nu_\mu + n \rightarrow \Delta^+ + \mu^- \rightarrow \mu^- + n + \pi^+$, as well as $\nu_\mu + n \rightarrow \Delta^+ + \mu^- \rightarrow \mu^- + p + \pi^0$.

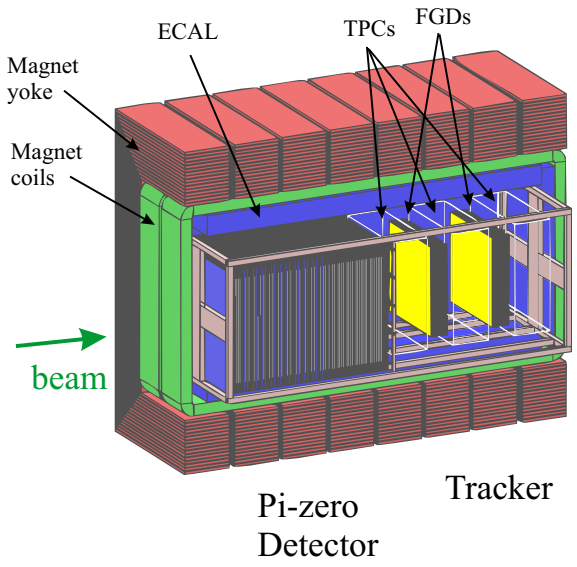

Figure 1.2: Side view of the near detector and its various components. Most of the Canadian effort is on the FGDs and TPCs.

Components of the Near Detector

The magnet that will be used by T2K's near detector is the old dipole magnet from NOMAD/UA1 that CERN donated to the collaboration. The presence of a magnetic field within the detector will greatly improve momentum reconstruction for quasi-elastic muons, also allowing charge identification. The total inner volume of the magnet is 80 m^3 and the total magnitude of the magnetic field will be 0.2 T, as opposed to NOMAD which used a field of 0.4 T. [16] Within the magnet and surrounding the inner parts of the detector, we find the electromagnetic calorimeters (ECALs). The ECALs, made of interleaved layers of lead and plastic scintillator, are optimized for measuring gamma rays – primarily coming from π^0 production – by studying electromagnetic showers. Such a shower is formed when a high energy photon (or electron) enters the material and creates a cascade of new particles due to successive pair production and bremsstrahlung. This process then continues until the energy becomes too low for any new e^+e^- pair to be produced; the radiation length determines the distance over which the shower develops. As the cascade develops, the ECAL records the energy deposited in each channel, therefore giving important information about the initial particle's energy.

The front portion of the inner near detector is called the π^0 detector or P0D. It is designed to make high statistics measurements of neutral-current π^0 events (several thousand a year). The P0D consists of interleaved plastic scintillator tracking planes and lead sheets. The tracking planes are assembled from co-extruded triangular polystyrene scintillator bars, each of which constitutes a channel, having a wavelength shifting fiber threaded through its center. The 0.6-mm thick lead sheets are introduced between the scintillator planes in order to increase photon conversion throughout the P0D. Moreover, a number of passive water layers are also interleaved with the plastic planes at the front end of the P0D in order to allow a statistical subtraction between neutrino interactions taking place in the scintillator (mostly on carbon nuclei), as opposed to the ones occuring on oxygen in pure water. Such a procedure is necessary to determine neutrino cross-sections on oxygen. [16]

The π^0 detector is then followed by the tracker, a sandwich of three time projection chambers and two fine-grained detectors forming a coherent unit and bounded by a solid structure, the basket. The tracker is optimized to study neutrino interactions that produce charged particles. It is the tracker's role to look at CCQE interactions and precisely measure the muon neutrino flux coming from the beam as well as its energy spectrum before any oscillation occured. It is also important to be able to measure differences in the spectrum as a function of time and location within the detector. [17] The tracker will also study charged and neutral-current inelastic interactions that could be interpreted as quasi-elastic events by the far detector, therefore assigning a wrong value for the ν_μ energy. Finally, it will study the ν_e flux and spectrum from the beam, an important source of background for ν_e appearance at Super-K. [16]

As an intrinsic part of the tracker, TPCs are gas-filled chambers divided in half by a high voltage electrode plate that creates an electric field between the center and the endplates. The chamber is positioned in a way such that the B-field coming from the magnet is parallel to the electric field of the cage. When a particle passes through the drift volume, it produces ionization along its track, and a measure of the drift time of electrons from the ionization event to the endplate gives information on the particle's location. It is then possible to reconstruct the path followed by the particle, whose curvature gives information on its initial momentum. More specifically, for the T2K experiment, TPCs will measure muon momenta produced in CCQE events, in order to determine the neutrino energy spectrum, and will determine

the charges of reaction products, distinguishing electrons and protons from pions and muons. In other words, TPCs are hollow boxes filled with gas used to catch the results of neutrino interactions mainly occurring in the FGDs where most of the mass is concentrated; this is the reason why the FGDs are located in between the three TPCs. Let's now take a closer look at these other elements composing the tracker.

1.3.4 A Closer Look at the Fine-Grained Detectors

As it has been claimed before, FGDs form the target mass for neutrino interactions in the rear part of the near detector. The FGDs however have a much deeper purpose than simply adding fiducial mass to the detector. The fine-segmentation of these components is a required feature in order to track all charged particles resulting from neutrino interactions, namely the muons as well as the low momentum recoil protons or pions. Such a reconstruction offers strong kinematic constraints and is used to reject backgrounds to CCQE events. Scintillator material has to be used rather than a Čerenkov detector in order to detect the protons having an energy below the Čerenkov threshold. Each FGD module has a size of 192 cm $\times$ 192 cm $\times$ 30 cm, which results in a total mass of $\sim$1.2 tonnes $\times$ 2 detectors (without considering the supports and electronics). Furthermore, a fundamental feature of the tracker is the fact that the two fine-grained detectors are quite different from one another: the first one, the plastic FGD, is entirely made of co-extruded solid scintillator bars while the second one, the water FGD, contains a significant admixture of water.

The scintillator bars forming the plastic FGD have a 1-cm^2 square profile and are stacked together in order to form solid planes. These planes are then positioned alternately in the x and y directions and similarly to the P0D, a wavelength shifting fiber runs through a hole in the center of each bar for channel readout; at this point, single- and double-ended readouts are still under study although single-ended may be favored. Each of these scintillating bars is furthermore coated with a thin layer of TiO_2, a highly reflective material in order to minimize light absorption as well as cross-talk problems. A detector quite similar to what is being described here has already been built for the K2K beamline experiment. Its highly inventive name is SciBar due to the fact it is composed of scintillator bars. A number of updates and modifications however have to be made from SciBar to fulfill T2K's requirements.

Firstly, SciBar had rectangular shaped bars larger than the 1 cm $\times$ 1 cm ones that are used for T2K. Because K2K's peak ν energy was larger than what T2K will be using, the detector needed not to be as finely segmented and coarse rectangular bars were adequate. Secondly, there is a major difference between the thicknesses of the two detectors: Scibar had a total thickness of 1.8 m in opposition to T2K's plastic FGD that is only 30 cm thick. The reason for such a difference is due to the presence of the TPCs which are in charge of tracking the longer range muons. In order to minimize the interactions between muons and scintillator – which complicate the reconstruction of the original vertex – as well as to maximize the probability for low momentum protons to reach the subsequent TPC, the FGDs must be thin. Thirty-cm thick FGD modules are then perfectly adequate to create fiducial mass as well as to track short range protons that may not reach the TPCs. Thirdly, the channel readout for SciBar was such that many fibers were connected to different pixels within the same photomultiplier tube. This design turned out to cause problems as cross-talk effects were observed between adjacent pixels, therefore not giving clear information about which cell the original interaction occured in. Such a cross-talk effect will be completely resolved for the case of T2K because every single cell will be connected to individual photosensors. On the other hand, cross-talk effects may still arise if the TiO_2 coating is thin enough for photons to cross from one cell to another; these effects will still have to be minimized for T2K. Finally, another major difference with SciBar is the fact that one of T2K FGD modules will contain a significant volume of water!

A fine-grained detector entirely made of plastic scintillator would offer a target mass mostly made of carbon whereas Super-K, made of pure water, uses primarily oxygen. Such a design would cause serious limitations due to systematic effects arising from the use of different nuclear targets between near and far detectors. The uncertainties in the measurements due to these nuclear differences come from the fact that nuclear Fermi momentum, Pauli blocking, charge exchange in the nuclear medium as well as nuclear absorption are poorly understood. The only way to get rid of these effects is by adding oxygen to the FGD in order to recreate ν interactions similar to what occurs at Super-K. In other words, the main motivation to add a significant volume of water in one of the FGD modules is to reproduce Super-Kamiokande's target material in order to cancel out the various nuclear effects. Consequently, by replacing some of the plastic modules with pure water in one of the FGDs, it will be possible to deduce the number of interactions occuring simply on water (oxygen) by mean of a statistical

subtraction between the interactions occuring in one FGD versus the other. This process is quite similar to what has been described for the P0D. Two main configurations have been considered for the water FGD: a passive design where simple pure water layers are interleaved with plastic scintillator modules and an active design where both the water and the plastic scintillator would be replaced with a water/liquid scintillator mixture. Both options have been under study and even though an active model is preferable for observing the recoil proton of a CCQE event, the concept causes serious engineering issues, as will be described later.

Active Versus Passive Detector Options

The active water module is an option that has been actively developed by the T2K Canada groups at TRIUMF and UBC. The main reason for designing the detector with an active water module is to eliminate any dead region within the detector, therefore allowing all recoil protons to be detected, no matter how small their momentum is after a CCQE event. Reconstructing low momentum protons is important in order to distinguish CCQE events from the backgrounds, but is also useful in understanding nuclear effects because these low momentum hadrons are mainly produced in nuclear reinteractions.[16] In both the case of an active or a passive design, part of the problem is simply to contain the liquid in a leakproof environment. However, in an active module design, numerous new challenges arise as a water "tank" has to be transformed into a finely segmented liquid detector. Firstly, extruded sheets of polypropylene with a twin-wall profile such as illustrated by figure 1.3 have been considered to contain the liquid in both scenarios. For the active design, each $\sim$1 cm $\times$ 1 cm cell will correspond to a different channel and the very shape of the extrusion will define the granularity of the detector. Secondly, in order for the volume to be active, the water target will be replaced by an admixture of water, liquid scintillator as well as some surfactant, an element necessary for the solution to remain homogeneous. This chemically reactive cocktail under its own weight will be under a total pressure of the order of a third of an atmosphere at the bottom of the panel. Leakproof seals will therefore have to be in place in order to sustain this pressure. The pressure will be equivalent for both passive and active configurations, but for the latter, the seals will have to be perforated to let through the wavelength shifting fibers for readout. As one may see, major complications arise when upgrading to an active water FGD; the following thesis specifically looks at these issues and tries from a research and development point of view to suggest and implement possible solutions.

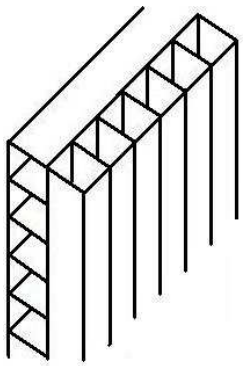

Figure 1.3: Successive x/y layers of the fine-grained detector liquid container. In the active water design, a wavelength shifting fiber will run through each cell, transforming a whole panel into a successive array of channels. The whole volume will then be filled with a mixture of water and liquid scintillator.

Research and Development in Solving Physics Issues

The following chapters describe the current status of the water FGD's design considering the various engineering and physics issues that need to be solved for both active and passive designs. Firstly, a general overview of the mechanical shape of the detector is described as well as the different materials that have been tested and the ones that are still under study. Many strength tests have been performed and prototypes have been built; here we present the setups and final results from these tests.

Secondly, we consider the fluid sealing issue, giving a complete update on the development of passive and active water seals. The method chosen for the passive case turned out to be quite simple, affordable and easily reproducible; it is described in great details throughout Chapter 3. A more complex possible design for an active detector seal is also described and viable prototypes involving thermal seals are presented. Problems that arose during the construction of these prototypes or future possible problems that might appear during the production are also addressed, and solutions are suggested. Long term tests looking to quantify the evaporation of water through the container as a function of time have also been set up with the use of one of the prototypes; the relevant details of the measurement are presented here.

Thirdly, the light yield issue is addressed. For an active water detector to be viable, the amount of light created by an event that gets to the photomultiplier must be significant; many criteria will affect light collection for a channel and understanding these effects is important. After a full description of the liquid scintillator that will be used for the experiment, painting test and beam test results are presented: in order to increase the reflectance of the container walls and to protect them against the scintillator, a massive painting job has been considered and the main observations are described. Results from beam tests performed at TRIUMF involving attenuation length measurements and long term stability of the liquid are also presented. Also, in order to study in detail various optical and geometrical effects of light propagation within a single detector channel, a computer program has been written and implemented using visual C as the programming language; the main results and subtleties of the program are described here.

Lastly, the long term effects of the chemically reactive liquid scintillator on materials have been studied. A description of how the aging process has been simulated, its inherent problems, and the various questions it may bring up are offered. With the use of a spectrophotometer and an integrating sphere, transmittance and reflectance measurements have been taken and the most relevant plots are presented. From these plots, we shall have a better idea what kind of effect the liquid scintillator has on the different materials and more specifically, on the polypropylene container the collaboration is considering for the active water detector configuration.

Chapter 2

Mechanical Structure of the Fine-Grained Detectors

2.1 Solid FGD Design

The total active volume to be filled by each FGD corresponds to 192 cm $\times$ 192 cm $\times$ 30 cm, the axis of the beam being along the 30 cm dimension. We may see this volume as a succession of thirty 1-cm thick layers having a surface of nearly 4 m^2 each. These thin planes are then combined together in order to form the modules which compose the FGD. For the solid FGD, a simple design of fifteen 2-cm wide modules has been chosen; a module being defined as an assembly of two layers of scintillator bars, one along the X axis and the other along Y. The two layers of plastic scintillator forming a module are built by gluing together 1-cm^2 co-extruded scintillator bars, machined by a B.C. company named CELCO. Inside each bar runs a wavelength shifting fiber. The orientation of the fiber defines the X and Y axes while the neutrino beam is along Z. The granularity for the solid FGD will therefore be of 1 cm $\times$ 1 cm $\times$ 192 cm and, supposing single ended readout, the total number of channels will be 5760.

CELCO has been chosen to extrude the bars as TRIUMF has had good experiences working with them. More specifically, CELCO worked on the KOPIO project, extruding the same kind of scintillator. Although the KOPIO experiment has been cancelled, the T2K collaboration greatly took advantage of the experience gained extruding these scintillator bars. Up to this point, a few preliminary runs have been done in order to adjust the die for optimizing the shape of the resulting bars. The main aspects that needed fixing were related to the overall square shape of the bar cross-section, the coating thickness uniformity on all four sides, as well as how well centered the fiber hole was. These points have been incrementally improved over the last three runs and various gluing tests have been performed. To form scintillator planes out of the individual bars, a two-part industrial epoxy has

been used: the resin is EPON 826 and the epoxy itself is called VERSAMID 140. This glue has good working time (∼1 hour) and has been used previously for TPC prototyping. On the other hand, small scale gluing tests are already showing that although the glued structure is quite rigid, it remains weak in one particular direction. Figure 2.1 shows a two-layers thick panel under its own weight. It is obvious here that the Y view will cause problems

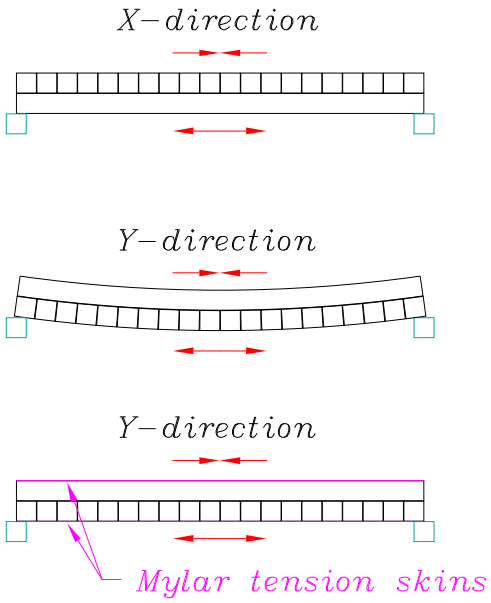

Figure 2.1: Two-layer thick scintillator module under its own weight. The upper part shows the X side view of the module: it is quite strong as the long side of the bars are under tension and the individual cells, under compression. The middle part shows the Y view: it is not as strong due to tension forces pulling apart the individual bars. The lower part of the drawing shows that strengthening skins around the module would solve part of the problem.

as tension forces pull apart the individal bars on the bottom layer. A solution would be to wrap a strengthening skin around each module. Mylar[†] could be used although it is unlikely to be found in such large dimensions. A

[†]Mylar is a trade name for biaxially-oriented polyethylene terephthalate (boPET) polyester film.

0.3-mm thick sheet of G10 will probably be used instead – such a thin sheet will make the scintillator module much stronger as it will absorb most of the tension strains. The fifteen solid FGD modules prepared and wrapped in strengthening cloth will then be positioned against one another to form a whole within the magnet; these modules will not be glued together as it would then be difficult to simply replace parts of the FGD. The details of how exactly these modules will be stacked and supported within the basket and between the TPCs are very similar to the way the water-rich FGD will be supported; it is therefore presented in the following section.

2.2 Water-Rich FGD Design

The number of modules composing the water FGD will be somewhat different from the solid FGD case. Initially, the water part of the FGD will be passive, but an upgrade may be considered later which would replace the passive modules by active ones. In the case of the passive water-rich FGD, interleaved solid scintillator and passive water modules will form the target mass for the detector. The solid module will still consist of the 2-cm thick X-Y modules previously discussed while the water module will be made of three 1-cm wide layers of extruded polypropylene having a hollow twin-wall (fluted) profile as illustrated in figure 1.3. For the passive water, all three layers of a single module may be oriented in an arbitrary direction since it will not be instrumented with fibers and we may as well choose the Y axis for practical purposes. Having all three layers along Y will facilitate the sealing process as only one end will be under water pressure. Figure 2.2 sketches half of the total side view of a passive water FGD. The figure is obviously not to scale considering only 10 out of 192 cells are shown on the X axis.

Let's recall that only water events are useful in order to offer a comparison with Super-K, a pure water detector. In first approximation, neutrino event distributions on water may be obtained by subtracting off the contribution from carbon measured in the plastic FGD as has been mentioned before. It may be possible, using more complex vertex reconstruction algorithms, to go further into the statistical separation of events in water and plastic; this particular aspect of the analysis has not been fully explored yet. [18] Moreover, the thickness chosen for the interleaved water modules is not arbitrary, but has been optimized from Monte Carlo simulations as well as from

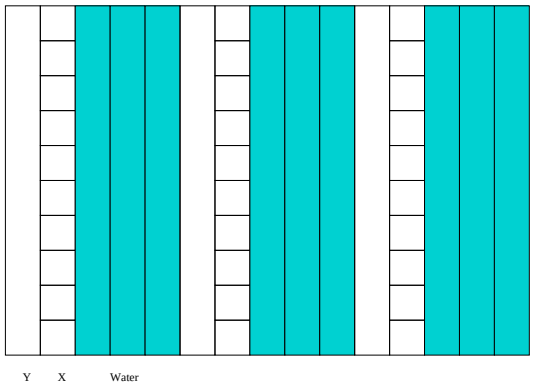

Figure 2.2: Side view for half of a passive water detector (horizontally). A complete detector is made of 6 solid scintillator modules (each composed by an X and a Y layer of solid scintillator) and 6 water modules (each composed of 3 Y layers of extruded polypropylene filled with water and perfectly sealed.)

K2K's experience with the SciFi detector that also used passive water as a target for neutrino interactions. Such a passive water design causes problems as a 3-cm dead region filled with passive water will fail to detect lower energy recoil protons that will lose all their momentum through the water, not reaching an active scintillator layer. This is the obvious reason why an active water design has been considered. In this more optimized case, the water FGD would simply be made of successive active layers of water with no plastic scintillator at all. A direct consequence would be to completely eliminate any dead region within the detector, therefore allowing all recoil protons to be detected. The adopted active configuration would therefore be quite similar to what has been described for the plastic FGD, the difference being that all the plastic would be exchanged for a liquid scintillator mixture contained in a hollow polypropylene extrusion. Consequently, the water FGD would be an assembly of 15 modules, each corresponding to an X and a Y layer glued together. Figure 2.3 shows a picture of the fluted profile polypropylene container manufactured by a company named Matra Plast Industries © located near Montreal.

There are many reasons why we are considering building the detector with these panels: they are easily found off the shelves, they are extremely cheap, strongly built, and they are easy to work with. It is possible other panels of

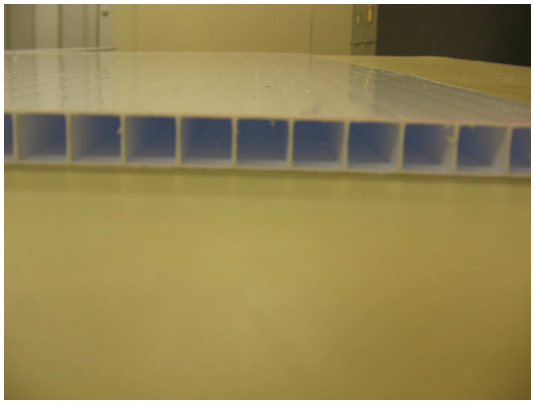

Figure 2.3: Profile view of a Matraplast Panel, the extruded polypropylene sheets likely to be chosen to contain the liquid. In the active configuration, a wavelength shifting fiber runs down each cell and leakproof endcaps seal the ends. The total thickness of the sheet is about 1 cm while the thickness of the inner walls is $\sim$0.6 mm.

the same type will be used for the real detector, but for the numerous tests that have to be performed, these ones work beautifully. The Matraplast sheets we have bought from a local distributor in Burnaby are 8 feet long, 4 feet wide and have a thickness of 1 cm. There is virtually no limit on the length the sheets may be manufactured with. However, the total width depends upon the extrusion machine used and as it turns out, 4 feet is the maximum. Consequently, to form a full-sized panel with the current material we have, we need to mechanically join together two sheets. The panel thickness we have been using is also the maximum dimension manufactured by the company: problems arise with larger cell sizes as the melted plastic gets difficult to handle during the extrusion process, resulting in a completely distorted cross-section. Various other companies and products similar to Matraplast have been investigated and depending on what will be found before the construction of the real detector starts, a different material may be used. A viable option would be to find 8×8 feet^2 panels rather than half this size; this would greatly facilitate the overall construction as it would not be necessary to externally link the panels together for them to fill simultaneously when the liquid would be inserted in. Other types of plastic have also been considered for containing the liquid at an early design stage, but as we will see explicitly in the *aging tests* section, the main problem has

been to find a product that remains inert to the liquid scintillator. White PVC turned out to be one of the worst possible choice one could make as it quickly turns yellow when in contact with the scintillator. High density polyethylene (HDPE) could have been a good choice as the scintillator itself is being stored in HDPE containers. The problem, however, has been to find a company that would sell small quantities of good quality extruded fluted HDPE. Matraplast could extrude HDPE, but only in ridiculously large quantities while companies such as Primex Plastics Corporation could sell in small quantities, but the product quality turned out to be much lower than what would be required to build the FGD.

Although most of the tests presented in this thesis have been done using Matraplast polypropylene, research towards finding a better material for the detector is still quite active. It has been pointed out that using polypropylene C_6H_{12} for the liquid container may not be the optimal choice for optimizing the oxygen/carbon ratio of the detector; this is because PP does not contain oxygen by itself.[†] To increase this ratio, polycarbonate panels $C_{16}H_{14}O_3$ could be used instead. These panels are mainly used for greenhouses and manufactured under names such as Lexan, Macrolux or Sunlite. Another great advantage of these products over Matraplast is the fact that they come in larger thickness, namely 10, 16, 20, 25 and 32 mm. Although a larger thickness may be problematic for an active detector as granularity goes down, it would be quite useful in the passive water case as it directly increases the oxygen/carbon ratio. Table 2.1 shows various possibilities of active and passive detectors as well as the corresponding ratios of the number of carbon to oxygen nuclei. [19] The passive detectors are built with 2-cm thick layers of polystyrene scintillator (C_8H_8) interleaved with passive modules of Matraplast or Lexan filled with water. The two last centimeters of the detector are also always made of polystyrene, consequently resulting in a structure made of n passive modules interleaved with $n+1$ plastic scintillator modules. The total thickness for a passive detector is therefore calculated from:

$$[\#\text{ layers HP} \times \text{thickness} \times n] + [(n+1) \times 2\text{ cm}] \tag{2.1}$$

with "# layers HP" being the number of layers of hollow panels in a passive module. For each configuration, the number of modules has been

[†] As previously discussed, it is important for the near detector to have a high oxygen concentration in order to replicate ν interaction in Super-K and to give an estimation of ν_e appearance backgrounds.

Det. Type	**Panel, # layers × thick.**	n	**Total Thick.**	**O:C**
Passive	Matraplast, 3 × 10 mm	6	32 cm	0.565
Passive	Matraplast, 3 × 10 mm	5	27 cm	0.550
Passive	Lexan, 1 × 20 mm	7	30 cm	0.491
Passive	Lexan, 1 × 25 mm	6	29 cm	0.606
Passive	Lexan, 2 × 16 mm	5	28 cm	0.703
Passive	Lexan, 1 × 32 mm	5	28 cm	0.752
Passive	Lexan, 2 × 20 mm	4	26 cm	0.832
Active	Matraplast, 30 × 10 mm	1	30 cm	1.174
Active	Lexan, 30 × 10 mm	1	30 cm	1.372

Table 2.1: Ratio of the numbers of carbon to oxygen nuclei for passive and active water FGDs of different water-bearing hollow containers. Each passive configuration is built from (2 polystyrene layers + a passive module) × n + 2 polystyrene layers, such that the detector starts and ends with 2 layers of plastic scintillator.

chosen so that the detector would have a thickness as close as possible to 30 cm. Not all the passive configurations give this exact number as one may see. On the other hand, the active detector does not contain any plastic scintillator and the hollow material is filled with a scintillator mixture (25% QSA, 70% water, 5% Triton-X – see *Chapter 4* for details) rather than with pure water. The total thickness in this case is simply # layers of hollow panel × thickness. The details of the ratio calculation are as follows: the density of polypropylene, polycarbonate and polystyrene as well as the areal density of the corresponding hollow panels are known from the manufacturer. The mass of a square foot panel filled with water may be calculated for the different configurations and from this value as well as from the thickness of the panel, the areal density may be deduced. By adding the carbon, oxygen and hydrogen components from all the different layers, the number of moles per square foot may be calculated for the three elements as well as the O:C ratio. The ratio is given per nucleus (or per atom) and would have to be multiplied by 16/12 to be per nucleon. Furthermore, for the active configurations, the whole chemical structure of the liquid scintillator mixture has been considered for the purpose of the calculation. From table 2.1, it becomes obvious that an active detector made of polycarbonate would be the best choice in order for the oxygen/carbon ratio to be maximized. This is, however, if the active configuration is not

ruled out due to other complications.†

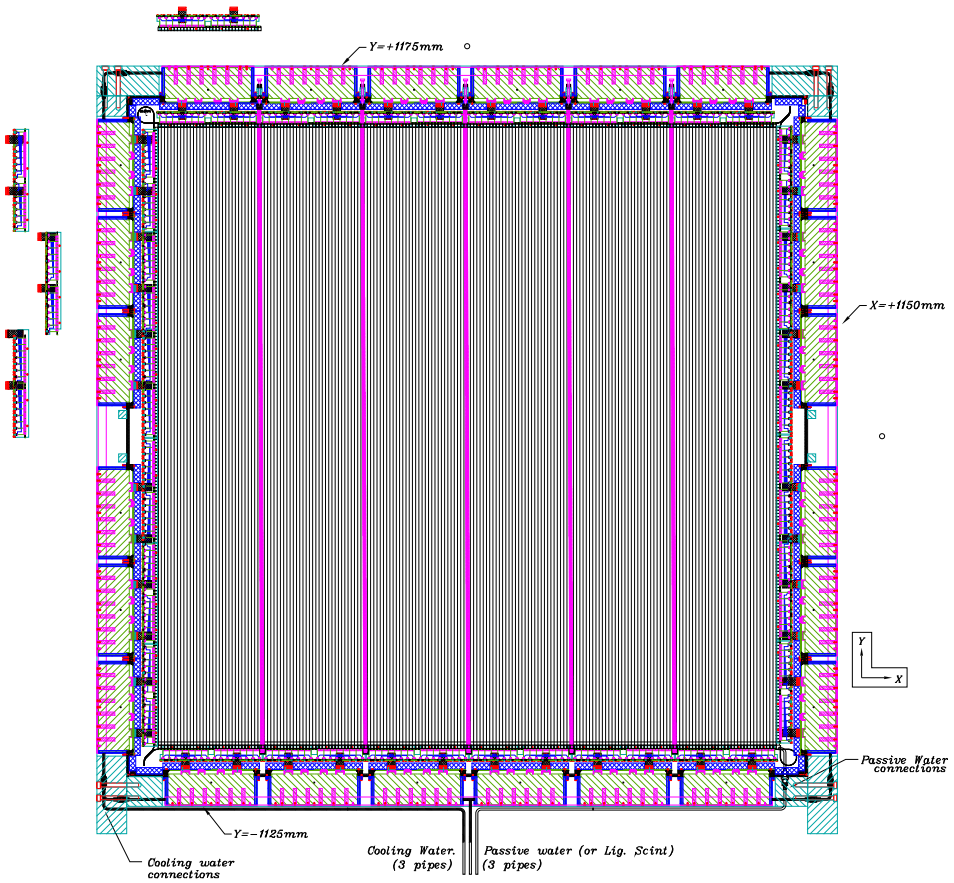

Figure 2.4: Front view of the latest FGD design showing part of the electronics, the water-cooling system and the top beams. The modules are supported from the top at five different locations by nylon straps represented on the figure by the thick vertical lines. Some bus-boards are also shown removed from the structure.

Let's now be more specific about how these plastic/liquid scintillator modules will be inserted and supported within the magnet and between the TPCs. Figure 2.4 shows the front view of a fine-grained detector module as well as the electronics surrounding it. Each module will be supported from

†As it turns out, PC is not suitable to be used with any chemically reactive scintillator and should therefore not be considered for the active configuration.

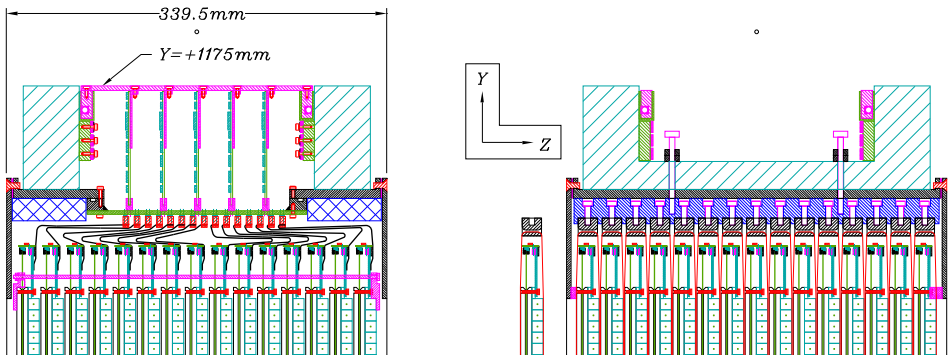

Figure 2.5: Side view of the FGD showing the details of how the modules are supported from above. The left part is seen through the ribbon cables and the right part is seen through the support system. The drawing is meant to be for a plastic FGD, but may very well show an active water FGD. In this case, only a liquid-recirculation system would have to be added, leaving the mechanical structure basically untouched.

above at five different locations in the X-Y plane by nylon straps running down both sides of the module. These straps are shown on the figure by the thick vertical lines every ∼30 cm, considering the module scale. Hanging the modules from the top will prevent the thin layers from bending under pressure; this configuration also minimizes the mass of the support structure. The figures in this section show what kind of space constraint the collaboration has to face in order to fit everything inside the basket; a great deal of engineering had to be done in order to come up with these designs. [20] Figure 2.5 shows two Y-Z views of the top part of the FGD, the left part being through the ribbon cables[†] and the right, through the nylon straps support system. All the straps from the different modules and located on the same Y-Z plane are securely attached to a common beam that spans the whole thickness of the FGD (30 cm) and is itself bolted in two points to the principal support structure outside of the dark box (see the right part of figure 2.5). The dark box is a thin-walled light-tight box that envelops each FGD and protects against any outside light that might reach the detector. Such a leak would be disastrous, basically making any interpretation of the

[†]Ribbon cables are what link the PMTs coming from the individual channels to the main electronics boards.

data impossible.

On a previous FGD design, each module had its own electronics board mechanically attached to it, but the constant need to optimize for space brought new ideas that evolved into the current design. In this sense, the latest update shows the boards not attached to the scintillator, but instead all gathered together in crates on the outside of the dark box as it may be seen from the left part of figure 2.5. Once all the modules will be completed, joined together, insulated, covered by the dark box and bolted to the main frame, the FGD will then be inserted in between the TPCs to complete the tracker as shown in figure 2.6.

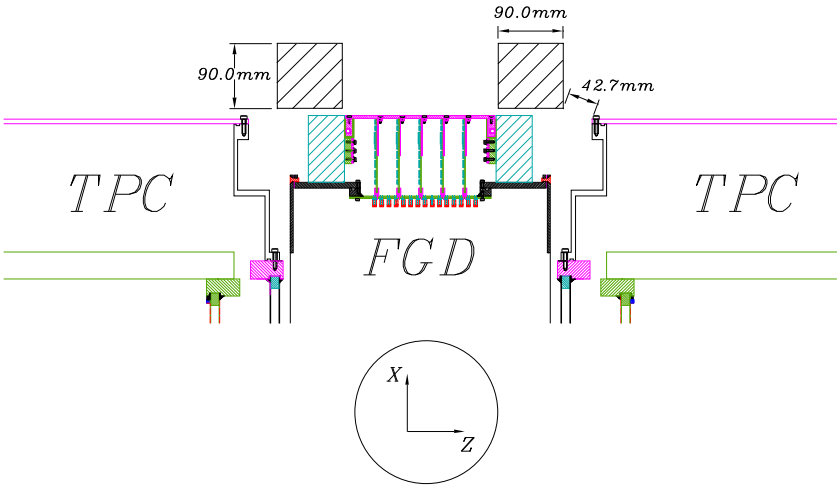

Figure 2.6: The FGD placed in between two TPCs and forming part of the tracker.

The detailed autoCAD drawings shown throughout this section are meant to represent the plastic scintillator, but they may easily be generalized for the active water-rich FGD. These two detectors are very similar to one another, both corresponding to a 15-module assembly, each of which is built juxtaposing an X and a Y layer of plastic or liquid scintillator. Their mechanical structure is essentially identical and only a liquid-recirculation system would have to be added in order to go from a plastic to an active water FGD, other than the obvious fact that the plastic has to be replaced with a liquid scintillator contained in plastic extrusions and sealed at both ends. It is a definite

advantage to have a design that may be easily adapted in order to satisfy the requirements of multiple detectors. On the other hand, the passive water would be somewhat different from this as three 1-cm thick Y-layers of water would be interleaved with plastic scintillator modules; this configuration would also lighten the total amount of electronics in the detector. Consequently, it is clear that plastic, passive water and active water detectors are all very similar mechanically, the only major difference being the layout of the modules as well as their orientation.

Furthermore, a cooling system will be necessary to keep the FGD modules inside the dark box at a temperature of $[23 \pm 2]^{\circ}$C. Insulation will be used to shield the FGDs against the magnet's heat load and an additional water cooling system will be used to remove the heat generated by the electronics. The electronics will most likely be kept at a temperature of $[27 \pm 2]^{\circ}$C, which is somewhat higher than for the FGD modules themselves. The cooling lines for each FGD will feed through the bottom of the magnet and in addition to this tubing, we may also want to use circulation lines as well as a pumping system to allow fluid circulation throughout the water FGD. Circulation of the scintillator mixture may be necessary in case mold growth becomes a serious problem or if any other types of inhomogeneity occur in sitting water/liquid scintillator mixtures.[†] Moreover, in case of water evaporation through the walls or the endcaps, we may need an easy way to top up the fluid level of the FGD.

2.3 Mechanical Strength Tests & Prototypes

The extruded panels of polypropylene we decided to use for most of the tests presented here were found at an early stage of the project design and the first questions we needed to answer were related to the mechanical strength of the plastic structure. In other words, could a plastic sheet be safely filled with water and hung from one of its extremities without collapsing under its own weight? Moreover, is it possible to glue two or three sheets together and then fill them with water? What kind of glue/tape could be used for this, and will it creep over time? These questions and numerous others needed answers and we therefore decided to realize these various mechanical tests in the basement of the Hennings building, in a lab where an old Van de Graaf generator used to stand. The room is quite large and a 2-ton crane has been

[†]Chapter 4 looks more specifically at the inhomogeneity problem as it directly affects light yield measurements

used to hang from the ceiling most of the prototypes built.

The goal of the first test (see figure 2.7) has been to get an idea of how strong the plastic container actually is. The setup is the following: a heavy duty 30-feet long chain runs through a hollow 9-feet long aluminum tube and is hung from the ceiling crane by two carabiners. The aluminum tube is 2 inches in diameter and is perforated by small holes every 15 inches. Length adjustable hooks are then locked through these small holes and metal straps attach the 8×4 feet^2 plastic panel to the hooks. Moreover, a 0.75×0.75 cm^2 steel rod is inserted in the top square cell of the panel, right over the metal strap supports. The rod tightly fits in the cell and redistributes the metal straps' pressure over the total length of the panel. In other words, the whole weight is supported by a steel rod located in the top cell of the panel. A panel by itself is quite light and strong, but the question was to under-

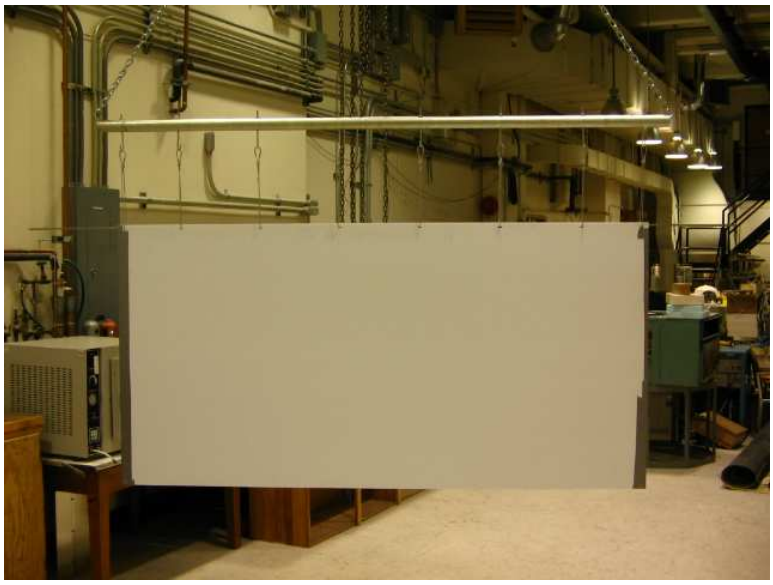

Figure 2.7: Plastic panel filled with sand and hung from the ceiling off a 2 ton crane in the Hennings Neutrino Lab. This setup was to test the mechanical strength of the panel when filled with a material whose density is close to water.

stand the effect of a full load of water on the structure. Because sealing the extremities of a panel is an issue by itself, we had to find a material whose density was close to water while not being as messy. Play sand seemed an

obvious choice as it is cheap and easily contained. Figure 2.7 therefore shows this Matraplast panel filled with sand simply contained by duct-tape, when the panel is hanging from the ceiling.

A quick engineering calculation has been done in order to estimate how far apart the supporting metal straps should be. What is happening with the steel rod supporting the whole structure is a simple beam deflection problem described by the Euler-Bernouilli equation. We therefore want to know how far apart should the two supports be (L) in order for the beam, which is under constant stress per unit length (ξ), to be deflected by some maximal amount between each support (δ_{max}). The maximum deflection equation corresponding to this specific force load is the following:

$$\delta_{max} = \frac{5\xi \mathrm{L}^4}{384 \mathrm{E} \mathrm{I_o}} \tag{2.2}$$

with E being Young's modulus, a constant depending on the type of material used ($\sim$200 GPa for steel) and $\mathrm{I_o}$ being the second moment of inertia related to the cross-section of the metal rod. In the case of a square cross-section, $\mathrm{I_o} = \alpha^4/12$, α being the dimension of one side of the square. Considering that we might want to support three whole 8×8 feet^2 fully loaded panels from the single rod, that is $\xi \sim$62.5 kg/m, and that the maximum deflection ought to be $\sim$2 mm, one get L $\sim$60 cm. As any engineer would do, I divided this number by 2, therefore increasing by the same factor the number of straps supporting the panel.[†]

As no significant distortion in the plastic of the hanging 4×8 feet^2 panel was observed over the first few weeks, it has been decided to try gluing other panels to the one already in place as well as filling them with sand. A total of six sheets forming a full-sized 3-layer detector were then assembled by simply gluing the new panels onto the old ones. The goal here was to investigate further the strength of the plastic as well as finding an effective glue to stick the panels together. Up to this point, two types of material have been used for gluing the pieces together: contact cement and double sided tape. Contact cement is a product quite effective for gluing plastic and wood surfaces. It comes both in a thick yellow liquid or gel. For it to

[†]To use such an equation, I assumed the length of the beam $\gg$ width and depth such that the stresses perpendicular to the beam were much smaller than the ones parallel to it. I also assumed the deformation remained small, no torsion was involved, the rod was considered perfectly isotropic and its cross-section remained constant throughout its length. These assumptions were more than reasonable in this case.

work, one needs to apply a thin layer on both surfaces to be glued and after only a few minutes of curing (before the cement completely dries out), the surfaces may be put in contact. Moreover, putting the piece under constant pressure while curing insures a better binding. From the experience I have gained, I may say contact cement is very effective, cheap, but quite messy and relatively difficult to work with even though it has a good working time. More specifically, it is difficult to make sure it is applied uniformly on all surfaces before they are put in contact and it is also non-trivial to put a large surface under constant pressure for a better result. Nevertheless, binding panels using contact cement turned out to work quite well as figure 2.9 shows.

The second material used for binding the plastic sheets together is double sided polyethylene tape. The tape is manufactured by Zhongshan New Asia Adhesive-Products Co. Ltd and comes as a very thin transparent film of about 4.5 feet wide; figure 2.8 shows a roll of this tape. The tape is of great

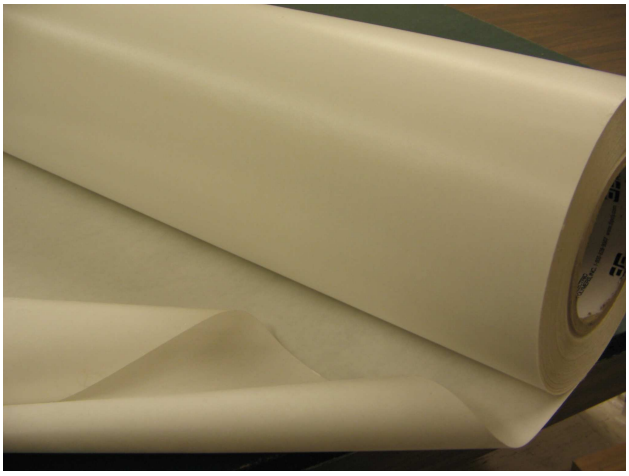

Figure 2.8: Double sided tape used for gluing panels together.

quality and has the advantage of being extremely easy to handle, without emitting any inconvenient odour when applied. Furthermore, both the cement and the tape adhere better to rough surfaces rather than to slippery ones. Therefore, to improve the quality of the binding between adjacent panels, all surfaces had to be roughened using sanding paper or a belt sander; this process is somewhat tedious, but turned out to be quite effective. In addition to the roughening and as a part of surface preparation, every panel

has been lightly washed with isopropyl alcohol prior to gluing in order to remove the remaining dust and large impurities. Other than cement or tape, it may also be possible to use the same epoxy as the one used for gluing the plastic FGD scintillator bars. There is no obvious reason why this would cause any problems, however, tests have yet to be performed with epoxy. The main issue raised by using either cement, tape or epoxy is to understand how the material reacts over time. Will it dry, creep and break or perhaps completely peel off under the shear forces exerted by adjacent fully-loaded panels? These non-trivial issues are best studied with the use of prototypes.

Consequently, as described above, a total of six panels have been assembled together, some using cement and others with tape. They all have been filled with sand and have remained suspended from the ceiling for over a six months period. Over this time, a monitoring of the relative positions of each panel (every week or so) allowed to look for any creeping caused by shear forces. None, however, have been observed. In other words, the full-sized module has remained suspended off the ceiling crane in a perfectly stable state over a long time and under full weight pressure. These observations, although rather qualitative, give strong insights on which materials are best to be used for building the real water FGD, for both the water-bearing material and the adhesive used to glue panels together.

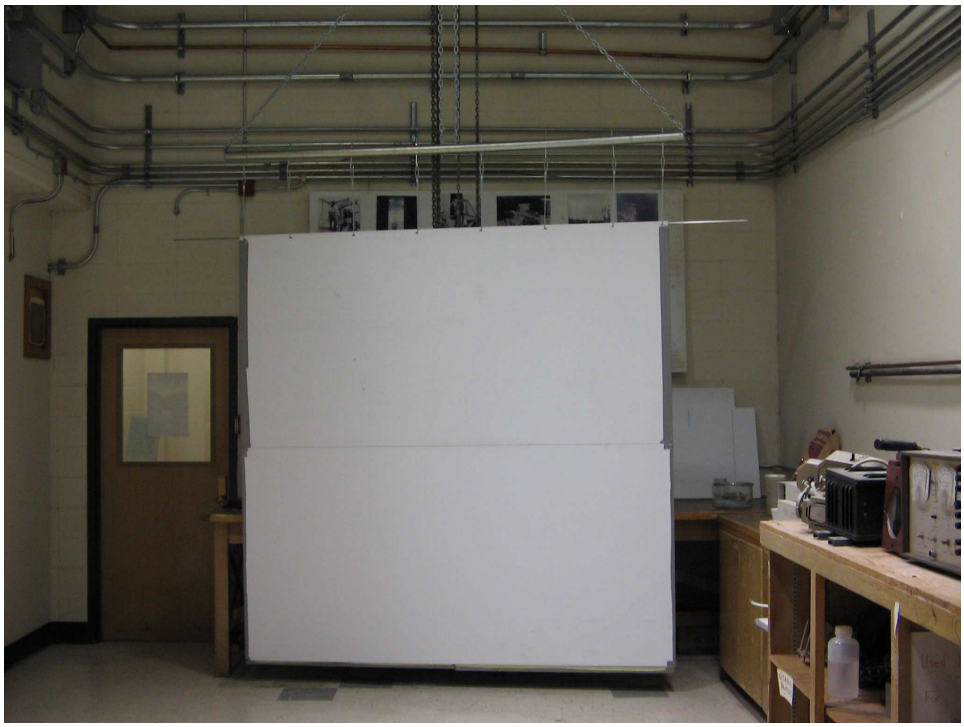

Figure 2.9: Full-sized detector filled with sand. The various panels have been glued to one another using contact cement as well as double sided tape. The whole structure has been hanging in the lab over a total period of 6 months.

Chapter 3

Fluid Sealing

The general design for both passive and active water fine-grained detectors has been presented in the previous section. It has been shown that the liquid mixture will be contained within hollow plastic extrusion panels glued together and forming independent modules. A serious issue that has been deliberately overlooked up to this point is the need to build leakproof modules in order for them to be safely inserted within the magnet. There is no need to say how dramatic the effect of a leak would be, considering all the electronics inside the detector. The present chapter will therefore address the fluid sealing problem, giving a complete update on the different approaches taken to seal both a passive and an active water detector.

3.1 Passive Sealing

We began by first attempting to seal a passive module, as it is a much simpler task than sealing an active one. Various designs have been tried over the last year or so which evolved into the method that will be most likely used in the real detector. Let's here present most of these ideas. One of the very first ideas consisted of gluing endcaps at the panel extremities in order to contain the water. The endcaps would be made of polypropylene, the same material as the panel itself, and a single piece would cover the whole length of the panel. The polypropylene that has been used for endcaps is of natural color, rather than white like the rest of the panel. There is no deep reason for this, simply the availability of the material at TRIUMF. Polypropylene has numerous advantages, namely, it is easily found, relatively cheap and may be machined into any kind of shape.

Although the ultimate goal is to seal a full-sized panel, the first series of tests had more modest objectives: 8-feet long by 6-cell wide pieces were sealed with plastic endcaps as well as with different types of glues, epoxies and RTV Silicones.[†] This has been done in the following way: a small

[†]RTV stands for room temperature vulcanization, a chemical process during which

polypropylene endcap having a depth of ∼2 cm is machined in order to fit over the extremity of a 6-cell wide extruded panel; the endcap is cut approximately a centimeter longer and larger than the panel itself. A 1-cm deep groove along the length of the endcap (longer than 6 cells, but not spanning the whole length) is then cut using a milling machine and after filling the groove with some gluing material, the Matraplast piece is inserted. Depending on the type of glue used, it may take up to a few days for it to fully cure. Figure 3.1 shows a close-up picture of one of these leakproof endcaps.

Figure 3.1: Passive water endcap sealed with white RTV

Various materials have been used for gluing these endcaps: 5-minute epoxy, 24-hour epoxy, and white and clear RTVs. Figure A.1 in the Appendix is a picture that shows this first series of tests. Although all of them provided a leakproof seal over a total period of 6 months, an unsuspected problem occured with the ones sealed with RTV. It seems as if the RTV was porous to ambient air, consequently allowing the water to evaporate very slowly as a function of time. It remains ambiguous at this point if the Matraplast panels are themselves porous to air, therefore also releasing evaporated water at a very slow rate. This aspect needs further investigation and is described in more detail in a subsequent section. Two other problems were also observed with gluing such endcaps to panels: firstly, trying to use a modified version

occurs a cross-linkage between the polymer chains of the rubber's molecules. When fully cured, the result is a springy surface that does not adhere to metal nor plastic.

of these endcaps for the active detector may cause difficulties, as both the polypropylene and the glue would be in contact with the scintillator. (It would be interesting to succeed in getting rid of the glue as part of the endcap.) Secondly, due to the fact that the endcap is thicker than the panel itself, a problem will arise when multiple panels will be glued and stacked together within the magnet. One may therefore ask how to get rid of this excess of plastic?

The second series of tests for the passive FGD specifically looked at the possibility of removing any glue from the sealing design. To succeed in doing so, one must consider thermally welded endcaps. The idea is to heat up the part

Figure 3.2: Small press used to thermally weld endcaps to the Matraplast panels. The press allows one to apply a constant pressure with a pointed metal piece heated up to the polypropylene melting point.

of the endcap that is in close contact with the extruded panel causing both plastic parts to melt together, forming a leakproof seal. The theoretical idea is simple, but technical issues soon appeared when prototyping. Firstly, the endcap design has to be somewhat modified: the single large groove previously described has to be removed and replaced by a much thinner one that follows the exact rectangular shape of the extruded Matraplast piece's

outside surface. The depth of this groove depends upon how deep we want to insert the Matraplast into the endcap; from experience (not extensive), it seems as if 5-6 mm was just fine. Now, cutting a groove 1 mm wide in a piece of plastic is far from being trivial, the main problem laying in the fact that there are no end mills having 1 mm in diameter. What has been used instead is a small saw blade that is precisely 1 mm in thickness; this blade mounted on an inch wide cylinder may therefore be used as a milling tool.

At this point, the inside walls of the Matraplast piece must be completely removed, up to 1-1.5 cm from the extremity. The piece may then be tightly inserted into the endcap as the extremity's cross-section now perfectly fits in the 1-mm thick groove (see figure 3.3). The final step consists of making the actual thermal weld by applying a constant and uniform pressure on the endcap with a sharp hot metal piece at the very position the panel has been inserted. The metal piece should be heated up and maintained at $\sim$250^{o}C, that is, the approximate melting point of polypropylene. The pressure should then be released when the edge of the metal piece starts to melt the Matraplast. The thermal press used for this purpose is shown in figure 3.2 and a close up of the metal-edged piece is found on figure 3.4.

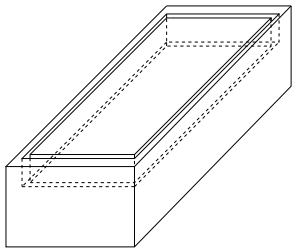

Figure 3.3: Endcap used to thermally seal the end of a Matraplast panel. A 1-mm thick groove is machined on the endcap and follows the exact shape of the Matraplast panel that will be inserted.

This thermal weld process has to be repeated for all sides of the endcap to ensure a perfect seal.

As soon as the press started being used for sealing 6-cell wide panels, interesting new results were obtained, but numerous issues and questions were raised as well. In my experience trying to seal about a dozen prototypes, a single thermal weld works beautifully as long as the pressure exerted is uniform over the surface. Problems however come from the fact that a total

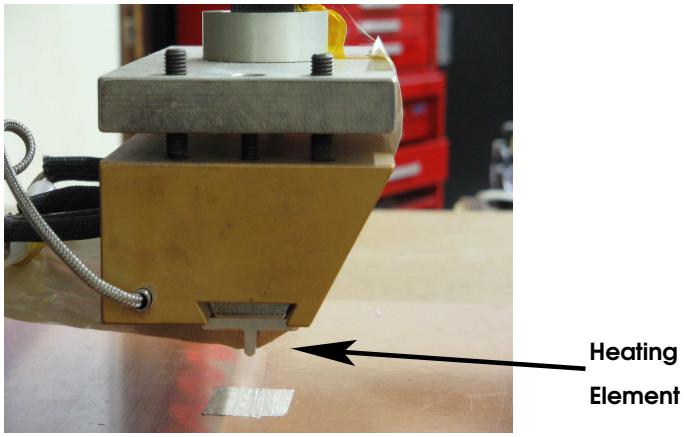

Figure 3.4: Close up of the heating element and the aluminum edged piece that melts the plastic. A thin heat tolerant piece of cloth partially made of teflon is covering the blade and prevents the melted polypropylene from sticking to it.

of four welds have to be done to seal a single panel due to the four sides of the endcap; making sure these individual welds overlap without leaving even the smallest gap is a definite problem. Further problems arise from the fact that, on each panel, there are two long and two narrow sides that have to be welded. Although the narrow side is only 1 cm wide, it could not be welded using the press, and a soldering iron had to be used with an appropriate end piece. This aspect has been the major cause of problems as it is very difficult to apply a constant pressure on the surface "by hand" using this tool; all the prototypes that failed leaked from the corners of the endcap, the very junction between welds. Consequently, a solution could be to design a press that would thermally seal all four sides simultaneously. Such a press would allow one to seal a full-sized panel in a single step, taking a few minutes only.

The thermal press idea is viable, although building a press capable of dealing with real-sized panels would still require a relatively large amount of engineering work. On the other hand, a thermally welded endcap remains larger than the panel itself, leaving the collaboration with yet another issue to solve. Consequently, for the passive FGD, because it is not critical for the epoxy to avoid any contact with pure water, a much simpler method may be considered. This last method consists of using a mould to seal the

ends of a panel, simply filling the mould with epoxy right before the panel's extremity is inserted in. The wet epoxy then cures in direct contact with the panel. Once the epoxy is fully cured, the mould simply has to be removed from the end of the panel. To avoid the epoxy sticking to the mould, teflon-based lubricant may be used prior to pouring the epoxy into the mould. By machining the mould to the exact width of the panel to be sealed, one may therefore completely get rid of any small rim of epoxy surrounding the end. It is also possible to build more complex moulds including small tubes as input/output for the water; these tubes may be used to link adjacent panels together. Four large prototypes (A-B-C-D) have been built using the mould method. The next sections present the details of these prototypes, how they have been built and what has been learned from them.

3.2 Passive Module Prototype A

This first prototype consists of a 3-layer thick, 30-cell wide and eight-feet tall module made of five individual parts sealed by a 1-cm thick epoxy endcap done with the *mould* method. The middle layer is made of a single 30-cell wide panel while the two outer layers are each built from two fifteen-cell wide pieces. The reason for doing so has been to simulate a similar situation that would occur in a real-sized detector: each individual layer in the detector will be made of two 4×8 feet^2 panels butted together, and in the passive design they will all be placed vertically along the Y direction as we saw. So, in order for a 3-layer module to hold together, the point of junction between the pieces in each layer must not be located at the same position from layer to layer; this is what has been reproduced to a smaller scale in the prototypes. (Obviously, the problem completely vanishes if 8×8 feet^2 panels are used instead.) These different pieces are then fastened together using double sided tape as it is easily handled, and the module is then ready for the sealing procedure. The first step consists of cutting a small 3-cm deep, 1-mm wide groove on all the inside walls of the panel using a small knife or more efficiently a jig-saw. This groove simply insures that water will freely flow between individual cells after the sealing procedure is completed. The choice for its depth is quite arbitrary, however, it must be deeper than the thickness of the epoxy seal in order for it to work and as we will see in the *prototype B* section, a groove that is too deep may cause problems. Moreover, it must not be too wide either, that is, the inner walls must not be completely removed or else there won't be enough plastic surface for the epoxy to bind to and the seal may fail. After

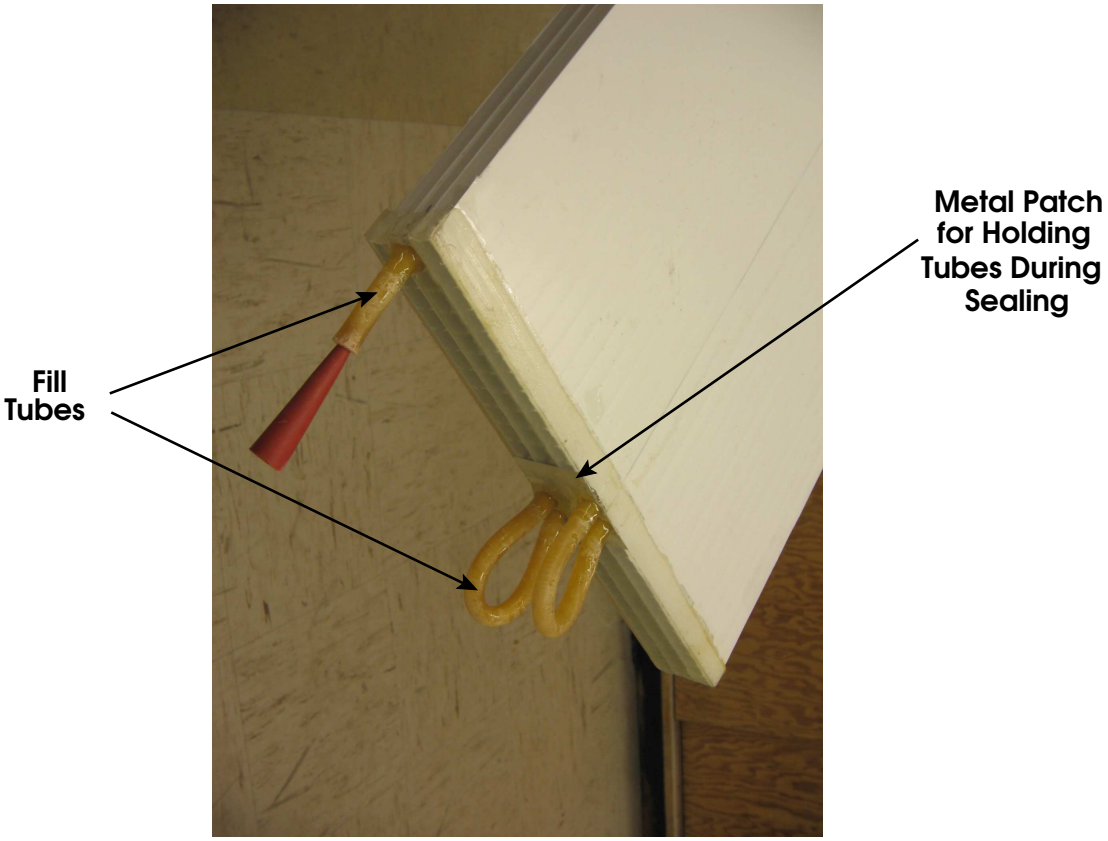

Figure 3.5: Close up of the epoxy seal for prototype A. Plastic tubes link adjacent parts, making sure the water flows throughout the module.

cutting such a groove, the inside surface of the cells that will be in direct contact with the epoxy has to be roughened to improve the binding; this may be done using files of different sizes although the process remains quite tedious. The final few steps consist of filling the mould with epoxy after it has been coated with anti-stick canola oil, inserting the 3-layer panel in the mould and waiting a few days for complete curing. The mould made of natural polypropylene itself may then be taken off and what is left is a pure epoxy seal (see figure 3.5). The picture shows yet another feature of the prototype, as small plastic tubes linking the different sections of each layer and a drain to flush the water have been installed. The small tubes linking adjacent pieces allow the water to flow and fill the module in a single

step. This will be a nice feature when both ends of the prototype will be sealed, leaving only one or two small inputs for water filling. Now, let's be more specific about how to integrate these tubes. Firstly, for prototypes A and B, they were not inserted after the curing process was completed, but the mould itself has been designed to incorporate them: holes through the mould were drilled for these tubes to pass through and small pieces of metal closely surrounding the tubes were placed inside the mould to prevent the epoxy from flowing out during the curing period. When the mould has been removed, these pieces of metal remained stuck to the panel as a part of the seal while the tubes freely passed through the mould.[†]

The prototype sealed at one end may then be hung from the crane in the lab and ultimately filled with water. For this purpose, inch wide, 12-feet long metal straps were epoxied onto the surface for supporting the structure from the top as figure 3.6 shows. Small pieces of aluminum were also bolted together at the very top of the panel to prevent the straps from peeling off (this area is by far the most fragile). For future prototypes, the metal straps should perhaps be replaced with nylon straps, often used for packaging purposes. These nylon straps would certainly be strong enough while being not as heavy as the metal ones. Prototype A remained in the lab, hung from the crane, for more than two months and no sign of leakage has been found during this time. Furthermore, as one may have observed from figure 3.5, all three layers are not interconnected by a network of plastic tubes. This was a design mistake and the whole panel could not be filled by a single input. Although corrected for prototype B, this error did not cause any serious issue here as only one end of the panel was sealed and all cells from the other end could be used as inputs.

3.3 Passive Module Prototype B

Prototype B is very similar to the previous one, but shows a higher level of complexity as it is longer (50 cells wide), and is made of 7 pieces all interconnected together by plastic tubes. It is also sealed at both ends. This second large prototype has been designed firstly to show the validity of the mould technique in the case of a more complex configuration, but secondly

[†]Metal probably is not the best material to be used here as we are trying to minimize the total mass that does not have an oxygen contribution. The point was simply to see if the chosen configuration would work; any material may therefore be used to replace the metal piece.

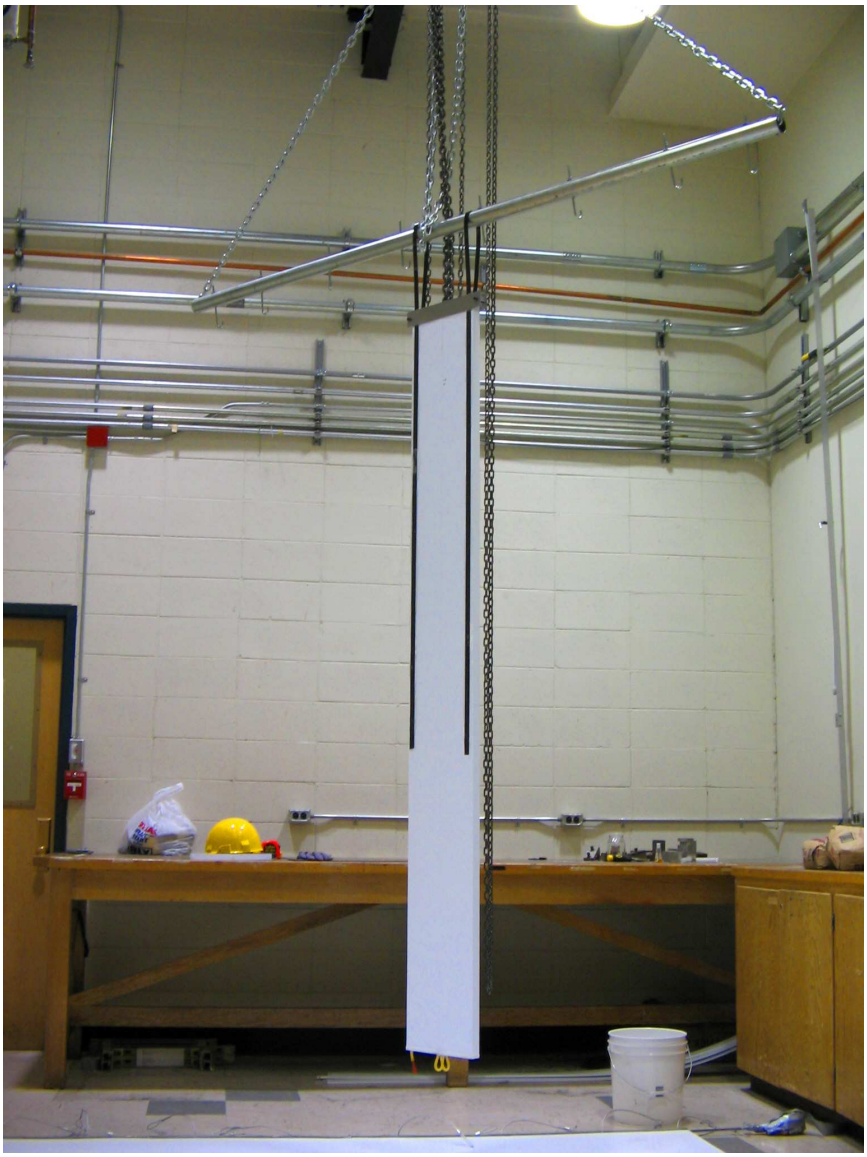

Figure 3.6: Prototype A hanging off the crane and supported by long metal straps epoxied onto the surface. The panel has been completely filled with water and remained in this position over a period of two months without showing any sign of leakage.

to investigate the water level inside the panel as a function of time. It might be possible for water to evaporate through the Matraplast or the epoxy endcaps, and this aspect has to be quantified. Needless to say both ends of a panel have to be closed for such an effect to be measurable. To seal the ends of this second prototype, the mould method has been used again, however, this time wood has been used instead of plastic to make the mould. The choice for a new material was simply to investigate the effect of epoxy on different surfaces. As it turned out, because wood is porous, it sticks very well to epoxy and is consequently a terrible material to be used for a mould. Figure 3.7 shows a picture of one of the moulds used for prototype B.

Figure 3.7: Mould used to seal the bottom end of prototype B. It is made of wood, a material that turned out to be quite terrible for this purpose. Plastic tubes are configured in such a way that they will interconnect all the panel pieces together once the sealing procedure is completed.

All the tubes that will interconnect the different pieces are visible on the picture as well as a drain to flush out the water. Just as was the case for prototype A, a very thin piece of metal is present at the bottom of the mould, closely surrounding the tubes; it will prevent the leakage of the epoxy when it is poured in the mould for sealing. Another very similar mould, but with only 2 inputs, has been used to seal the top of the panel; one may see that two inputs are necessary to allow a constant air flow during the water filling.

An unexpected issue however arose when sealing both ends of this prototype. As figure 3.8 shows and unlike prototype A, the sealing procedure somehow induced a distortion in the panel ends; a single look at the cross-section shows how important this effect turned out to be. This problem had to be investigated further to understand its cause; such a distortion in the final detector would be inadmissible. The two main hypotheses we thought

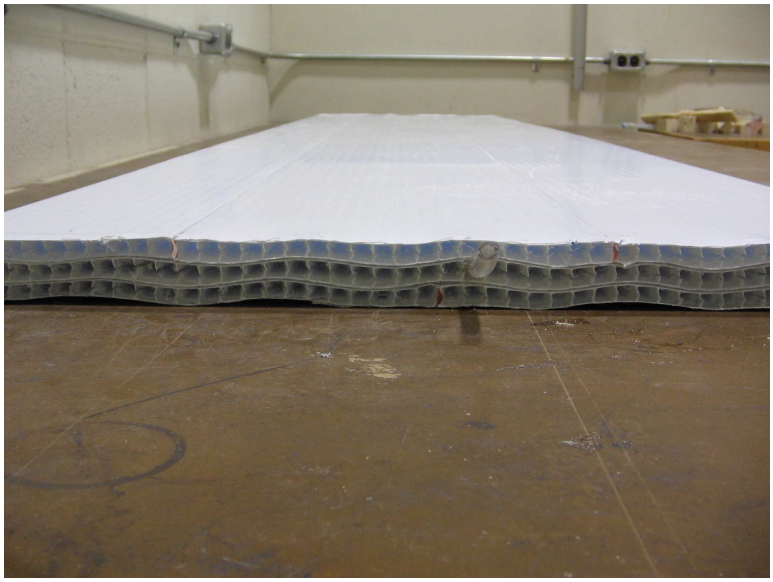

Figure 3.8: Prototype B top seal showing a completely distorted cross-section due to a combination of a too deep groove and the epoxy's strong exothermic reaction.

could explain this phenomenon were either that the groove cut into the inner walls was too deep, or the use of an epoxy that heats up too strongly as it cures, therefore melting the plastic. As a matter of fact, for the first time on this prototype, the jig-saw was used to cut the groove on the inner walls. Consequently, it turned out to be almost twice as deep as the one from prototype A. On the other hand, the epoxy used was the "New Clear Epoxy" from Industrial Formulators and it does show a highly exothermic reaction during the curing process. Two tests have been done on a smaller scale to understand the causes of the distortion: the first one used the "New Clear Epoxy" with a much shallower groove and the second one kept the deep groove, but used a type of epoxy that does not heat up when it cures. In both cases, the problem completely disappeared, proving the problem

was caused by the combination of a too deep groove and the specific type of epoxy used. The situation is consequently under control and can be avoided for the real detector.

After its completion, prototype B has been hung from the ceiling and also partially filled with coloured water (figure A.2). The whole module was simultaneously weighed with a hanging scale directly attached to the crane. The idea was to monitor the water level as well as the mass of the structure as a function of time to see if the water evaporates. Prototype B, however, turned out to show signs of leakage between two adjacent pieces of the module. The exact reason for this leak remains unknown, but is most probably due to a perforation in an outer wall. Because the perforation was not accessible, the problem could not be solved, and ultimately the panel failed to offer a leakproof seal for a passive water module. This prototype made clearer some of the difficulties one encounters when forming a module made of many pieces. It therefore reinforced the need to find plastic panels as large as the detector's total cross-section.

3.4 Passive Module Prototype C

Prototype C consists of a single Matraplast layer, 4×8 feet^2, sealed with epoxy at both ends. This configuration is simple as no tubes link adjacent parts, the whole panel being made of a single piece. Sealing this piece turned out to be much simpler than what has been experienced for the previous prototypes. A 1-cm wide metal mould has been used to seal both ends of this panel and unlike the previous prototypes, the input/output have been installed after the sealing procedure was completed. The two inputs and the output consist of 1/4 inch copper tubes inserted in holes of the exact same size carefully drilled through the epoxy seal. Once the tubes are tightly inserted and positioned, a thin layer of epoxy may then be applied around the tube and on the end of the panel in order to complete the sealing. Figure A.3 in the Appendix shows the mould used as well as one end of the panel being sealed. Copper has been chosen over plastic for the tubes in order to increase the binding with the glue. As was the case for the previous trials, prototype C was hung from the crane and held by narrow nylon straps running 4.5 feet down each side of the panel.

Prototype C proved to be perfectly leakproof and it has been fully filled with coloured water. The main objective of this prototype, other than the

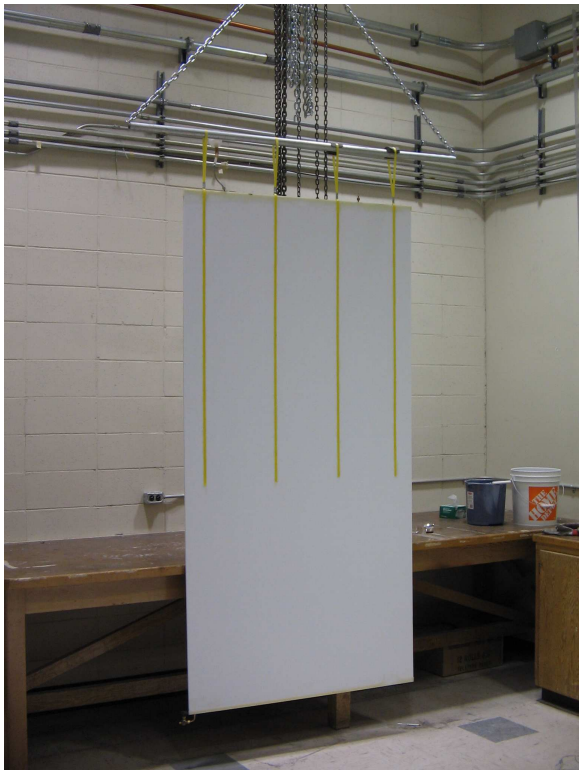

Figure 3.9: Prototype C hanging off the crane in the lab. It is sealed at both ends and is supported by narrow nylon straps. The panel has been filled with water and showed no leakage signs after many weeks. Prototype C is being used as a long term test to monitor the water level as a function of time.

obvious one of building a viable half-size passive water layer, was to quantify the evaporation of water through the Matraplast walls as a function of time. Although the detector still currently hangs from a fish scale, it might be quite difficult to measure the weight of the panel as a function of time and it might be simpler and more accurate to simply monitor the water level through the plastic. This is one of the reason the water used has been colored with a dark colorant. From May 9^{th}, 2006 to August 5^{th}, 2006, the water level has dropped by 10.3 mm (for a 125-cell wide panel), which seems to indicate the evaporation through the matraplast and/or the epoxy endcaps is not negligible although being quite small. To fill the panel with water, a

funnel has been attached to one of the two inputs and as water was poured in one of them, the air was allowed to flow out of the other. The filling procedure took about an hour while draining the panel takes about half this time.

3.5 Passive Module Prototype D

In addition to the epoxy endcap supporting the load of water within a panel, it may be possible to completely eliminate any leak by putting the panel under negative pressure, that is, under a pressure lower than 1 atm. or 101.325 kPa. As we may see from figure 3.10, this may be accomplished with the use of a small *bubbler tank* positioned at the top corner of the FGD. A water pump is used circulate the water in and out of the module

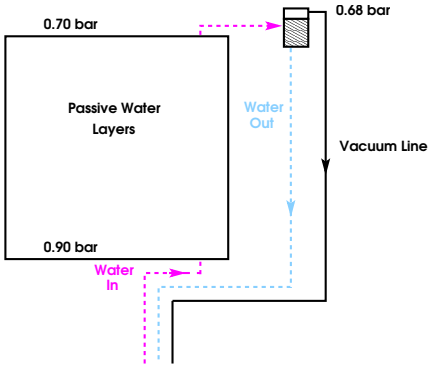

Figure 3.10: Schematic of the negative pressure system. The dotted lines correspond to the water flowing in and out of a small *bubbler tank* positioned at the top of a passive module while the solid line represents the air pumped out of the system by a vacuum pump. With such a configuration, the whole panel is placed under a negative pressure between 0.70 and 0.90 bar.

while the air is pumped out of the *bubbler tank* by a vacuum pump. The result is a pressure varying from 0.70 to 0.90 bar between the top and the bottom of the panel. Although this procedure may be very interesting in order to control the possible leaks, it was initially quite unclear what would be the impact of such a pressure on a Matraplast piece. This obviously needed further investigation and this is the reason why prototype D was built. Prototype D consists of a 25-cell, 8-feet long Matraplast piece sealed at both ends by a 1-cm thick epoxy seal. At one end of the panel, an input

for the pump to connect to has been inserted and epoxied to the endcap. The objective of this prototype was to bring the pressure inside the panel as close as possible to the vacuum while monitoring the appearance of the extrusion. Although this procedure is not an accurate description of a water-filled negative pressure system, pumping the air out of a sealed panel remains an easy way to test the strength of the material.

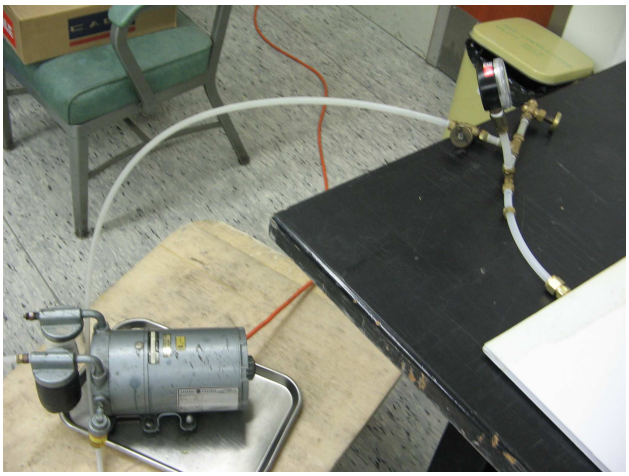

Figure 3.11: Prototype D as well as the vacuum pump used to bring the internal pressure as close to vacuum as possible.

More specifically, the deformation of the panel has been quantified measuring the deflection of the surface as a function of the negative pressure within the panel. The tool used for the measurement was a deflection gauge having a precision of 0.001 inch. Figure 3.12 shows the deflection of the panel as a function of the internal pressure. In this sense, 0% vacuum corresponds to 1 atm. while 100% vacuum corresponds to 0 atm. For this set of data, the deflection has been measured in the middle of the panel, both along its width (middle of 12^{th} cell out of 25) and length. The first thing to observe is the fact that the deflection shows a linear relationship with the exerted pressure. More importantly, perhaps, is the fact that the deflection remains extremely small, even when the panel is brought to a pressure under 0.1 atmosphere (deflection of 0.003 inch $\approx$ 0.075 mm at 90% of vacuum pressure). This is very good news for the collaboration and it is clear that a Matraplast panel will sustain, without significant deformation, the pressure we intend

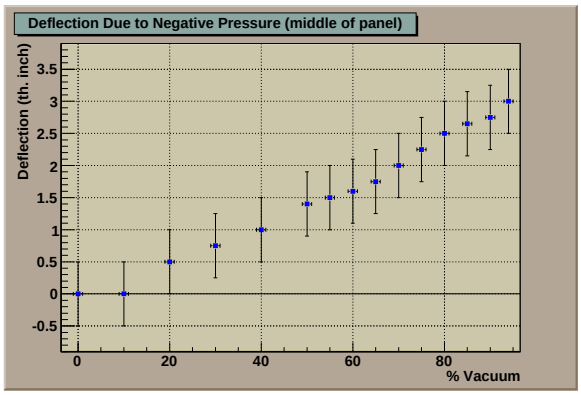

Figure 3.12: Plot showing the deflection of a Matraplast cell as a function of the vacuum pressure exerted inside the panel. The maximum deflection measured is 0.003 inch at a pressure of 90% of vacuum.

to use to counter-balance the weight of water (∼0.3 atm.).

Prototype E as well as the subsequent ones will probably consist of improvements on what has been presented here. For instance, the next prototype may be made out of polycarbonate rather than polypropylene. The mould could also use some improvement because the current design still leaves a small rim of epoxy all around the panel. This has no particular use for the strength of the seal or for any other purpose. The filling method could also use some improvement: rather than having someone slowly pouring water inside the panel, it would be simpler and more efficient to link a tube from the sink to the bottom of the panel and fill it from there.

3.6 Active Sealing

Let's now consider the case of the active water-rich detector. Such a configuration puts further constraints on the seal design. Obviously, the seal still has to be perfectly leakproof, but it must also be perforated in order for the fibers to pass through for readout purposes. Furthermore, although the fiber's cladding is QSA resistant, the core is not and the end of the fiber must in no circumstances get in contact with the scintillator. It would be also interesting to develop a design that would make easy the replacement

of the fibers in case one gets damaged. With these ideas in mind, a small prototype has been built for the active water configuration.

The thermal weld technique has been used with a modified version of the endcap previously described (see figure 3.13 for a cut view of the active endcap and figure 3.14 for the actual prototype). In this version, small holes in the endcap let through the wavelength shifting fibers and larger holes that don't go all the way through are also drilled from the outside to partially insert rubber plugs. This rubber, the Dow Corning 28004-V BLU

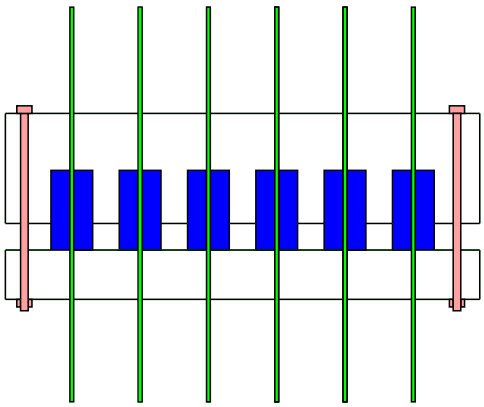

Figure 3.13: Schematic view of the inside of an active seal. The wavelength shifting fibers are hold in place by blue fluorosilicone rubber. The seal is made of two individual pieces bolted together, squeezing the rubber plugs onto the fiber and ensuring a leakproof seal.

fluorosilicone, comes as a blue powder mix and may be molded into any kind of shape depending the purpose it is used for. Here, it is molded into small cylinders which are then pierced through their central axis with a needle for the fiber to pass through. These small blue fluorosilicone rubber plugs are then partially inserted in the "recessed sockets" described above. They are slightly larger than the holes themselves and they consequently squeeze the fiber into place as well as seal the liquid coming out of the fiber's hole. To add some pressure to the rubber plugs, and in order to complete the sealing, a small piece of polypropylene is bolted to the main frame. The rubber itself moreover seems to remain quite inert to the contact with the scintillator mixture; this is a good feature as the material is to be used in an active FGD. The protoype displayed on figure 3.14 did not show any sign

of leakage through the fibers holes and it seems the rubber plugs serve their purpose. On the other hand, only one active prototype has been built like this and it turned out to be one of the few that could not be perfectly sealed at the joint between the endcap and the extruded panel using the thermal press. As one of the corners leaked and could not be fixed via the melting method, a layer of epoxy has been applied around the thermal seal to fix the problem. The point here was to see if the blue rubber plugs could offer a leakproof environment rather than showing the viability of the thermal weld method.

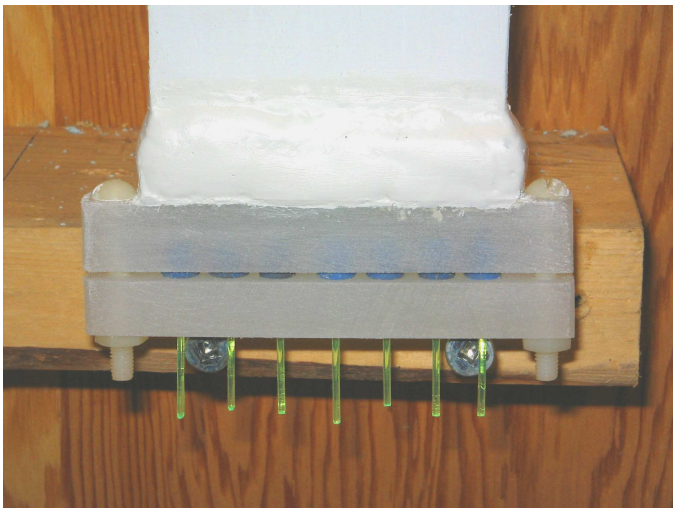

Figure 3.14: Active water seal prototype for a 7-cell wide panel.

The T2K collaboration is under a very tight schedule and although an active water-rich FGD is preferable for the detection of recoil protons, it may not be possible to build a complete and viable prototype before the project starts. Consequently, it may be preferable to see the active configuration as an upgrade that may become possible over the years, simply replacing the pure water with active modules within the FGD.

Chapter 4

Light Yield

This chapter closely looks at the light yield aspect of an active water-based detector as well as a plastic scintillator detector: that is, how much light is actually being detected from the original interactions on the target mass. In this process, the incoming charged particles deposit energy that is absorbed by the scintillator, which then reemits the same energy by fluorescence of blue photons. These photons will travel through the channel, bouncing off the reflective walls numerous times on average before hitting the fiber or getting absorbed (lost) by the environment, either liquid or solid. Once a photon hits the fiber and gets absorbed, it is re-emitted at a longer wavelength (green), and about 10% of this light remains trapped by internal reflection within the fiber which then acts as a wave-guide to the PMT. The name "wavelength shifting fiber" (WLS) comes from the fact that the fiber re-emits the light it absorbs at a different wavelength. To give a simple order of magnitude, for light yield to be adequate, one requires a minimum of $\sim$5 photoelectrons per minimum ionizing particle reaching the PMT; this light yield strongly depends on the properties of the materials used.

The MINOS collaboration at Fermilab, also studying neutrino oscillation using a man made neutrino beam, has looked at the possibility of building a liquid scintillator detector quite similar to the one designed by T2K, but with no water. In 2001, they published a paper giving great details of their design as well as presenting an analytical formula for the probability P of a given blue photon to hit a WLS fiber of diameter d located within a square cell of width w and having an average wall reflectance R: [21]

$$P = \frac{1}{1 + Aw/d} \tag{4.1}$$

In this expression, A is the surface absorptivity and corresponds to $1 - R$ (assuming the transmittance through the opaque wall is negligible). This equation allows one to see what elements have direct or indirect impacts on the light yield. For the plastic FGD, the light yield strongly depends upon the scintillator choice and shape as well as the fiber's diameter. For the liq-

uid scintillator, however, it might be more complex as the light yield depends on the scintillator cocktail chosen, on the reflectance of the water-bearing container as well as on the dimension of the fiber, its position throughout the channel and the shape of the cell. Furthermore, it is important for the light yield not to degrade too much over time, and *Chapter 5* addresses this question, taking a look at the aging of the materials.

Another way one may be able to observe more light from an event, without really changing any light yield variable, would be to simply consider double-ended rather than single-ended readout. Up to this point, physics studies for T2K have shown that the absolute light yield for the water scintillator detector remains too low to even consider using single-ended readout. The choice, however, is not so simple for the plastic FGD. Although double-ended readout would improve the uniformity of the light output, it may not systematically improve the physics performance of the detectors. [22] Double-ended readout would also greatly complicate the mechanical design due to thermal expansion and the fact that if the coefficients of all the different pieces are not matched, the pressure exerted on a fiber fixed at both ends may cause damage. For this reason and the obvious fact that heavy costs would be spared, the collaboration is leaning towards choosing single-ended readout for the plastic FGD.

4.1 Water-Soluble Scintillator Mixtures

Although the construction of a fully active water-rich FGD may not be the immediate objective of the T2K collaboration, it certainly is its ultimate goal and a great deal of research and development has been done in this area. The liquid scintillator that was chosen early in the design phase is manufactured by Zinsser Analytic and is called "QuickSafe A" (QSA). This commercial scintillator is based on the active element di-isopropylnaphthalene and is described by the manufacturer as being an economical and safe scintillator optimized for aqueous samples. More specifically, it is characterized by the following:

- Flash point[†] >150°C
- Environmentally friendly and biodegradable

[†]The flash point of a liquid is the lowest temperature at which it can form an ignitable mixture with air (see Wikipedia.org).

- Safe, no hazardous component
- Odourless, emitting no dangerous fumes
- Costs $50 per litre

Moreover, the product is highly tolerant of water and has a light yield 80% that of the plastic scintillator when undiluted. On the other hand, QSA remains a reactive chemical and as mentioned before, it causes mechanical damage to some materials while leaving others seemingly intact. For instance, it strongly attacks PVC and polystyrene but does not touch Teflon or polyethylene. Another interesting property of QSA is the fact that it can be made into a gel with the use of an appropriate gelling agent. The collaboration spent a significant amount of time and effort trying to take advantage of this property, and such a gel could be part of an interesting solution to eliminate any leak as well as to slow down the aging process. Many gelling agents used in agriculture and food industry have been tried and mixed with water and QSA, but unfortunately only a very few formed clear gels. Adding 0.6 % of carbopol EZ-3 polymer neutralized with NaOH did form a clear gel having the viscosity of hair gel. However, under full pressure – which we define as being 1/3 atm. – such a substance would still leak through a 1-mm hole. Ultimately, because the QSA itself shows signs of degradation, a liquid mixture that could be recirculated is believed to be best for the detector in order to avoid any significant decrease in light yield over time. Due to these difficulties and the problems one would encounter trying to pump a high viscosity substance into the detector, the gel idea was abandoned.

Efforts have also been put into developing the liquid mixture to be used in order to get a compromise between the light output – directly proportional to the amount of QSA – and the proportion of water, our primary target. The current favoured cocktail consists of 70% water, 25% Quicksafe A and 5% Triton-X 100. Triton-X is a surfactant used to lower the interfacial tension between QSA and water, consequently making the solution homogeneous. One of the most salient feature of the solution is the fact that it turns cloudy for temperatures that reach or exceed the cloud point $> 29^{o}$C. This is due to the very nature of the surfactant that starts creating molecular agglomerates when some temperature is reached, thus becoming cloudy. Although the ambient temperature within the detector will be carefully monitored and should not exceed 25^{o}C, one may argue that the current cloud point is dangerously low. Adding or substituting a variety of surfactants may raise

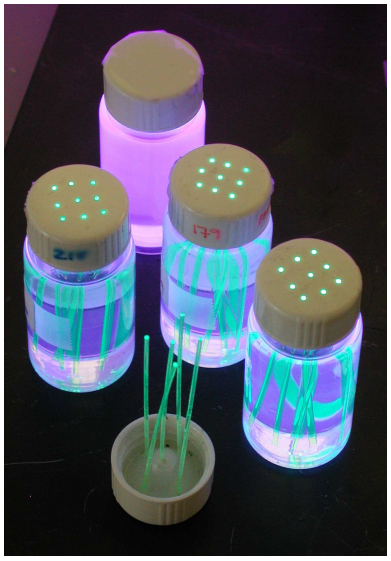

Figure 4.1: Vials filled with the scintillator cocktail under ultraviolet light. Wavelength shifting fibers also are submerged in the solution.

the cloud point to a more acceptable value. For instance, adding 10% by volume of Tergitol NP-13 raises the cloud point to 37°C, but dilutes quite drastically the water fraction down to 64%. On the other hand, adding 1.05% by volume of Tergitol NP-15 raises the cloud point to 35°C without greatly changing the water fraction, but lowers the light yield by about 10%. The question remains to find an appropriate mixture that will maximize the cloud point temperature while not greatly affecting the water fraction as well as the light yield itself.

4.2 Painting the Inside Walls of the Detector

As has been mentioned before, the light yield directly depends upon the reflectance of the inside walls of the extrusion. It may be possible to ask the extrusion company to increase the amount of TiO_2 to the plastic mixture to increase its total reflectance[†], however, this may not be extremely effective nor cheap. Another suggestion has been to coat the interior of each cell with

[†]TiO_2 is already present in the plastic mixture: it is the component that gives the white color to the plastic as well as its reflective property.

a highly reflective paint. Such a process could increase the reflectance of the walls, but also create a protective barrier for the plastic against the liquid scintillator. On the other hand, such a painting process would be extremely tedious and quite expensive as nearly 6000 individual cells would have to be painted. We therefore have to determine if it is better to coat the inner walls with paint, trying to completely eliminate the aging process, or if we should just replace the detector after a year or so of operation or when signs of aging become important. If the painting method is pursued further, one also has to find an effective way of painting these cells.

Eljen Technology is a company that produces solid as well as liquid scintillators and paint. Eljen-520, a reflective paint made of a two-part polyurethane base and designed specifically for liquid scintillator cells, has been used in an attempt to paint the inside of individual 1×1 cm^2 cells. The spectral response of the paint's absolute reflectance remains quite constant above 425 nm at a value of $\sim$92%. Under 425 nm, however, the reflectance starts dropping linearly and ends up $\sim$60% at 375 nm. [23] According to the company's website, the paint should primarily be used for metal cells bearing the liquid scintillator, rather than plastic. This is due to the strong solvents composing the paint that may attack the plastic surface. This paint has however been tried on the polypropylene surface and as it turned out, no significant negative effect has been observed. On the other hand, it has been discovered that wavelength shifting fibers get completely destroyed after being put near the fumes emitted by the curing paint. Fully cured paint however seems to remain totally harmless to the fibers from what is visible to the naked eye. The main problem we had to face for the whole painting story has been to make the paint stick to the plastic surface. For this matter, different types of plastic primers have been investigated: Krylon, Rust-Oleum and Dr. A. Schoch. The first two are cheap commercial primers one may buy in every hardware store while the third one has been imported from Switzerland and is supposedly designed to adhere to polypropylene without any surface preparation. All three were quite different to handle and showed different properties when put in contact with QSA. For instance, Dr. A. Schoch primer was completely intolerant of QSA (the next chapter will closely address this problem) while the other two remained unchanged. Krylon and Rust-Oleum however had their share of problems: although they would stick quite well to the paint itself, one could easily peel them off the plastic surface without effort. For this reason, it turned out being preferable not to use any primer at all prior to applying the paint.

Another difficulty arising from painting the inside of the detector is the need for the paint to be applied uniformly all over the walls of the cell; three layers of paint are necessary to optimize the reflectance according to the Eljen website. Firstly, we have tried to simply pour paint inside a cell, letting it run back and forth from the extremities and draining the excess. This method turned out not to work properly, as the paint would stick mostly in the four corners due to surface tension, therefore not forming a uniform layer over the surface. The next technique we have tried was to attach a small 1-cm^2 sponge imbibed with paint to a wire and run it through the cell. This method turned out to work a little bit better than the first one. However, because three layers of paint are needed, it so happens that running a sponge through a painted cell badly scrapes the previous applied layer. Needless to say this method too needed improvements. The best technique yet developed consists of using an airbrush with a long nozzle having a small diameter in order for it to fit within a cell and covering its whole length. [24] A custum-built airbrush has been built for our purpose: as compressed air moves through a venturi, suction pulls paint from the interconnected reservoir and the high velocity of the air atomizes the paint into fine particles. This results in a very thin and uniform layer of paint being applied on all the inner surfaces of the cell. Needless to say this process is a very tedious one that would have to be repeated for every single cell of a full-sized panel.

Moreover, roughening the surface prior to the coating process seems to increase the binding of the paint to the walls. This is simply done by running a squared-profile rod coated with sand paper (# 180) back and forth along the Matraplast cell. Many cells have been painted following this procedure. They have been opened up and although no quantitative analysis has been done to measure how strongly the paint binds to the surface, one can see it holds quite strongly. Also, to see how uniformly the paint is applied onto the surface – because it is not absolutely obvious considering the Matraplast is also white – we have tried coating the surface with a black primer before applying the paint. The result is conclusive and every layer of paint is applied very uniformly, all over the surface. Finally, it remains yet to be discussed what is the effect of QSA on the paint. According to the Eljen-520 website, the paint should not develop a yellow cast as it ages, however, it is not clear what would be the consequences of soaking painted plastic samples in the scintillator on the liquid itself. This is an important issue that will be discussed in *Chapter 5*.

4.3 Beam Tests

Unequivocally, the best way to study light yield in a quantitative manner consists of performing beam tests where accelerated particles are incident onto the scintillator sample under study (see figure 4.2). Ionizing particles passing through the scintillator create light which gets collected by the fiber and is then seen by the light collecting device located at the end of the sample. This is definitely the best test one can do to simulate the real activity of the detector. Beam tests have therefore been performed using the M11 beam channel at TRIUMF. When the channel magnets are set for a momentum of 400 MeV/c, the emerging beam consists almost exclusively of protons. To acquire significant data from these tests, part of the problem consists of being able to trigger the counter exclusively on meaningful events, that is, on protons from the beam having the desired energy and going through the scintillator bar.

To implement this and because the width of the beam is much larger than the size of the sample itself, two plastic trigger scintillators are used. The first one is placed right at the output of the beam and before the sample under study; the second trigger is placed 4.4 m downstream. The three components are therefore in perfect alignment with the beam and the only particles recorded are the ones producing light in both the front and the rear triggers. This procedure is used to significantly reduce noise in the observed signal and it also allows one to trigger on particles having a specific momentum. This momentum may be deduced looking at the time of flight, the elapsed time between when a particle is detected in the front and when it is detected in the rear trigger. Let's note that all recorded particles did not necessarily pass through the sample under study and as we will see, this results in a large pedestal in the histogram of the number of events as a function of the energy deposited in the sample. By measuring the energy deposited in the rear scintillator and plotting it as a function of the time of flight, one can get information on the type of interactions that occur in the triggers – that is, to know if the protons go right through both scintillators or if they are slow enough to be completely stopped by the material encountered, depositing their total energy. The energy deposited by an ionizing particle passing through the scintillator may be expressed as the following for non-relativistic particles or slow protons in our case:

$$\Delta E = \frac{dE}{dX}\Delta X \qquad \text{with} \qquad \frac{dE}{dX} \sim \frac{1}{v^2} \tag{4.2}$$

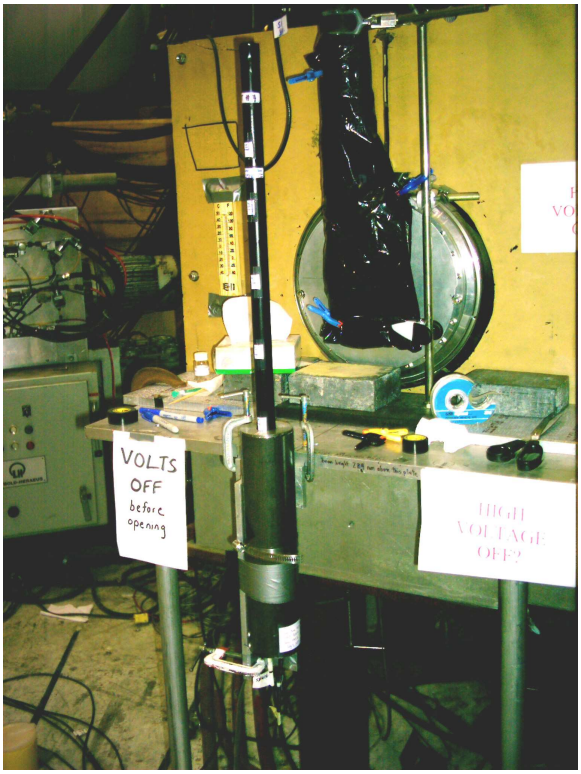

Figure 4.2: View of the M11 beam channel output at TRIUMF as well as the first trigger (wraped in a black plastic bag) and the sample currently under study (black elongated cylinder).

where v is the velocity of the incoming particle and X, its penetration depth. For particles energetic enough to pass right through the scintillator, it is obvious that the faster they go, the less energy they deposit as ΔX remains fixed. The locus observed when plotting ΔE as a function of the time of flight consequently is relatively linear with a positive slope. Slower particles, on the other hand, may be completely stopped by the rear scintillator detector, therefore losing a maximum of energy. The energy deposited by these particles will mostly depend upon the total distance they have travelled within the scintillator slab and a typical plot of the energy as a function of the time of flight will show protons with lower pulse heights for slower particles $\sim$300 MeV/c as one may see from figure 4.3. Furthermore, software cuts are used to simply trigger on events located within a desired range

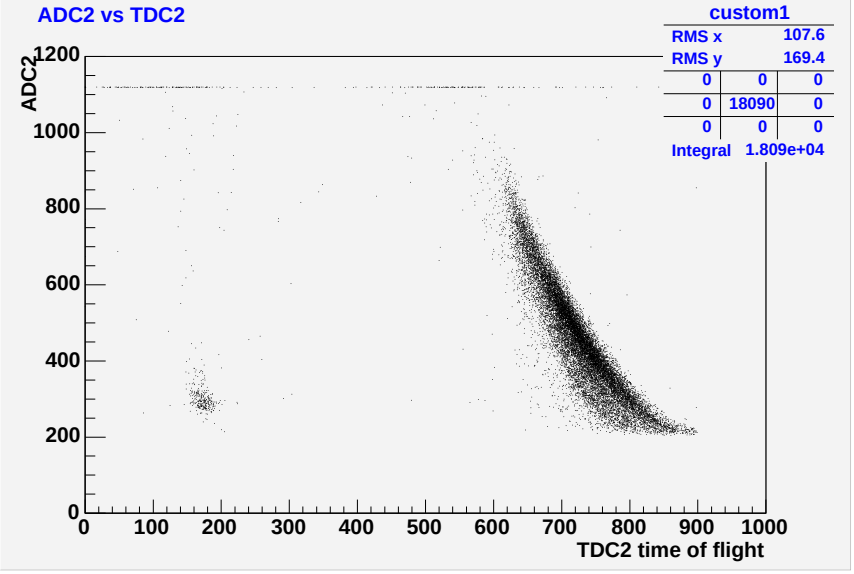

Figure 4.3: Scatterplot showing the energy deposited in the rear trigger scintillator as a function of the time of flight for ∼300-MeV/c protons. The locus is consistent with particles stopping within the scintillator, depositing their total energy. Events located around the 175 TDC2 channel may possibly be associated with electrons contaminating the beam, which would be consistent with a smaller time of flight. The X and Y axes are respectively a measure of the time of flight and the energy deposited – however, the numbers shown represent channels rather than explicit values of time and energy.

of energy and time of flight (TOF) channels. The beam tests that have been performed at TRIUMF over the last fall may be divided in two main categories: attenuation length measurements and long term stability tests.

4.3.1 Attenuation Length Measurements

The first series of tests consisted of measuring the attenuation lengths and relative light yields of Kuraray Y-11 wavelength shifting fibers of different diameters. [25] Measuring the attenuation of a fiber corresponds to quantifying the loss of light observed at a specific point along the fiber as the light-producing event gets further away from this point. More specifically, the attenuation length is the length at which the initial intensity (I) has

dropped to I/e. It is directly related to the light yield of the system and it is important to be able to understand it quantitatively.

These measurements have been done up to this point using only solid bars rather than liquid scintillator for convenience. The first attenuation length measurements used a sctintillator plank originally extruded for the KOPIO experiment as T2K had not done an extrusion run yet. The KOPIO bars are somewhat different from what T2K will be using. The bars have a 0.8 cm $\times$ 7 cm rectangular profile and have holes of 1.4 mm diameter extruded 1.06 cm apart along the length of the bar. The three holes in the center of the bar were respectively threaded, from top to bottom, with a 1-mm fiber, some black O-ring material and a 1.5-mm fiber. The plank was about 2.5 m long and the total length of the fibers was 255.5 cm. They were read out at one end by a Russian silicon photomultiplier and at the other end stood a simple photomultiplier tube. Rotatable masks located right between the end of the fibers and the PMT allowed one to choose which fiber was being analysed. The plank was also wrapped in white Tyvek, an extremely reflective material, in order to minimize light loss at the edges. The M11 beam channel was tuned to a momentum of 300 MeV/c, which is quite slow for protons, therefore implying that the majority of particles will deposit a maximum of energy in the rear trigger. At this point, software cuts were used to trigger simply on the most densely populated part of the proton locus, namely, 680 $<$ TOF $<$ 780 and 300 $<$ ADC2 $<$ 600 (see figure 4.3). Consequently, no event outside of these boundaries have been considered for further analysis. Data points necessary to estimate the attenuation length were obtained by moving the plank normal to the beam, taking measurements every $\sim$20 cm along its length; the procedure has been repeated for both the 1-mm and the 1.5-mm fiber. The light yield for both fibers (number of photoelectrons) as a function of the distance between the beam and the position of the PMT have been plotted and analysed. The curves for both fibers are not quite smooth as one may see from figure 4.4 and we suspect it is due to the marginal nature of the range of the particles. The fact that 300-MeV/c protons are not energetic enough to pass through the rear trigger implies that different particles may have very different penetration depths within the scintillator, therefore depositing a different amount of energy. This could possibly explain the non-uniformity of the results. Undoubtedly, a better measurement is needed.

The second setup used for beam tests was quite similar to the one previously described, but the KOPIO plank was replaced by samples of the first

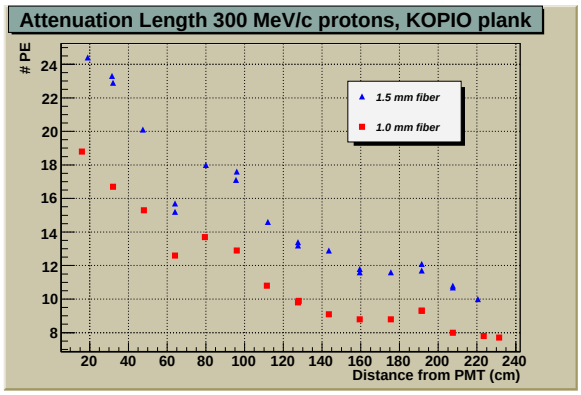

Figure 4.4: Light yield as a function of the distance between the beam and the PMT for both a 1.0-mm and a 1.5-mm fiber inserted in a KOPIO scintillator plank. Results are difficult to interpret and further measurements are needed.

T2K co-extrusion CELCO run performed on November 30$^{\text{th}}$, 2005. The bars had a length of 2.5 m and the cross-section had the following dimensions: 0.95 cm (along the beamline) by 1.05 cm (perpendicular to the beamline). Let's recall that the scintillator bars are meant to have a perfectly symmetric cross-section in the final design and obviously, the first run was not quite accurate. The reason is, after each run, the die – the tool determining the exact shape of the extruded bar – is slightly reshaped to improve the cross-section appearance for the subsequent run. Such an iterative process ultimately leads to the final acceptable shape within tolerance. Although not perfectly symmetric, the bars from the first run have been used to offer an approximation of the fibers' attenuation lengths. The setup therefore consisted of two scintillator bars placed next to one another and respectively threaded with a 1-mm and a 1.5-mm fiber. As before, a Russian SiPM collected light at one end of the apparatus and a regular PMT did the same at the other end; masks have been used to select the fiber under study. To eliminate problems similar to the ones encountered for the first series of tests, the momentum of the protons coming out of the M11 channel beam has been increased to 400 MeV/c, therefore insuring the particles will pass right through the rear scintillator. Figure 4.5 shows what one should expect from fast protons passing through the rear trigger: a positive slope is observed from the graph of the pulse height as a function of the time of flight. This is consistent with the fact that slow moving particles (large

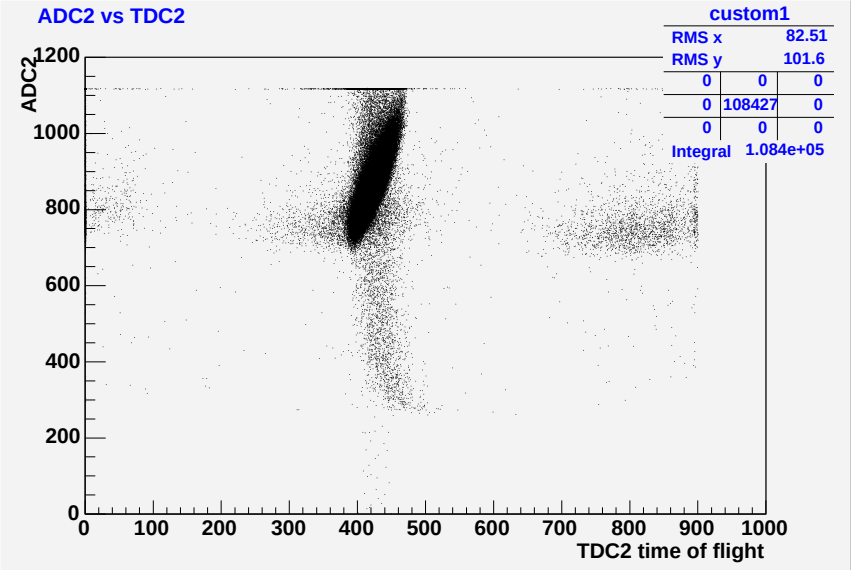

Figure 4.5: Scatterplot showing the energy deposited in the rear scintillator as a function of the time of flight for ∼400-MeV/c protons. The shape of the proton locus is consistent with fully penetrating particles. The *good* protons are selected by mean of a software cut where the counter only triggers on events with $370 < \text{TDC2} < 480$ and $675 < \text{ADC2} < 1075$.

TOF) deposit a larger amount of energy in the detector in opposition to fast particles. A fainter and almost vertical band is also evident at TDC2 = 420 and stretching from $300 < \text{ADC2} < 1100$. This cluster may be explained by particles grazing the rear trigger, not suffering the full energy loss. Finally, the scatterplot also shows accidental coincidence events between particles from different beam bursts occuring every ∼43 ns (430 TDC units) and located at ADC2 ∼800.

Now, because we want to plot the intensity of the light seen by either the SiPM or the PMT as a function of the position of the scintillator in reference to the beam, we have to determine the average number of photoelectrons observed for each position. This is done by plotting a histogram of the light yield as a function of the energy as figure 4.6 shows. What is actually plotted is the number of events as a function of the ADC value when the beam hits the middle of the scintillator bar. The large peak around 50 is called the pedestal and corresponds to particles that hit both the front and the

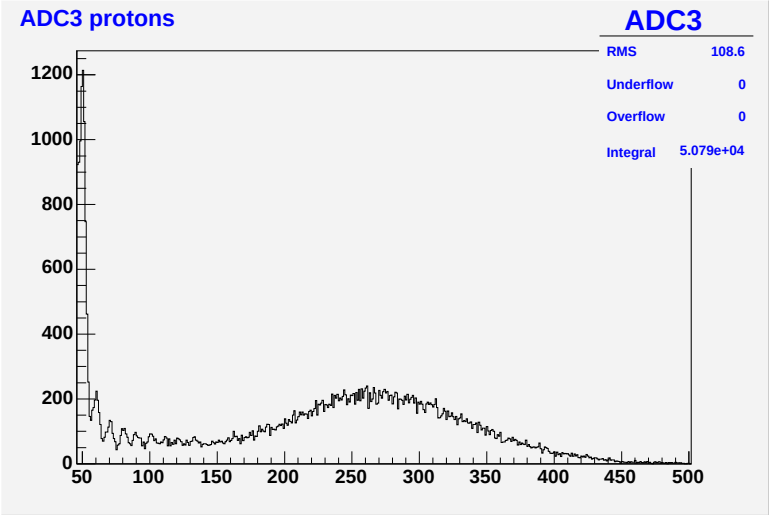

Figure 4.6: Histogram showing the number of events as a function of the ADC value for a 1-mm fiber seen by the SiPM. The pedestal is visible as well as the first 5 photoelectrons peaks. These are useful in order to estimate the number of photoelectrons in the main signal.

rear trigger scintillators without passing through ADC3, the extruded bar itself. The first few photoelectrons peaks are also visible from the graph, the first one being around channel 60. At higher energy, it becomes impossible to distinguish individual peaks as they are all smeared together, resulting in a Gaussian-shaped signal. The first photoelectron peak is particularly important as it may be used to calibrate the light yield of the main proton signal:

$$\#\,\mathrm{PE} = \frac{\text{Mean of main signal} \;-\; \text{Mean of Pedestal}}{\text{Mean of } 1^{\text{st}} \text{ photoelectron peak} \;-\; \text{Mean of Pedestal}} \tag{4.3}$$

Moreover, the continuum observed at ADC counts below 175 is probably the result of particles grazing the bar or simply touching the corners, depositing a smaller amount of energy. Figure 4.7 shows the result of the measurements for 1.0-mm and 1.5-mm fibers read by the PMT as well as the 1-mm fiber read by the SiPM. Results for the 1.5-mm fiber seen by the SiPM are non-reproducible because the SiPM itself has a diameter of 1.0 mm. This causes a major problem because the fiber being larger than the photosensor, the relative position of one versus the other greatly affects the readings. Reproducibility of the results could indeed not be demonstrated by simply taking

out and putting back on the SiPM. They are therefore omitted here. As one

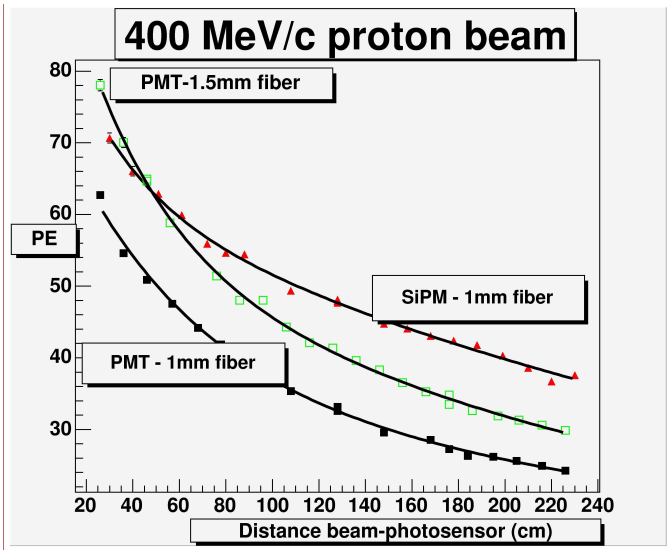

Figure 4.7: Mean photoelectron yield as a function of the position of the beam for different sets of fibers and light collecting devices. The attenuation length may be modeled by a sum of two exponentials, therefore showing a short as well as a long attenuation component.

may see, the plots are best fitted by a sum of two exponentials rather than a single one: $Y = A\ e^{-x/L_1} + B\ e^{-x/L_2}$. Each fiber therefore shows a short as well as a long attenuation length. An explicit calculation that considers the relevant uncertainties on Y leads to the following conclusions: [25] for the 1.0-mm fiber, the short attenuation length has a value of [40 $\pm$ 10] cm while the long one is of the order of [375 $\pm$ 25] cm. For the 1.5-mm fiber, the short attenuation length is [39 $\pm$ 4] cm and the long one is [358 $\pm$ 28] cm. The reason for using a 2-component model is twofold: the reality of the fiber's self-absorption as well as the wavelength dependence of the light collecting device. As it has been previously discussed, once a fiber has absorbed blue light from the scintillator, it reemits a continuous spectrum of light centered at a longer wavelength (green). The lower part of this spectrum however gets rapidly reabsorbed by the fiber and this is the process called self-absorption. Furthermore, the sensitivity of the light collecting device is wavelength dependent: PMTs are more sensitive to low wavelengths while

SiPM are more sensitive to higher wavelengths. The overall effect may be observed from figure 4.7. One may see the light yield for the PMT dropping faster than the one for the SiPM. Due to self-absorption and because PMTs are more sensitive to shorter wavelengths, these are more rapidly attenuated and the total light yield turns out to drop faster than for the SiPM. This is also the reason why the SiPM curve remains higher than the two others at longer distances.

4.3.2 Long Term Stability Tests

The beam tests described up to this point have been done using solid scintillator. Because the main goal was to study the attenuation length of the fiber, the use of solid over liquid scintillator was preferable because solid scintillator produces more light. Other tests, however, have also been performed in order to understand the evolution of the light yield produced by the liquid scintillator as a function of time. Small 50-cm long single cell prototypes have been built for this purpose. Here is the procedure followed:

- A single cell, 50 cm in length, is cut from a Matraplast panel. If the cell is to be painted, this step has to be done at this point; no fiber must be near the fumes of curing paint, else it will be damaged.

- A WLS fiber is then inserted in the cell and threaded through a hole drilled in a plastic cap. A generous excess of fiber is left sticking out of the cap and both are held in place on the cell by clear RTV.

- Once the RTV is fully cured, the Matraplast cell is cut to slide inside an acrylic tube. The cap is held on to the tube only by black vinyl tape, so it is possible to open up and refill the cell if necessary.

- The excess fibre has to be trimmed, sanded and polished to be perfectly flat with the plastic cap.

- The active liquid may then be poured in the cell and the second end may be sealed if desired. In case the second end remains open, the sample will obviously have to be kept vertical throughout all manipulations or otherwise the liquid will leak everywhere inside the acrylic tube.

- The acrylic tube is then wrapped in black vinyl tape in order to exclude ambient light.

- In the beam area, the sample is placed vertically, such that the plastic cap is in contact with the PMT. Mineral oil is used to allow a perfect coupling between the fiber and the face of the PMT. Figure 4.2 shows one of these samples in front of the beam as well as the PMT.

Ten different samples have been studied, each either painted or unpainted, sealed or unsealed and either containing a mixture of 70% water + 25% QSA + 5% Triton-X, or 100% QSA. Only five of the possible combinations have been considered, and two identical samples of each have been built in order to study reproducibility, as identical samples should in theory give the same result. Table 4.1 describes each of these samples. Light yield measurements have been taken at four different times over the year 2005: on July 18^{th}, on August 15^{th}, on October 12^{th} and on November 22^{th}. Table 4.2 presents both the absolute light yield measured for each date (number of photoelectrons: PE), as well as percentage values quoted relative to the light yield of the same sample initially measured on July 18^{th}.

Table 4.1: Samples Built for the Long Term Light Yield Tests.

Sample #	**Cell Type + Liquid**
1	Unpainted 25% QSA, Sealed
2	Unpainted 25% QSA, Sealed
3	Unpainted 100% QSA, Sealed
4	Unpainted 100% QSA, Sealed
5	Painted 25% QSA, Unsealed
6	Painted 25% QSA, Unsealed
7	Painted 100% QSA, Unsealed
8	Painted 100% QSA, Unsealed
9	Unpainted 25% QSA, Unsealed
10	Unpainted 25% QSA, Unsealed

Table 4.2: Long Term Light Yield Tests for the Liquid Scintillator. Samples 7 and 9 have been tested twice on October 12^{th} in order to eliminate possible discrepancies due to the apparently low light yield detected.

Sample #	PE / %	July 18^{th}	Aug. 15^{th}	Oct. 12^{th}	Nov. 22^{nd}
1	PE	8.6	6.5	3.55	3.37
1	%	100%	75%	41%	39%
2	PE	7.62	5.81	4.14	3.75
2	%	100%	76%	54%	49%
3	PE	46.7	38.4	27.3	25.9
3	%	100%	82%	58%	55%
4	PE	25.2	19.7	13.0	12.45
4	%	100%	74%	52%	49%
5	PE	10.7	9.36	9.27	7.45
5	%	100%	87%	87%	70%
6	PE	11.3	10.8	10.0	8.41
6	%	100%	95%	88%	74%
7	PE	58.2	54.7	44.1, 50.7	45.1
7	%	100%	94%	76%, 87%	77%
8	PE	36.3	31.2	23.2	21.7
8	%	100%	86%	64%	60%
9	PE	7.8	5.35	3.52, 3.22	—
9	%	100%	69%	45%, 41%	—
10	PE	9.5	8.1	8.1	7.3
10	%	100%	85%	85%	77%

As one may see, the results show great discrepancies between samples that were supposedly identical. Looking at the values quotes relative to the light yield originally measured on July 18^{th}, one may approximate the uncertainty on the data to be $\sim$8%, which is relatively large. Trying to interpret absolute light yield measurements taken the same day for samples again supposedly identical leads however to an even more radical conclusion as the number of PE observed differs by more than 100% for some samples! (See sample 3 vs 4 or 7 vs 8 for the October and November measurements.) The most likely reason for this non-reproducibility may lie in the appearance of the scintillator cocktail contained in each sample, namely how homogeneous is

it exactly? It is quite possible mold growth or other types of impurities have started to appear inside some of the samples. Obviously, this assumption may not be directly verified because the liquid is contained in opaque black tubes, but mold growth has already been observed in some sitting water/liquid scintillator mixtures. Further beam tests will soon be performed on the samples and once these completed, the tubes will be opened and a look at the solutions will confirm/refute the previous hypotheses.

Furthermore, such an apparent non-reproducibility makes an accurate interpretation of the results very difficult. At this point, it is quite impossible to conclude anything about the effect painting the inside walls actually has on the light yield. Moreover, although 100% QSA samples seem to initially give more light than 25% QSA samples – which certainly makes sense –, the interpretation of what happens over time is disputable. In fact, measurements for samples 7 and 9 were repeated twice. Because the light yield of sample 9 was so low, even on August 15^{th}, it was believed that some kind of contamination occured to the liquid as previously described. In an attempt to solve this, the sample was opened, and the liquid was drained and completely replaced on October 12^{th}. The second value obtained on that date has been taken after the liquid change, but as we see, the light yield did not recover. The measurement for sample 7 was taken twice as well on October 12^{th} simply to eliminate any possible discrepancy.

Further beam tests measurements have to be performed in order to reach any meaningful result and this is the reason why a series of 32 samples have been carefully prepared following the steps described above (see figure 4.8). The goals of this new series of measurements are threefold: to see if painting and sanding the inner surface of the cell increases the light yield, to see the exact effect of using a 70% water mixture rather than pure QSA, and to study the consequences of adding biological inhibitors to the scintillator mixture. The reason for the last element is related to the fact that over the last few months, mold growth has been observed inside some of the samples kept at room temperature. Needless to say such a problem could be quite dramatic if it were to occur within the real detector. The samples built are as follows:

- 4 samples of 100% QSA
- 4 samples of the standard 70% water cocktail
- 4 samples of the standard cocktail + 0.5% Germall-Plus (biological inhibitor)

Figure 4.8: A total of 32 samples have been built for long term tests with liquid scintillator

- 4 samples of the standard cocktail + 0.5% Germall-Plus + 3000 ppm by weight of Zn^{++} (the ions come in the form of zinc acetate).

There are unpainted as well as painted versions of all of these samples, for a total of 32. To date, only a single measurement has been taken for all of these samples, so it is not quite possible to get any interesting results yet. The T2K collaboration will be taking the second set of measurements over the summer of 2006 and the results will be ready shortly after.

4.4 Simulation Programs

To study the effect on the light yield when some variables are changed, small programs have been written using the C programming language. The variables considered are the position of the fiber within the cell, the shape of the cell itself and the reflectance of the inner walls. Many versions of the program have been written, each upgraded and aiming at different objectives. The program's general idea consists of creating photons within a fictitious cell and estimating the percentage of them that will eventually reach the PMT as a function of the distance between the initial photon creation position and the PMT position.

More specifically, the program follows these steps:

a) Firstly, it creates a photon within a cell at a known position, but with a random direction. In the original program, the cell is set up to have a square 1-cm^2 cross-section. The probability for a photon to be emitted in a specific direction is isotropic and normalized in spherical coordinates. For this purpose, the simple random generator from the *math.h* library is being used. This simple method for generating random numbers may not be suitable if a great number of photons are created, but seems appropriate for our purpose. When created, each photon is given a weight of 1.0. This weight is reduced anytime the photon encounters an absorbing medium, such as a wall or the fiber.

b) Secondly, the program calculates the minimum distance between the photon path and the center of the fiber. If this distance is smaller than the radius of the fiber itself, it is assumed the photon gets absorbed and transmitted to the PMT with some given attenuation; the weight of the photon therefore goes as $\sim e^{-x/\tau}$ for some fixed attenuation length (τ) explicitly included in the program. This step corresponds to the simple geometric exercise of finding the minimum distance between two lines in a 3D space.

c) Thirdly, if the initial photon does not get absorbed by the fiber, it will therefore get reflected off a wall. The exact position where the photon hits the wall is found from the intersection between its direction vector and the wall plane it hits. From this intersection point, a new completely random direction (isotropic over an hemisphere) is assigned to the photon, and the process repeats itself until the photon finally hits the fiber. For every wall the photon hits, its weight is multiplied by a factor of 0.9, implying a 90% wall reflectance. This part of the program models the plastic surface as being isotropically reflective into 2π (Lambertian surface). This type of simulation may be somewhat different from what is usually done: in GEANT, for instance, individual photons either reach or don't reach the light collecting device and the light yield is deduced from this. In my case, however, every photon reaches the PMT, but with different weights, depending the path it followed. One may see this *weight* as some sort of light intensity that goes down on the path to the PMT. It is however important to understand that, technically speaking, it does not make physical sense to speak about the intensity of individual photons.

d) The previous steps are then repeated for many photons, always keeping the same starting position. Adding up the final weights when each photon reaches the PMT and dividing the result by the number of times the procedure has been repeated gives a good approximation of the probability for a photon to reach the PMT when initially created at a specific position. For the approximation to be valid, statistics must be adequate and repeating the procedure ∼1000 times seems to give results that are consistent.

The first thing studied with this program was the effect of the cell geometry on the total effective attenuation length of the fiber. The fiber intrinsic attenuation length (τ value) has been set to 200 cm and the idea was to check if the effective attenuation length observed was any different from this value: that is, does the square geometry of the cell has any impact on the effective attenuation length as might be caused if photons bounce a long distance along the cell's length? Results are shown on figure 4.9. For each

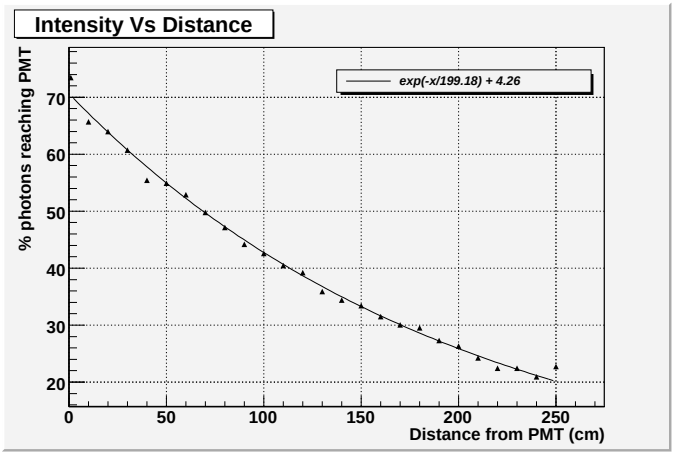

Figure 4.9: Plot of the percentage of photons reaching the PMT as a function of the position of the initial photon created. The closer to the PMT a photon is created, the larger is the probability it will reach it, and the larger the intensity of the light seen by the observer is. An exponential fits the curve, showing an effective attenuation length essentially identical to the theoretical one assumed in the program. This implies the geometry of the cell does not have an important impact on the effective attenuation length of the fiber.

data point, a total of 1000 photons have been created away from the PMT (at a position given by the x axis value). Adding up the final weights for all of these photons and dividing the value obtained by 1000 gives a good approximation for the probability a photon created at point x will reach the PMT. This is what has been plotted as a function of the position x. An exponential function fits the data with an effective attenuation length very close to 200 cm. Let's add the fact that this is a relative light yield prediction rather than an absolute calculation. In no case am I stating that the percentage of photons reaching the PMT in the actual detector will follow this curve. Light absorption in all mediums has indeed not been considered for this particular analysis and as previously mentioned, only about 10% of the light absorbed by the fiber will reach the photosensor. From this result however, we may conclude the geometry of the cell does not have any significant impact on the effective attenuation length.

In what has been described so far, the initial photons have always been created at a fixed position within the cell, but this is obviously not what would happen physically in any real detector. Instead of having 1000 photons emitted at a fixed position, we might actually see the same amount of photons emitted along some line across the cell, referring to the path the incident ionizing particle followed, exciting the atoms on its way. This more realistic view has been implemented in one version of the simulation, creating n photons uniformly spread over some arbitrary line running through the cell. This is simply a better way to look at the simulation, closer to the physical reality of proton ionization along its path through the detector.

The next test performed consisted in creating photons all over the cell, varying the reflectance of the walls and finding the percentage of the photons hitting the fiber in order to reproduce equation 4.1. The same program as before has been used for this test, however the attenuation length of the fiber had to be brought to infinity not to affect the simulated light yield because what is measured is the probability for the photons to get in the fiber, not to reach the photosensor. Furthermore, to improve the smoothness of the results, photons have been created in a three-dimensional grid pattern spanning the whole cell's volume. A total of 50^3 initial photons have therefore been created within the cell. Results are presented in figure 4.10. Because the percentage of photons getting absorbed by the fiber goes exponentially with the wall reflectance, maximizing this variable is of crucial importance for an active water-rich liquid scintillator; this is why painting the inner walls or adding TiO_2 to the plastic are important possible up-

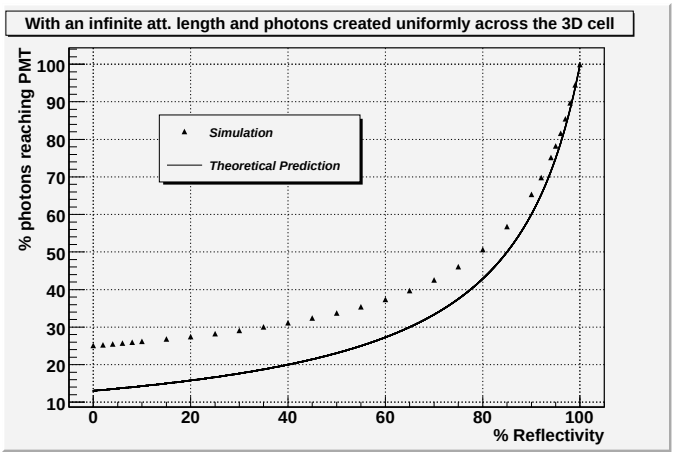

Figure 4.10: Plot of the percentage of photons reaching the PMT as a function of the wall's reflectance. One may see the light yield rapidly increases with the reflectance of the walls. For the purpose of this analysis, the photons have been created in a grid pattern in the middle of the cell's length, 125 cm away from the PMT. An overlay of the predicted model (from equation 4.1) is also shown on the graph.

grades for the detector. The figure also shows what may be predicted from equation 4.1. The overlap between the two curves is obviously not great and at this point, the reason for such a difference is not completely understood. It is possible for a computing mistake from the simulation to be responsible for the divergence of the curves, but let's also consider the following: the MINOS paper [21] is not particularly clear about how exactly the equation is obtained or if any approximations/assumptions have been made. From the rest of the paper, however, in no case is a calculation or simulation made which considers a reflectivity lower than $\sim$94% (for a wavelength $\geq$ 420 nm). In this sense, perhaps the reflectivity is assumed to be of the order of 1 in the equation. The fitting of the data with the theoretical curve is indeed much better for $R \sim 1$ and after all, the MINOS paper does say the equation is an *approximation* to the probability calculation.

Another test performed has been to compare the *light collection efficiency* given by the T2K square cell relative to the rectangular cell from the SciBar detector. This actually measures the probability of photons produced at

a specific distance from the photosensor to also be detected. Let's recall the size of a SciBar cell is 1.3 cm × 2.5 cm. This time, a two-dimensional grid pattern spanning the cell's cross-section has been used to create the original photons (a total of 1000^2) at a given position along the length of the cell. Results are shown on figure 4.11 and we see the use of square cells improves the *light collection efficiency* by a factor of about 1.4. This seems to make sense: for a rectangular-shaped cell, there is a higher probability for photons to get "stuck" in the corners, bouncing off adjacent walls back and forth numerous times. One must however be careful interpreting the results because the *light collection efficiency* is not the same thing as the light yield and it would not be accurate to assume the T2K bars will provide a light yield higher than SciBar. A proton passing through a SciBar cell will create a larger amount of photons on average due to the larger size of the cells. This obviously also affects the light yield.

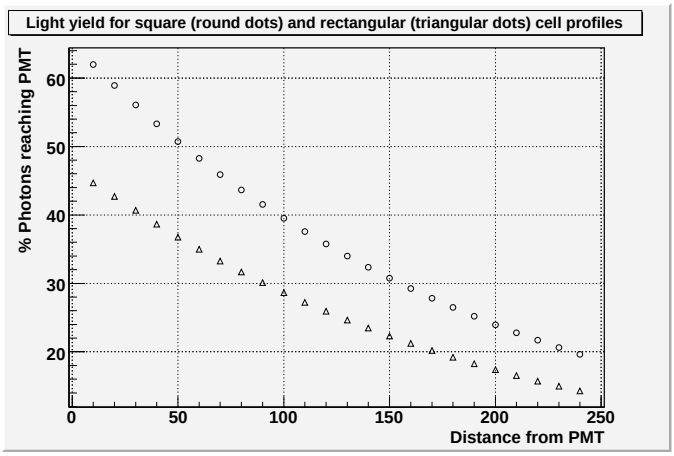

Figure 4.11: We see the total probability for photons to be detected for square cells is larger than what is offered by larger rectangular cells. The light yield is larger by a factor of about 1.4 for the 1 cm × 1 cm cell.

The last test performed has been to study the effect on the light yield as the position of the fiber is moved away from the center of a square cell. Again, the grid pattern of 1000^2 photons has been used for this purpose with the grid positioned in the middle of the cell along its length. The fiber has been moved up/down (Z-axis) and left/right (X-axis) when looking at

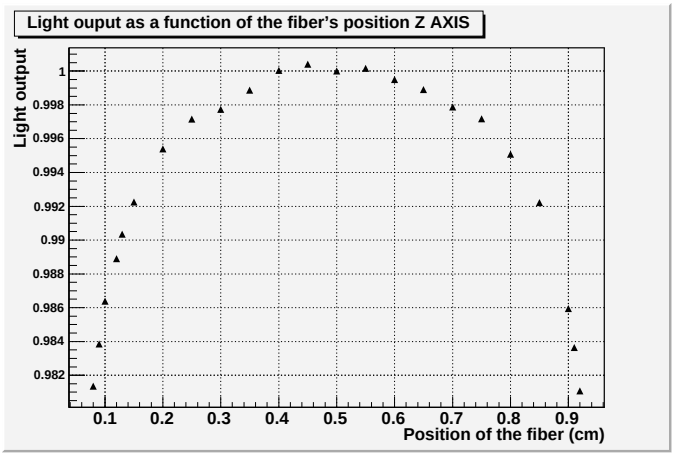

Figure 4.12: Relative light output for a square cell and a fiber off-centered. One may see such an effect remains quite small as the light yield barely drops by 2% when the fiber touches the wall. Here, the position 0.5 cm corresponds to the middle of the cell while 0 and 1 cm correspond to the walls.

the cell cross-section and assuming its length is along the Y-axis. Results shown by figure 4.12 represent the light output when the whole length of the fiber is moved up and down the Z-axis; the graph obtained when moving the fiber along X is very similar to the one presented here due to the obvious symmetry of the geometry. Moving the whole length of the fiber like this does not model well what may happen in a real cell, but could be referred as being a worst-case scenario. The observations are consistent with MINOS paper, agreeing on the fact that the position of the fiber within the cell does not have a great impact on the observed light yield. On may see this from the graph as the light yield only drops by $\sim$2% when the fiber is moved away from the center of the cell, all the way up against the wall.

Chapter 5

Aging Stability Tests

5.1 Quantifying the Aging Process

The aging of all materials we are planning to use for the active water FGD is an important issue that needs understanding. What is the effect of QSA on plastic, on the reflective paint, and on various epoxies and RTVs? Aging of the materials may take different forms such as the yellowing of QSA, the yellowing of the plastic or some other change in appearance for any material soaked in the scintillator. It is possible a water/liquid scintillator cocktail does not remain homogeneous with time and the individual components may separate into layers. To observe these effects, one must therefore prepare samples and let them sit for a long period of time. However, is there any way one can accelerate the aging process and accurately observe these effects on a smaller time scale? What would be the best approach to use for this measurement? This chapter seeks answers to these numerous vital questions.

According to the MINOS collaboration,[21] it seems one might be able to accelerate the aging process by incubating the samples at higher temperature. This comes from assuming that the interaction rate causing the aging process (R_{ag}) is proportional to the exponential of the reaction's activation energy divided by k_BT, with k_B being the Boltzmann constant and T, the absolute temperature.

$$R_{ag} \sim e^{-E_a/k_BT} \tag{5.1}$$

$$ln(R_{ag}) \sim 1/T \tag{5.2}$$

Consequently, the logarithm of the time necessary to produce some effect is inversely proportional to the temperature and one may extrapolate how long it should take at room temperature to observe an effect seen at higher temperature. It is difficult to predict how accurate this assumption actually is and what could the temperature upper limit be for these types of measurements. According to the results obtained by the MINOS collaboration for the accelerated aging of scintillator incubated at high temperature, it is believed 8 months of aging at 50°C corresponds to 10 years at 25°C. [26]

From this statement, one can therefore deduce a simple *rule of thumb* saying that the aging rate doubles for every 6°C increase in temperature. The activation energy may also be calculated and gives $E_a \approx 0.89667$ eV. Such a rule will be somewhat useful to compare the result of tests performed at different temperatures and see if the previous hypotheses actually hold. Let's note however that for such a rule to hold, I am assuming the activation energy is essentially the same for liquid and solid scintillators.

As no further information was available concerning the aging of QSA and its long term effect on various materials, the only way we could approach the problem was to actually try putting QSA in contact with various materials using small samples and bringing these samples to higher temperatures. For our purpose, measurements have been taken at approximately 35°C as well as 50°C using small incubators for the samples. These incubators consisted of styrofoam boxes heated up from the inside by simple light bulbs; a 60-W bulb has been used to bring the temperature up to 50°C and a 40-W one has brought it to 35°C. It was unclear at the beginning, when the project started, if heating up the samples to 50 degrees would give meaningful results or if perhaps at these temperatures we would be simulating a very different type of aging, something that would never happen at room temperature, even after a very long period of time. The analysis of the results presented here will give more details on this matter. Furthermore, because light itself degrades QSA over time, all samples have been kept in the dark within the incubators. This is also the case at room temperature, and all QSA samples have been kept away from any intense light source.

The aspect of material aging that is the most worrisome for the collaboration is related to the yellowing of QSA as plastic or other substances are soaked in it. A scintillator that slowly becomes yellow causes a drop in light yield as it ages and may be dramatic for the detector. The objective here has been to quantify this yellowing or, more specifically, this loss in transmittance for the mixture. The best method for taking these measurements consists of using a spectrophotometer that measures the relative transmittance of the samples for all relevant wavelengths. The spectrophotometer used for this purpose was a *Perkin-Elmer Lambda-3B Spectrophotometer*. It works by comparing the intensity of two beams of light, one passing through a reference sample and the other one passing through the sample to be analysed. By the way it is designed, the machine therefore only takes relative measurements rather than absolute; these types of measurements are perfectly adequate for our purpose because all we want is a measure of the aging of QSA at

high temperature in comparison with pure QSA kept at room temperature. The only apparent problem is the fact that QSA itself does slowly age, even at room temperature and in the dark. Our measurements will be completely insensitive to this factor. A first solution could be to measure the absolute transmittance of QSA, however, this remains particularly difficult. It could also be possible to use a liquid that does not age as a reference, such as water. This has been tried, and as it turns out, the relative transmittance of QSA in reference to water is very small, so no meaningful results may be obtained from this. On the other hand, the relative transmittance has been measured between a year-old sample of QSA (kept at room temperature) and a brand new one. The difference observed was less than a 2% drop in transmittance. Consequently, because the aging of QSA at room temperature is extremely slow, we will consider its effect to be essentially negligible for further analysis.

Furthermore, it seems the kind of vial used for the measurements affects the results. In this sense, two types of vials have been tried: the first one being cylindrical and the second having a square-based prism shape. Transmittance values obtained with the cylindrical vials turned out to create reproducibility issues because the spectrophotometer did not have proper sample holders for such vials. Because the light path crosses two curved surfaces when passing through cylindrical vials, the exact position of both samples is absolutely crucial – this is what could not be accurately reproduced. For square-based prism-shaped vials, the problem disappears as the light does not cross curved surfaces and consequently, only the relative transmittance between the solutions is measured. These vials turned out to give reproducible results and were specifically designed by the manufacturer to be used with the *Lambda 3B Perkin-Elmer* spectrophotometer; all the results presented in this section have been obtained with such vials. The spectrophotometer therefore measures the transmittance of some small 1-cm thick liquid sample for a specific wavelength. The range of wavelengths spanned by the machine is relatively large and covers the ultraviolet as well as the visible. What we want is to measure the transmittance spectrum for each sample as a function of time. This implies a great number of measurements, and the use of a computer program is suitable for such a repetitive process. To remotely control the spectrophotometer, a computer has been hooked to it via a COM port and a small C program has been used to automatically take series of measurements.

Let's now be more specific about how exactly measurements have been taken.

Figure 5.1: Spectrophotometer used for all measurements as well as the integrating sphere that can be added to the configuration. Commands to the spectrophotometer are given via a COM port controlled by the computer.

As described previously, the spectrophotometer works by comparing the intensity of two beams of light, each going through a vial, the one used as a reference and the one we want to study. For pretty much all samples, the reference used has been 100% QSA maintained at room temperature and away from any ambient light. The program measures the relative transmittance (in percent) for every integer wavelength between 400 and 600 nm. Prior to taking a valid series of measurements, however, a calibration must be done:

Firstly, two identical samples of pure 100% QSA are inserted in the spectrophotometer at a wavelength of 450 nm (value quite arbitrary at this point) and *auto-zero* is pressed. This exactly calibrates the machine such that the relative transmittance at this particular wavelength gives 100%. At this point, if one takes a single transmittance measurement at any other wavelength, 100% should be theoretically obtained as the two samples are identical. This is however not quite what is observed and when inspecting the whole range of wavelengths, transmittance may give values oscillating between 90% and 105%. These systematic errors will have to be corrected for

and it is therefore necessary to take a series of measurements spanning the whole range of wavelengths with two identical samples. The values obtained will give the data necessary to correct for every subsequent measurement. This procedure has been called *the zero-correction*. From experience, it seems this must be done every time the machine is turned on.

One may legitimately ask: "What if another wavelength is chosen instead of 450 nm for *auto-zero* to be pressed at? Does anything change in this case? Will the exact same result be obtained in the end?" This has been tested, setting the *auto-zero* at different values from 400 nm to 600 nm. Essentially, the result is the following: the same result is obtained (within very small variations) for wavelengths between 420 nm to 600 nm. Below 420 nm, results diverge greatly. It is known that the absolute transmittance of QSA at these wavelengths is extremely small, all the light getting shifted to longer wavelengths (this is an intrinsic property of QSA). In this case, because the absolute value is so small, the uncertainty becomes comparable to the result itself, making it irrelevant. Therefore, for transmittance measurements, it does not seem to make much sense to consider results below 420 nm. This is the reason why no data points have been plotted below this wavelength (see the numerous plots presented below in the *Transmittance Measurements* section). Another nice feature of the spectrophotometer is the fact that it may be turned into an apparatus designed to measure the reflectance of diffuse surfaces. This may be done with the use of an integrating sphere[†] specifically built for the Lambda-3B spectrophotometer. The integrating sphere (which actually consists more of a hemisphere) has been used to measure the reflectance of Eljen-520 painted surfaces. As we will see, however, numerous difficulties arise when interpreting reflectance results.

5.2 Transmittance Measurements

Let's now try to understand the effect of QSA on various materials, quantifying the transmittance as a function of time. Three-dimensional plots are best used to present the results, showing the transmittance (%), the spectral wavelength and the time elapsed since the material has initially been put in contact with QSA, on three different axes. Although such a visual plot

[†]See Appendix B for the complete procedure to follow in order to hook up and use the integrating sphere appropriately.

gives a good appreciation of what physically happens to the scintillator over time, it may get a little bit heavy to manipulate as the drawing software has to plot 3D data sets getting more and more numerous every time new data is taken. ROOT has been used for such a purpose and although it is a very powerful tool, difficulties arose while plotting some of the results. Incidentally, for the plots not to suffer from a lack of clarity, no error bars or uncertainties have been added to them. They may however be approximated as follows for all 3D plots presented:

- The uncertainty for the *number of days spent in contact with QSA*-axis may be of the order of ± 3. This is due to binning by the ROOT plotting packages.

- The uncertainty for the *wavelength value*-axis depends only on the accuracy of the spectrophotometer and it is believed to be quite small, essentially negligible for our purpose.

- The most important uncertainty is without any doubt the one along the % transmittance-axis. Although the spectrophotometer gives extremely precise transmittance measurements, the uncertainty here is not quite of the same order of magnitude. The overall value obtained strongly depends on the vial used to contain the liquid when the measurements are taken as well as on the liquid itself. Is the vial perfectly clean? Is it scratched? Is the liquid sample perfectly homogeneous? Are there any bubbles mixed in the solution or other various impurities? These elements may have dramatic impacts on the results. To approximate the uncertainty, the best way probably is to compare two identical samples and see, week after week, how different the results are. If we define the transmittance as $[0 \leq T \leq 100]\%$, its uncertainty may be approximated as being of the order of $[T \pm 1]\%$.

A summary of all the results presented in this section is found at the end of the chapter for sake of completeness and clarity.

5.2.1 Aging of Pure QSA

The first results shown here are for the aging of pure QSA: small samples of pure QSA have been put at 35°C as well as at 50°C. Let's recall that all measurements have been taken in reference with pure QSA kept in the dark and at room temperature. Room temperature remains relatively constant, the lab being in the basement, and it has been measured to be $[23 \pm 2]$°C. The first obvious thing one may see from figure 5.2 is the fact that the

aging process is strongly wavelength dependent. Although practically no signs of aging are perceptible around 600 nm, it is quite different below 500 nm where the transmittance dropped by up to ∼8% around 420 nm over a period of 330 days. The data taken on the 110$^{\text{th}}$ day may be a

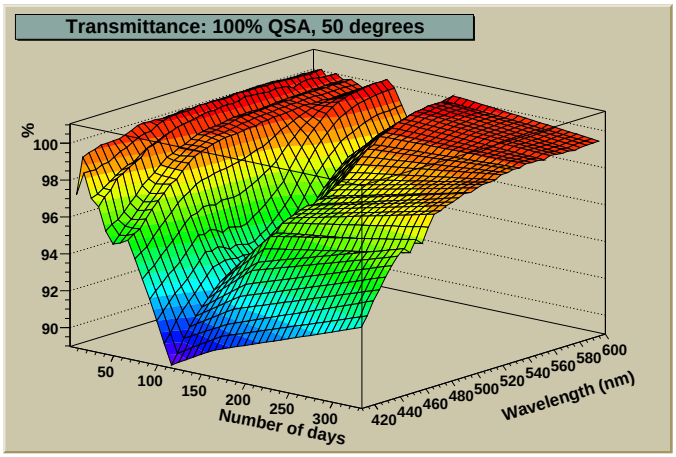

Figure 5.2: Transmittance of pure QSA aged at 50°C relative to pristine QSA as a function of time.

little bit puzzling as it shows lower transmittance than even the last set of measurements. This is most likely due to a systematic error that happened that specific day: either a dirty or a slightly scratched vial could have had been used. It would be hard to believe a transmittance going up and down as a function of time. Although vials were meticulously cleaned before each use, systematic errors could not be completely avoided and this explains why the uncertainty on the transmittance-axis remains relatively large. Figure 5.3 shows the transmittance of pure QSA incubated at 35 and 50 degrees as a function of time, and for a wavelength of 420 nm. Although one may argue that the points taken the same day for the two temperatures are close of being within each other's uncertainty ranges, the sample incubated at 50 degrees continuously shows lower transmittance than the one at 35 degrees. This seems to confirm the hypothesis that higher temperature increases the aging effect. Now, let's see what happens when one adds plastic to the mixture.

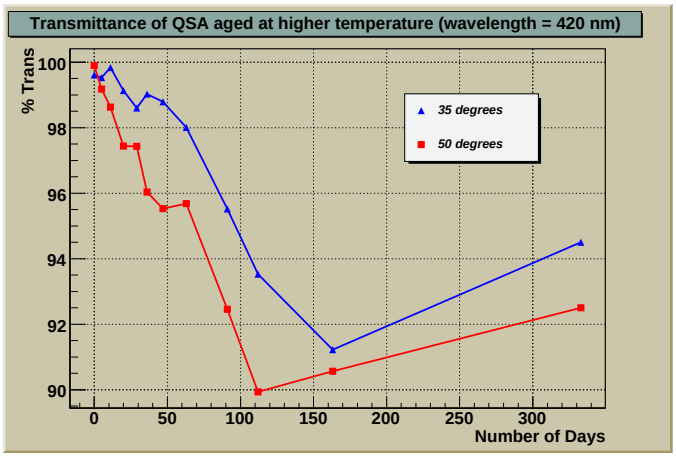

Figure 5.3: Transmittance of pure QSA at 35 and 50°C for a wavelength of 420 nm as a function of time.

5.2.2 Aging of QSA When in Contact With a Small Amount of Plastic

Figure 5.4 shows the transmittance of pure QSA having been in contact with the Matraplast white plastic. More specifically, a small plastic piece having a mass of 4 g was soaked in ∼20 mL of QSA. The material/QSA ratio therefore remains much smaller than what would characterize the real detector. As one may observe, the values obtained at room temperature over the period of 330 days oscillate between 98% and 101%. The results are basically within uncertainties and we may conclude that aging of QSA is negligible when put in contact with small amounts of plastic at room temperature. Things are somewhat different at higher temperatures. At 35 and 50 degrees, an aging effect is obviously observed and it seems plastic in the solution accelerates the aging process (see figure 5.5). When simply looking at the worst-case scenario, that is ∼420 nm, we see that results for incubated samples at 50 degrees with plastic (89% transmittance) are a little bit worse than what is obtained at the same temperature, but without any plastic (92%). Adding plastic therefore seems to aggravate the aging effect, although significant signs of degradation have yet to be observed at room temperature. Another feature of the high temperature plots is the fact that the aging process is not linear with time, but rather seems to plateau

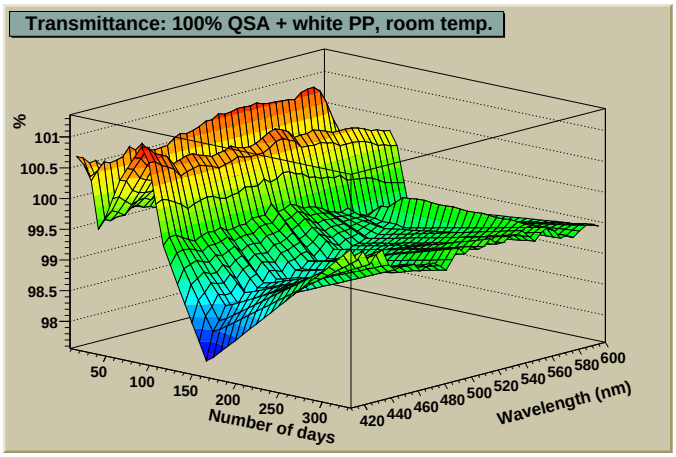

Figure 5.4: Transmittance of pure QSA put in contact with a small amount of white PP. The sample has been kept at room temperature over the time period; only the effect of plastic is therefore measured.

to some definite value of transmittance. This may actually be a good sign for the collaboration: the plastic may be leaching some constituent in the solution, but once this process is over, the transmittance of the scintillator remains relatively constant, even after a long time.

Up to this point, plots have shown the results for white PP in contact with QSA. Another color has also been considered: the natural polypropylene, also manufactured by Matraplast. This natural color looks relatively transparent, perhaps even yellow-ish. The material by itself could not be used for building our detector, but it could perhaps be used after being coated with the Eljen-520 reflective paint previously discussed. Small 4-g samples have also been soaked in the scintillator and the aging has been monitored. At room temperature, as one may see from figure 5.6, no sign of aging is perceptible. This type of graph has been actually quite useful in determining the order magnitude of the uncertainty along the transmittance axis due to its numerous ups and downs which sample the uncertainty itself. When looking at the plot, one may ask why the part between 200 and 330 days is so flat in comparison with the rest. This is simply because initially, measurements were taken at relatively small time intervals, every 2 weeks or so. Later in the process, measurements were not taken as often and more specifically,

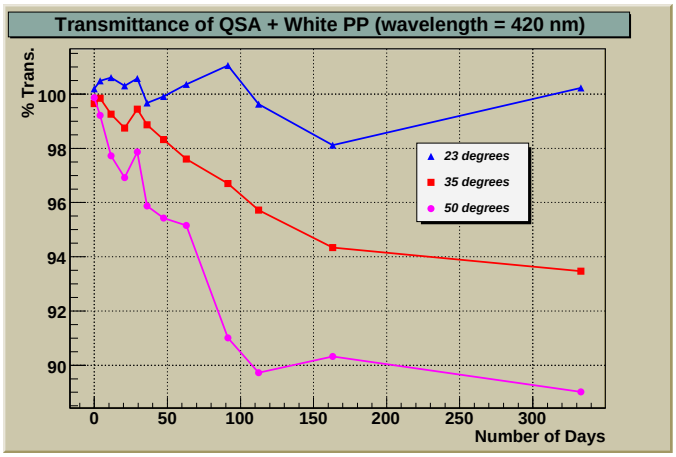

Figure 5.5: Transmittance of QSA when put in contact with white plastic at 3 different temperatures. The results are shown for a wavelength of 420 nm.

the last measurement has been taken a long time after the previous ones. In order to present the results in an appropriate manner, forming a continuous surface joining all data sets, linear approximations had to be done (that is, it has been assumed the scintillator changes linearly with time in between data sets) and this explains the look of the plot. This last comment is valid for all plots presented in this chapter.† Figure 5.7 shows the transmittance of QSA when it is put in contact with natural polypropylene as a function of time for samples kept at three different temperatures. The lower curve on the plot corresponds to a heated sample that has been put in contact with two identical pieces of matraplast (each weighing 4 g). The objective here was simply to get an idea about how important is the plastic/scintillator ratio on the aging. Results are conclusive: just like incubating a sample to a higher temperature, adding more plastic to it increases the rate of aging.

†ROOT does not do a great job plotting data sets that are very far apart in time. The problem is similar to the one described earlier concerning the uncertainty for the *number of days*-axis. In this case, however, the problem is more dramatic and ROOT just won't fit data sets very far apart. A simple solution has been to create "virtual data sets" where needed, linearly approximating the transmittance that would be obtained if a measurement were taken on that specific day. For instance, for the last measurement to appear on the plot, 4 of these virtual data sets had to be used. Such a procedure is perfectly transparent as ROOT itself does linear approximations between "real" data sets.

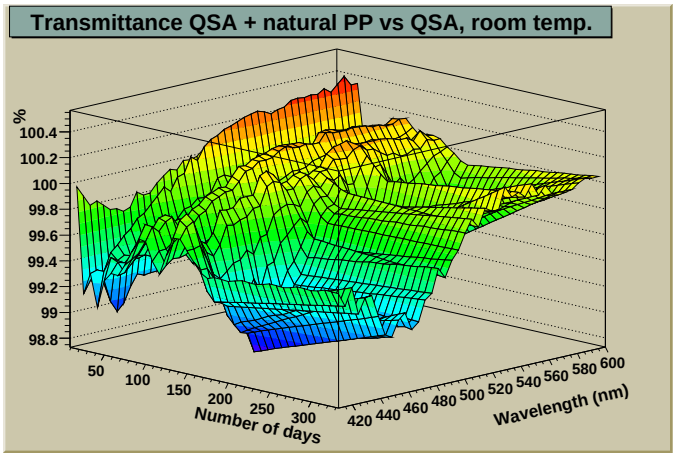

Figure 5.6: Transmittance of pure QSA put in contact with a small amount of natural PP. The sample has been kept at room temperature over the time period.

While pure QSA alone (without plastic) drops to ∼92% in transmittance over 330 days when kept at 50 degrees, the transmittance drops down to 89% when a single piece of plastic is added to the solution and drops to 86% when two pieces are added at the same temperature. It is unclear at this point what would be observed for the plastic/liquid scintillator ratio characterizing the real detector. Further investigation is definitely needed in this area and this is what the next section addresses. Also, these results are for samples having been incubated at 50 degrees and it is still quite unclear how exactly these results can be trusted. In this sense, a problem arises when comparing the actual drop in transmittance at room temperature with what may be predicted from the activation energy equation and the data taken at higher temperature. From figure 5.7, we observe a drop in transmittance of about 10% over the first 110 days at 50 degrees (sample having a single piece of plastic), and on the basis of the "rule of thumb" previously stated, one should have expected a drop of about 2-3% over a period of 330 days at room temperature, something that is not observed. This same drop of 2-3% over 330 days may be predicted from the results taken at 35°C as well, so at least the results extracted from the two incubated samples seem to be consistent with one another even though one may argue they do not agree with what is seen at 23°C. On the other hand, it is possible the reason why

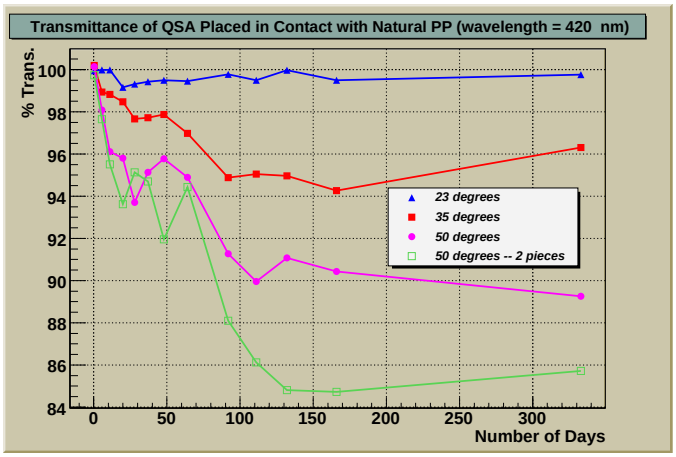

Figure 5.7: Transmittance of QSA when put in contact with natural plastic at 3 different temperatures. The results are shown for a wavelength of 420 nm.

no drop in transmittance has been observed at room temperature lies within the uncertainty of the measurements, considering the predicted drop is of the same order of magnitude as the uncertainty itself.

5.2.3 Increasing the Plastic/Scintillator Ratio

From the previous plots, it seems the amount of plastic versus the volume of scintillator in each sample is quite important to consider. At this point, it is therefore necessary to simulate the real conditions of the detector. For this purpose, an equivalent surface of 48 cm^2 has been put in 12 mL of QSA; what is important here is not quite the plastic mass, but rather its surface area in contact with the chemical. These data sets presented in this section have been taken for samples left at room temperature as well as for samples incubated at 35°C only. It has been argued at this point, looking at all the results previously discussed, that incubating QSA at 50 degrees may just be too extreme and not representative of the reality of aging. The argument is based on the fact that although a higher temperature accelerates the aging process, no significant drop has yet been observed at room temperature, and this, for a period of over 330 days. As previously discussed, we should

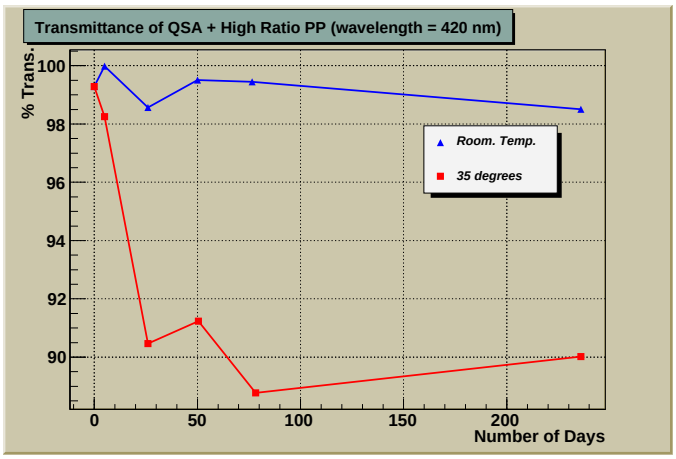

Figure 5.8: Transmittance of pure QSA put in contact with a large amount of white plastic both at room temperature and at 35 degrees; this is to simulate the real plastic/scintillator ratio seen in the real detector. The results are shown for a wavelength of 420 nm.

have seen some decrease in transmittance at room temperature if the high temperature aging simulation were completely true. Also, the plateau value differs at 35°C and 50°C, which prevents extrapolations. One should therefore be careful when interpreting results obtained at 50 degrees; it is not clear if samples kept at 35 degrees give any better results, but the temperature gain is at least not as radical. Figure 5.8 shows the transmittance of a high PP/QSA ratio at 23°C and 35°C. This confirms the hypothesis that the aging effect is proportional to the size of the plastic surface being in direct contact with QSA when the sample is brought to a higher temperature: 90% in transmittance for a large amount of plastic in 220 days versus 94% for a single piece of plastic in QSA at 35°C for 330 days (see figure 5.8 vs figure 5.5). We may also observe the fact that adding more plastic to the solution does not seem to change the behaviour that a plateau is reached after some time and no further degradation is observed afterwards. The value of transmittance at which the plateau is reached also seems to be quite temperature dependent: apparently, the plastic leaches a certain amount of material in the solution over time, but this amount depends upon the temperature the sample has been brought to. This gives yet another argument against the validity of material aging tests at high temperature. This may

moreover be a good sign for the collaboration: perhaps the plateau reached by the solution at room temperature is so close to the initial value that the aging process is essentially negligible. It remains unclear, however, how flat exactly this plateau is and what are the effects over a very long period of time. The question remains whether if the plateau will be flat enough over the time period the active water detector will be in use that further aging can be completely ignored.

5.2.4 Aging of QSA When Put in Contact With Painted Samples of Plastic

As previously discussed, painting the inner walls of a Matraplast panel has been considered and one of the important questions to answer concerns the effect of the paint on QSA. To study the question, samples of white as well as natural plastic have been painted and soaked in 100% QSA. Transmittance of the liquid and the physical appearance of the paint itself have been monitored as a function of time: does the paint crack over time, does it peel off? High temperature aging has also been used for this purpose. When these numerous samples were prepared and when these series of measurements started, it was still quite unclear what was the best method for making sure the paint would stick to the plastic. It was believed at the time that coating the surface with any kind of primer would be better than no primer at all. This turned out not to be true, but there was no such evidence at the time. Three types of primers have therefore been used: Krylon, Rust-Oleum and Dr. A. Schoch. The following results are divided into the type of primer used prior to coating the plastic surface with EJ-520 paint. In theory, a primer should simply affect the adhesion of the paint onto the plastic and the QSA should not get in contact with any of the primers due to the layers of protective paint. This may not be the case however if the paint starts to crack severely over time. The results from the third primer will clearly show the effect a primer may have on QSA.

Krylon Primer

Krylon is a paint formulated to adhere to plastics without a primer, but we have been using it instead as a primer undercoat to the EJ-520. Krylon is relatively cheap and may be found in essentially any hardware store. It comes as a spray and various colors are available; simple white has been used for our purpose. As we may see from figure 5.9, there is still no apparent

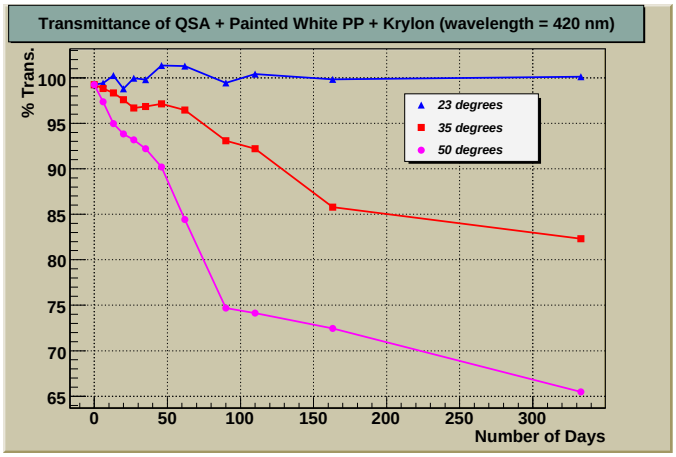

Figure 5.9: Transmittance of QSA when placed in contact with white painted PP coated with Krylon primer. Results are shown at a wavelength of 420 nm for 3 different temperatures.

sign of aging for the QSA at room temperature after having been in contact with the painted plastic. However, it has been noted that the paint itself shows a slight sign of damage. The paint has cracked on one of the sharp edges of the sample, possibly a place where there was only a very thin layer of paint due to surface tension. This is an observation that is common to all painted plastic samples left at room temperature in QSA: the paint shows evidence of cracking around any sharp edge after only a few months of being in contact with the scintillator. This apparent problem, however, may be of negligible importance because only the interior of a cell would be painted in the real detector and such a surface does not show any outside edge. In this sense, the inside corners of a cell are not problematic because once the paint is applied (but not cured), surface tension forces act to redistribute it, thinning the coating layer at outside corners and thickening it in the inside as the free surface (the paint) contracts to minimize surface energy. Natural plastic painted and left at room temperature basically shows the same properties as white plastic. At higher temperature, however, the picture is quite different. The transmittance suffers an important drop compared with unpainted plastic over the same period of time, but it is difficult to compare the two because the paint badly reacted to any high temperature treatment. Figure A.4 presented in Appendix shows the three layers of paint

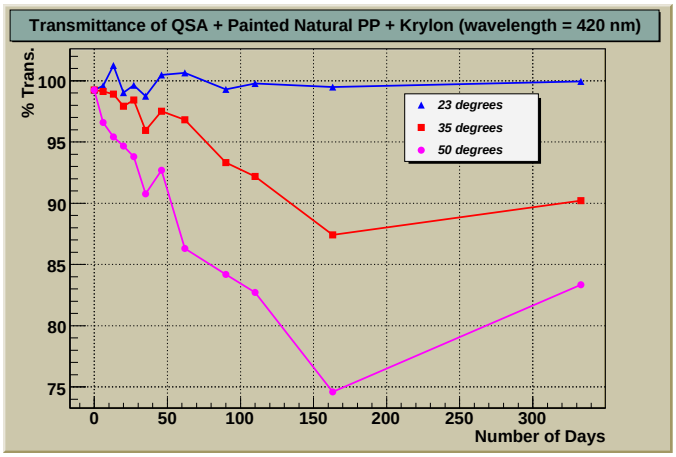

Figure 5.10: Transmittance of QSA when placed in contact with painted natural PP coated with Krylon primer. Results are shown at a wavelength of 420 nm for 3 different temperatures.

completely peeling off the white plastic surface. A similar result is obtained with natural plastic although the drop in transmittance is not quite as bad as it is the case with white PP (90% for natural versus 82% for white plastic at 35°C over 330 days). The cracking of the paint, perhaps due to the activation of various chemicals at high temperature, makes the interpretation of the results very difficult for various reasons. Firstly, the paint has been applied to improve reflectance, but also to protect the plastic against the chemical attack of QSA. Once the paint cracks, it does not protect the plastic anymore and a transmittance measurement quantifies not only the effect of the paint, but also the effect of plastic on QSA. It would therefore be questionable to compare these results with the ones obtained with unpainted plastic samples in order to see if the paint slows down the aging in some way. Furthermore, once the paint cracks, the primer gets in contact with QSA which may certainly affect the results. Looking at figure 5.9 and using our *rule of thumb* for the aging, it is possible to predict that a drop of ∼3% should have been observed at 23°C according to the high temperature results. The difference between the prediction and the actual result leads once again to the questioning of how exactly can one trust the results obtained from incubated samples. Although the results may be arguably non-significant, it is possible to observe the fact that painted natural plastic

gives a larger transmittance than white plastic (see figures 5.9 and 5.10) with a difference of ∼7% at 35°C and >10% at 50°C.

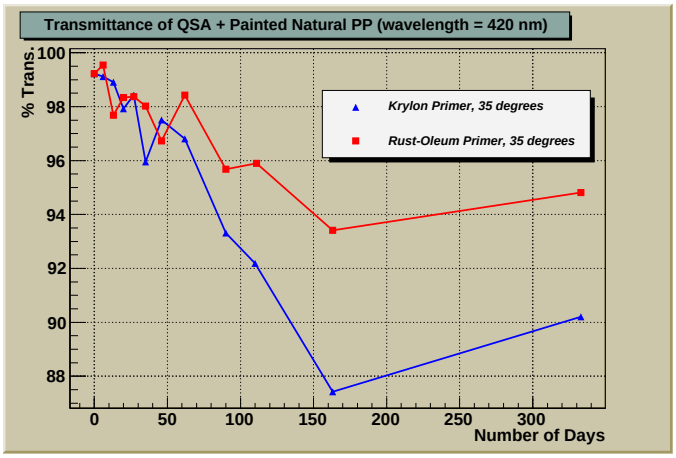

Figure 5.11: Transmittance of QSA when placed in contact with painted natural PP coated with Krylon primer versus Rust-Oleum primer. Results are shown at a wavelength of 420 nm for samples incubated at 35 degrees.

Rust-Oleum Primer

The Rust-Oleum primer is also a relatively cheap primer that may be found in any hardware store and it also comes in a spray can. The results obtained with this primer are very similar to what has been already presented with Krylon. In this sense, no apparent signs of aging have been observed at room temperature although small cracks have appeared over time around sharp edges. At 35°C, the paint has also completely peeled off the surface as it was the case with Krylon. Moreover, when looking at the white versus the natural plastic treated with Rust-Oleum and incubated at higher temperatures, we see that again, natural plastic seems to do better than white (see lines 25 versus 22 and 26 versus 23 in table 5.1). Another thing one may observe is the fact that for the same type of plastic and for samples incubated at the same temperature, Rust-Oleum shows a better transmittance than Krylon (see figure 5.11). The conclusion therefore is: although it may not be correct to interpret too closely results from incubated samples, it seems preferable to use natural rather than white plastic if painting the

inside walls of the detector is serously considered; also, Rust-Oleum would be better than Krylon in case a primer is needed (which seems to be unlikely at this point).

Dr. A. Schoch Primer

This last primer, imported from the UK, turned out to give interesting but puzzling results as we may see from figure 5.12. At room temperature, the

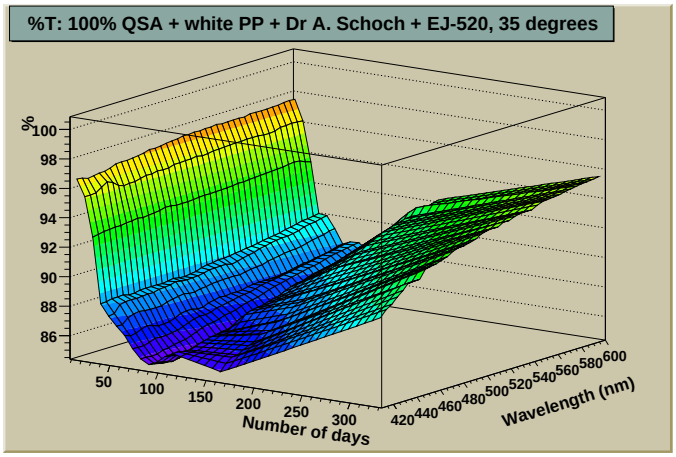

Figure 5.12: Transmittance of pure QSA put in contact with a painted sample of white plastic; Schoch primer has been used prior to applying the paint. The sample has been incubated at 35°C over the time period.

same result as for the other primers is observed, but as soon as samples are incubated, unexpected – and perhaps ridiculous – results are obtained. At 35 degrees, within the first 100 days, the transmittance has uniformly dropped to 84%, but then went up almost linearly for the subsequent 200 days to reach a value well above the 90% for all wavelengths! The effect is even more pronounced for samples that have been incubated at 50 degrees. In this case, the transmittance dropped down to 70% in less than 50 days and went back up over 90%. These two specific examples are not rare exceptions caused by any systematic error or contaminated samples as it is common to all that have been coated with Dr. A. Schoch primer and maintained at higher temperature. Obviously, such results don't make much sense when purely interpreting them as signs of aging, but they might make more sense

when considering the following: a few days after the painted samples have had been incubated, the liquid solution started to look milky, just as if some component was being released. Weeks later, looking at the vials, it was as if the milky solution turned into a clearer one having thousands of tiny particles in suspension. These small particles were only present in the samples treated by the Schoch primer and it is suspected they may be responsible for the radical drop in transmittance early in the aging process by simple diffusion of the incident light; this phenomenon could also explain the fact that the change in transmittance is almost wavelength independent. Over the next few months, these particles slowly fell to the bottom of the vial to form a sediment still visible today. The solution consequently went back completely clear and this probably explains why the transmittance went back up quite strongly. In table 5.1, no final transmittance value has been given for these items as it is impossible to conclude anything meaningful whatsoever.

5.2.5 Aging of QSA When Various Materials Bathe in it

Various materials have also been tested in order to improve our understanding of the effect the scintillator may have on them over time. Small pieces of these materials have been cut, weighed and soaked in ∼20 mL of QSA. These samples have only been incubated at 35 degrees because it is believed 50 degrees corresponds to a too intense treatment. RTVs, cements and epoxies have been studied in order to see what should and what should not be used in the real detector as any part of sealing. When these measurements were started, it was quite unclear what design would be chosen to bear the active cocktail (even now, such decisions are not final) and therefore many different gluing materials had to be tried. Furthermore, if the thermal press sealing method is being used for the active configuration, we may be able to completely eliminate the use of such constituents (with the exception of the fluorosilicone rubber) or at least restrict the surface area in contact with QSA. Results are still presented here, however, in case any of these materials are considered for later use.

RTVs

Four different RTVs have been studied, two being an opaque white and the others clear. For all RTV samples, a small piece weighing 3.0 g has been put in contact with 20 mL of QSA. At room temperature, only the white RTV 162 from General Electric shows signs of interaction with QSA, as the

transmittance has dropped by a significant 8% at 420 nm over 330 days. At

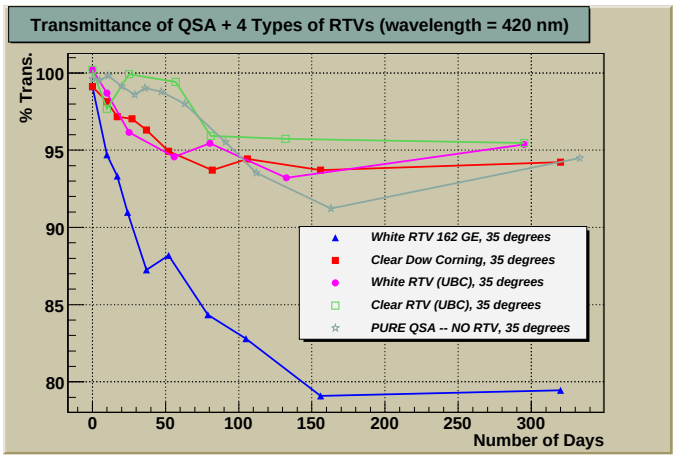

Figure 5.13: Transmittance of pure QSA put in contact with 4 different types of RTVs. The transmittance of QSA alone (no RTV) is also plotted as a reference. Results are shown at a wavelength of 420 nm for samples incubated at 35 degrees.

35 degrees, this same RTV also shows the worst effect out of the four (see figure 5.13) and should probably not be used for any further purpose. The three other RTVs however show quite similar effects – or an absence of effect – on QSA and it would be difficult choosing the best one at this point. On the other hand, let's recall that an apparent problem with any RTV is the fact that it is porous with air, and therefore water may evaporate through it.[†] Another positive point concerning the aging of RTVs is the fact that the material itself does not seem to be physically changed by contact with QSA, that is, the color, the shape as well as the rubber-ish texture and the general appearance do not change over time, even when incubated at high temperature. Such an observation has been made comparing aged RTV that has been soaked in QSA with aged dry RTV; as we will momentarily see, this is not quite the case for all substances and some changed appearance over time. A few other types of RTVs have also been studied although none of these results are presented here. These RTVs were brightly coloured and within only a few days of being in contact with QSA, they turned the whole

[†]This may end up not being too much of a problem if the RTV is thick enough, but it would be still inconvenient.

liquid into that specific color; the impact is an obvious dramatic drop in QSA transmittance.

Epoxies

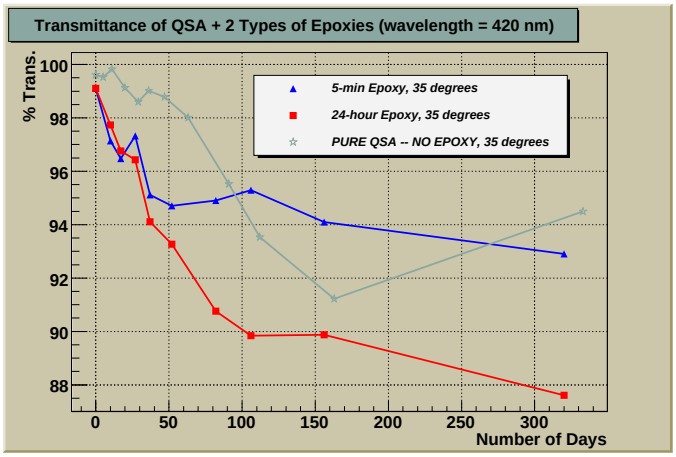

Figure 5.14: Transmittance of pure QSA put in contact with two types of epoxy maintained at 35°C.

Two specific epoxies were studied, a fast curing 5-minute epoxy as well as a 24-hour epoxy, both manufactured by Devcon. As it was the case for the RTVs, a small 3.0-g piece has been put in contact with 20 mL of QSA and incubated at higher temperatures. The QSA containing the 5-minute epoxy shows a moderate drop in transmittance at both room temperature and 35 degrees, the results being quite similar to what has been obtained for the RTVs. On the other hand, the small 5-minute epoxy piece itself incubated at 35 degrees completely changed color over time: it went from pale yellow to dark orange, also emitting a strong smell that does not seem to dissipate much over time. The smell is also something perceptible from the sample left at room temperature, although it may not be quite as pronounced. The 24-hour epoxy, however, turned out quite differently. Although the piece did not change appearance, shape or texture over time, the transmittance dropped significantly more than it did for the 5-minute epoxy. These are signs that both the 5-minute as well as the 24-hour epoxy should probably not be used

for further purpose. Many other types of epoxy could be used instead as long as the tolerance to QSA has been verified. One could therefore conclude that different epoxies behave quite differently when put in contact with the liquid scintillator. It is not possible to generalize in any way to all epoxies what has been observed for two of them.

Others

Two other RTV-like substances have also been studied: a clear cement (Held-On) as well as a product called Kwick Seal. Both show similar results to the RTVs previously discussed, without showing any special interesting characteristics.

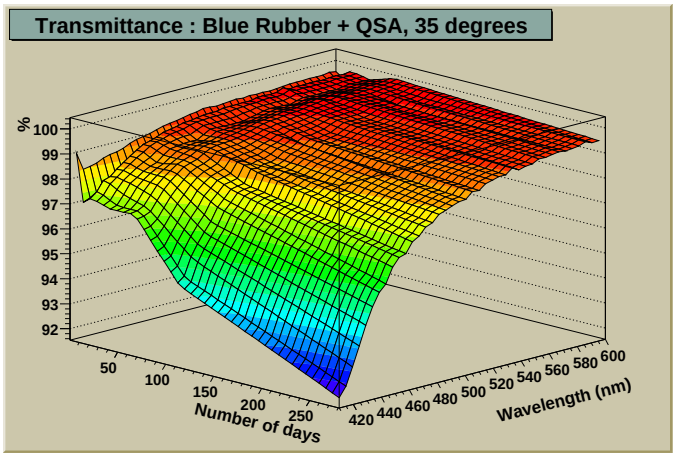

Figure 5.15: Aging of QSA at 35°C when a small rectangular piece of Blue Fluorosilicone Rubber is inserted in the solution.

Blue Fluorosilicone rubber has also been put in contact with QSA at both room temperature and 35 degrees. This product is actually the only one still actively considered as being a future component of the detector. It therefore is particularly important for it to remain relatively inert to QSA. After 290 days, no significant drop in transmittance has been observed at room temperature and at 35 degrees, it dropped to 93% (figure 5.15) which is within the uncertainty of QSA alone at this temperature. Consequently, no significant drop in transmittance caused by the rubber has been observed.

One thing to consider however is the fact that the drop has been quite linear in time at least for wavelengths near the UV, and a plateau is yet to be reached.

5.2.6 Inconclusive Tests

Some other different tests have also been performed and perhaps due to limitations of the spectrophotometer, they did not give easily interpretable results. For instance, it has been hypothesized that perhaps if we coat the plastic samples with silicon oil, we could prevent the active cocktail from attacking the plastic. Silicon oil is a waterproof substance that is supposedly chemically inert and once it gets in contact with any material – such as polypropylene – it gets quite difficult to remove; no matter how much the piece is rinsed, a thin layer of oil always remains stuck to the surface. It was argued that such a thin layer of oil could create an organic barrier protecting the plastic against the scintillator. Consequently, small plastic pieces have been dipped in different kinds of silicon oils, rinsed and then soaked in QSA. Trying to measure the transmittance for these samples turned out being quite difficult as no matter how little oil is left on the piece of polypropylene, it seems to dissolve (or at least partially) in QSA, making it relatively inhomogeneous. Such inhomogeneity in the solution leads to completely incoherent results from which no viable analysis may be done. Furthermore, small samples of optical fibers treated with silicon oil and dipped in QSA for testing showed serious signs of degradation within only a few days and the silicon oil idea has been dropped ever since.

Another series of tests performed was to study the aging of plastic in a scintillator cocktail made of 70% water, 25% QSA and 5% surfactant rather than pure QSA. The motivation for this was to see the real aging effect rather than the exaggerated effect seen from soaking the samples in pure QSA. Two major problems had however to be overcome at the very beginning: what would be used as the reference sample and what would be the real effect of putting such cocktails at elevated temperatures to simulate the aging? The first question may be simpler to address as it would not make much sense trying to compare solutions with different proportions of QSA, that is, solutions not even identical at time zero. In order to resolve this, what has been used as a reference was the cocktail itself, having the same percent of water and scintillator. The result is the following: at room temperature, absolutely no signs of aging are perceptible when plastic is added to the cocktail. This is not particularly enlightening as plastic in pure QSA kept

at room temperature has not really shown any signs of aging either, so it would have been surprising if a diluted version had. At higher temperature, however, a more fundamental problem arises due to the very nature of the cocktail's cloud point. As we saw earlier, the cloud point of the solution is well below 35°C, so when samples are incubated at 35 and 50 degrees, they turn almost instantly milky, a densely opaque white. Obviously, for the measurements to be taken, the samples need to be cooled back down to room temperature, until they turn transparent again. In theory, this should have been simple, however, the results were once again extremely difficult to interpret. Although the solution turns back relatively clear after it has been cooled down, it seems as if it is not quite as homogeneous as it was originally. Perhaps the accelerated aging of the cocktail's components once they have separated is quite different from the aging of the cocktail itself. In any case, the results obtained will be omitted rather than being subjectively discussed.

5.2.7 Complete Summary of Transmittance Results

Here is a table that summarizes all transmittance results obtained and discussed throughout this chapter. The table states what has been added to QSA, the temperature it has been brought to, the number of days it remained incubated as well as the final transmittance for the worst case secenario, that is, at a wavelength of 420 nm. To lighten the table, let's define the following configurations.

- Configuration A: A piece of white plastic coated with Krylon primer as well as 3 layers of EJ-520 reflective paint.
- Configuration B: A piece of natural plastic coated with Krylon primer as well as 3 layers of EJ-520 reflective paint.
- Configuration C: A piece of white plastic coated with Rust-Oleum primer as well as 3 layers of EJ-520 reflective paint.
- Configuration D: A piece of natural plastic coated with Rust-Oleum primer as well as 3 layers of EJ-520 reflective paint.
- Configuration E: A piece of white plastic coated with Dr. A. Schoch primer as well as 3 layers of EJ-520 reflective paint.
- Configuration F: A piece of natural plastic coated with Dr. A. Schoch primer as well as 3 layers of EJ-520 reflective paint.

Table 5.1: Summary for all relevant transmittance results.

	Added to QSA	**Temp.**	**# Days**	**% T. at 420nm**
—	———	±5°C	±3	±1%
1	Nothing	35°C	330	94
2	Nothing	50°C	330	92
3	1 piece white PP	23°C	330	100
4	1 piece white PP	35°C	330	93
5	1 piece white PP	50°C	330	89
6	1 piece natural PP	23°C	330	100
7	1 piece natural PP	35°C	330	96
8	1 piece natural PP	50°C	330	89
9	2 pieces natural PP PP	50°C	330	86
10	2 pieces white PP	23°C	320	98
11	2 pieces white PP	35°C	320	92
12	3 pieces white PP	23°C	320	99
13	3 pieces white PP	35°C	320	91
14	Large amount white PP	23°C	220	99
15	Large Amount white PP	35°C	220	89
16	Configuration A	23°C	330	100
17	Configuration A	35°C	330	82
18	Configuration A	50°C	330	65
19	Configuration B	23°C	330	100
20	Configuration B	35°C	330	88
21	Configuration B	50°C	330	78
22	Configuration C	23°C	330	99
23	Configuration C	35°C	330	92
24	Configuration C	50°C	330	78
25	Configuration D	23°C	330	99.5
26	Configuration D	35°C	330	94
27	Configuration D	50°C	330	86
28	Configuration E	23°C	330	99
29	Configuration E	35°C	330	—
30	Configuration E	50°C	330	—
31	Configuration F	23°C	330	99
32	Configuration F	35°C	330	—

Continued on next page

Table 5.1 – continued from previous page

	Added to QSA	Temp.	# Days	% T. at 420nm
33	Configuration F	50°C	330	—
34	White RTV (162 GE)	23°C	320	92
35	White RTV (162 GE)	35°C	320	79
36	White RTV (UBC)	23°C	290	99
37	White RTV (UBC)	35°C	290	95
38	Dow Corning RTV (Clear)	23°C	320	99
39	Dow Corning RTV (Clear)	35°C	320	94
40	Clear RTV (UBC)	23°C	290	98
41	Clear RTV (UBC)	35°C	290	96
42	Clear Cement	23°C	320	100
43	Clear Cement	35°C	320	88
44	Kwick Seal Caulk	23°C	290	98
45	Kwick Seal Caulk	35°C	290	86
46	5-min. Epoxy (TRIUMF)	23°C	320	97.5
47	5-min. Epoxy (TRIUMF)	35°C	320	93
48	24-Hour Epoxy (TRIUMF)	23°C	320	96
49	24-Hour Epoxy (TRIUMF)	35°C	320	87
50	Fluorosilicone Rubber	23°C	290	99
51	Fluorosilicone Rubber	35°C	290	93

5.3 Reflectance Measurements

As previously discussed, small plastic samples have been painted with different primers, coated with three layers of reflective paint and then soaked in QSA. In addition to quantifying the evolution of the liquid transmittance as a function of time, the problem of reflectivity degradation has also been addressed using the spectrophotometer as well as the integrating hemisphere provided. In reflectance mode, just as it was the case for transmittance measurements, the sample under study is also compared to another sample – the reference. In this configuration, the samples are both pressed against an opening/window connecting the integrating hemisphere; two beams of light are incident onto the samples and the integrating hemisphere measures the relative light intensity reflecting off both samples. These "openings" actually consist of small 0.75 cm $\times$ 2 cm rectangles cut in a flat piece of metal

adjacent to the hemisphere. The objective pursued here is to measure the reflectivity of all the different painted plastic samples put in contact with the liquid scintillator as a function of time in reference to a painted sample that is kept dry at room temperature and away from any intense light source. Many difficulties were however encountered while taking the measurements and this section elaborates on what exactly happened and how could one get significant results from future tests.

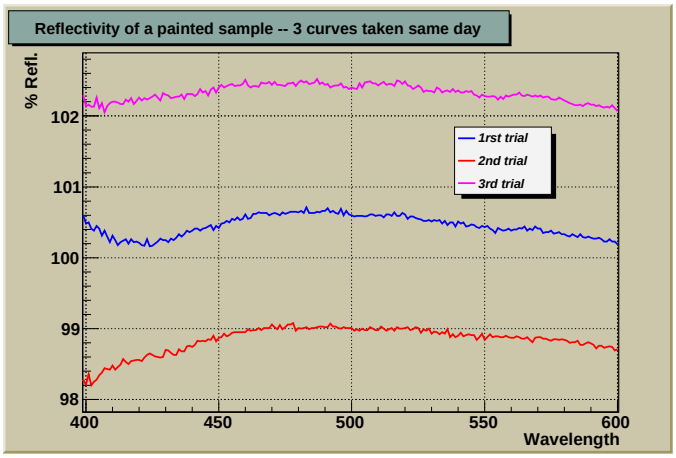

Figure 5.16: Example of the non-reproducibility of the results once the painted sample is slightly displaced. It therefore seems the exact position of the sample relative to the integrating hemisphere's opening is crucial.

The main issue definitely lies in the fact that the results are not reproducible, showing large systematic errors between data sets taken only a few minutes apart. These systematic errors are however only observed if the sample is moved/touched between the measurements. In other words, two sets of data taken subsequently without the operator ever touching the painted sample will give very similar results, but if the sample is taken out of the spectrophotometer and put right back in, then the errors become large. This may be a good argument for believing these effects to be caused by systematic errors rather than simply being a hardware uncertainty.[†] It therefore seems

[†]In this sense, no such differences were ever observed in transmittance mode between numerous measurements of the same sample taken the same day.

the exact position of the sample relative to the opening for the integrating sphere is of crucial importance. Because the window itself is smaller than the painted sample and because the sample may be placed quite arbitrarily behind this window, it is extremely difficult to position the sample at the exact same place between the measurements. Figure 5.16 shows an example of this non-reproducibility as the three data sets were taken the same day and should consequently be identical.

In theory, the exact position of the sample relative to the opening should not matter because the reflection of the surface is diffuse and the hemisphere should integrate the light coming from all directions. In this sense, even if the thickness of the coating was very uneven over the painted surface – which is really the case, each sample being characterized by its own surface smoothness – the reflectivity measurements should not be affected whatsoever. So, what causes the non-reproducibility of the results then? It is possible the integrating hemisphere does not really sum over all directions, or perhaps the reflection of the paint is not quite perfectly diffuse. I however personally suspect the variable smoothness of the painted surface to cause another problem.

Because of the non-uniformity of the paint, it is rather difficult to position the sample against the opening in a way such that absolutely no gap is left at any position all around the junction between the painted sample and the piece of metal. Any gap left, no matter how small, will absorb part of the light that should be collected and this may certainly affect the results. These conclusions were not particularly trivial to get to and before serious doubts were expressed concerning the validity of the results, a few reflectivity measurements were taken for most of the painted samples. Figure 5.17 shows an example of such measurements. Three sets of measurements have been taken over the first month and as we may see, it is difficult to really conclude anything considering the variation between the results is similar to what has already been observed between measurements taken the same day. After a month of active reflectivity studying, the decision to stop acquiring new data was taken for numerous reasons: firstly, I personally could not reconcile with the non-reproducibility of the results and I would not have believed any further analysis. Secondly, the cracking of the paint became quite severe for samples incubated at elevated temperature and in no way was it possible – or did it make any sense – to measure the reflectivity of paint peeling off the plastic surface. As previously stated, the samples soaked in QSA and maintained at room temperature did not show as severe cracking

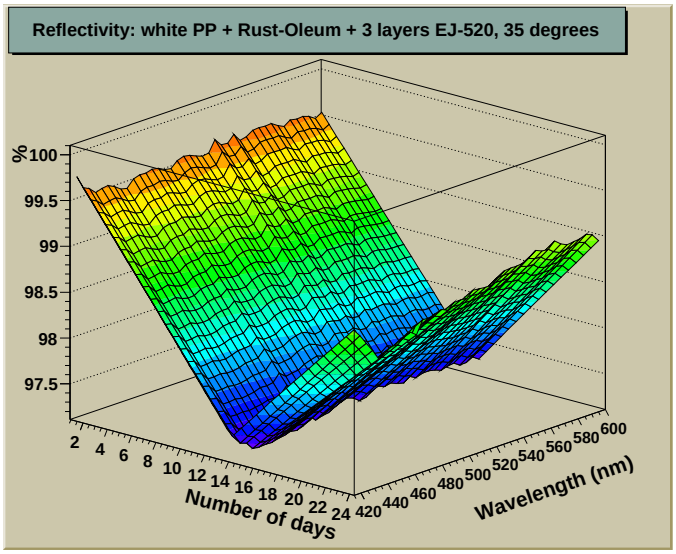

Figure 5.17: Reflectivity measurements for sample painted with 3 layers of EJ-520, put in contact with QSA and maintained at an elevated temperature of 35°C.

and peeling of the paint, so it could have been possible to continue taking data from these samples. On the other hand, reflectivity measurements also require one to significantly manipulate the painted samples before putting them back into the QSA solution to resume the aging. It was unclear what would be the effect of all these manipulations on the paint (would it weaken faster over time?), but I was also worried the whole procedure of *taking the painted sample out of QSA, washing it, taking the reflectivity measurements, washing it again and putting it back in the original vial* would ultimately also affect the QSA itself and consequently, the transmittance measurements.

From this whole discussion, it seems the main reason for the reflectivity measurements not to be successful for samples maintained at room temperature[†] is the fact that the coating has not originally been applied very uniformly over the plastic surface.[‡] That was due to the fact that a simple

[†]For incubated samples, the cracking of the paint is probably too quick and severe to ever consider measuring the reflectivity.

[‡]The fact that the QSA may be affected by repeated manipulations of the painted

brush was used to apply the primers as well as the three layers of paint, the airbrush method not having been developed at the time. Now that such a method may be used to apply very thin and uniform coatings of paint onto plastic surfaces, perhaps it would be a good idea to restart a new series of reflectivity tests. It would also be interesting to investigate further what exactly causes the systematic errors observed between measurements.

sample may not be significant if one does not need to monitor the transmittance of the solution as well.

Chapter 6

Conclusion

The research process leading towards a complete understanding of neutrino physics is far from being definite and is by no means a linear one. The tortuous path followed over the last decades, punctuated by major experiments and discoveries, continues to evolve in such a way that any further contribution may have significant impact, not only on particle physics, but on all fields of science. In this sense, confirmation of neutrino oscillation gave birth to numerous new theories and experimental possibilities acknowledging neutrino mass and therefore opening the door to a new era beyond the Standard Model requiring precise measurements of lepton flavor physics. Such new physics may give insights into understanding the relation between quarks and leptons and may even lead to new theories of mass generation. As for now, it remains fundamentally important to get accurate measurements of the missing variables in the MNS matrix, namely θ_{13} as well as the CP violation parameter δ.

Long baseline neutrino experiments such as T2K are designed for such a purpose. The experiment will compare neutrino interactions in near and far detectors, trying to observe muon to electron neutrino appearance as well as muon neutrino disappearance via an off-axis neutrino beam directed from J-PARC in Tokai to Kamioka where stands the massive Super-Kamiokande pure water detector. Because the far detector is already built, most of the efforts are put into building the near detector as well as the neutrino beam at J-PARC. The Canadian group is working on parts of the near detector, namely the time projection chambers and the fine-grained detectors, together forming the tracker as a whole. Most of the efforts at TRIUMF and UBC have been devoted to building the two fine-grained detectors, one made entirely of solid scintillator bars coated with TiO_2 and the other one bearing large quantities of water, in order to reproduce the far detector's target material. Two design possibilities have been considered for the water detector: either an active or a passive configuration. The former implies using a liquid scintillator mixture contained in large extruded polypropylene sheets, each cell being threaded with a wavelength shifting fiber, while the

latter replaces the cocktail with simple water and alternates layers of plastic scintillator with passive water layers.

The present thesis have addressed four of the main issues that must be solved for the realization of the project. The mechanical design for both fine-grained detectors has been presented as well as results from mechanical tests and prototypes. To test the strength of the water detector's extruded plastic, a three-layer full-sized prototype has been built, filled with sand and hung up from a crane at UBC. As it turned out, the material undoubtedly supports the pressure, showing incredible strength due to its twin-wall cross-section design. How to seal these panels is also a predominent problem that has been studied for both the active and the passive configurations. A relatively straightforward method has been developed for sealing passive panels, using a mould and epoxy as sealing material; a four by eight-feet^2 successful prototype has been built and remains hanging off a crane down in the lab. Sealing an active panel, however, turned out to be much trickier and it is safe to say a complete leakproof procedure remains yet to be fully developed for such a purpose. The light yield issue has also been examined in the case of the active water detector configuration, trying to optimize the QSA cocktail as well as trying to paint the inner walls of multiple cells. Furthermore, beam tests done at TRIUMF have allowed us to approximatively quantify the attenuation length of the fibers using solid scintillator bars while new beam tests with the objective of quantifying long term effects on liquid scintillator are underway. Lastly, the aging of all materials when put in contact with QSA has been studied at room temperature as well as at 35 and 50 degrees. Such a treatment has been used to accelerate aging effects, but turns out to be a rather questionable method of accelerating aging because although we may predict a drop in transmittance at room temperature from incubated sample results, no such drop has been observed. After over 200 days bathing in QSA at room temperature, the same ratio of plastic versus QSA as the real detector does not show any significant signs of aging. Moreover, QSA does not show any signs of aging when put in contact at room temperature with a variety of materials (with an exception of certain types of epoxy and RTVs).

Such results are certainly quite encouraging for the collaboration as no major difficulties have been encountered that would make a water-scintillator detector impossible. Although developing a working water scintillator detector may not be possible right at the beginning of the project due to a tight schedule, it is still being considered as a future upgrade to the experiment.

The immediate steps to be followed by the collaboration consist in building a full-sized plastic scintillator and passive water detectors. Numerous improvements will possibly be made over the next year of prototyping and the plan is to have completed the construction of the FGDs by March 2008. By this time, the TPCs should also be completed and beam tests will be performed at TRIUMF with the fully integrated tracker. The disassembling of the detector and its subsequent shipping and installation in Tokai, Japan is planned for the winter of 2008-9. If everything goes as planned, the neutrino beam construction should be completed by April 2009, and interesting data on neutrino interactions from the first T2K beam should be expected shortly after. It remains quite difficult at this point to predict what will happen following the publication of T2K's main results. If the experiment is successful, a second phase may be undertaken with possibly a greater beam power, a phase that would more specifically look into leptonic CP violation and the δ parameter, perhaps even improving further the precision for some mixing parameters.

Other than T2K, various other experiments currently in development will delve deeper than simple neutrino oscillation confirmation, such as the NOνA experiment. NOνA, an American project still in the proposal stage, is quite similar to T2K, but will be characterized by greater beam energy, a longer beamline and a different far detector. [27] On the other hand, new types of experiments such as building a detector close to a nuclear reactor may actually be able to give an alternate measurement of θ_{13}. Such a project creates vast interest due to its apparent low cost ($50M) and high statistics; many proposals have been made for such an experiment. Finally, in the very long run, numerous imaginative ideas may be considered in order to study neutrinos such as a Hyper-Kamiokande detector and even very long baseline experiments across the US. One should perhaps expect interesting surprises when studying neutrinos, surprises ranging from sterile neutrino states, neutrino decay or even CPT violation! One thing is for sure, the future is bright for neutrino physics as well as for physics in general and although we may be far from knowing everything – or perhaps anything – the road we are following certainly is an exciting one.

Appendix A

Supplementary Figures and Tables

Table A.1: Exhaustive list of all interaction modes for the near detector. The number of events is given per ton and per 10^{21} protons on target. [16]

Interaction Mode	**Fraction**	**Nb of Events**
CC - QE	38%	65038
CC - $p\pi^+$	11%	17846
CC - $p\pi^0$	3%	4887
CC - $n\pi^+$	3%	5107
CC - Coherent π^+	1%	2189
CC - multi π's	7%	11943
CC - DIS	8%	13057
NC - Elastic n	9%	15671
NC - Elastic p	8%	13581
NC - $n\pi^0$	2%	2837
NC - $p\pi^0$	2%	3519
NC - $p\pi^-$	1%	1931
NC - $n\pi^+$	1%	2300
NC - Coherent π^0	1%	1099
NC - multi π's	2%	3639
NC - DIS	2%	4022

Table A.2: Fraction of interaction modes around oscillation maximum for the 1 ring muon-like event as predicted by the Monte Carlo simulation.

Interaction Mode	**Fraction**
CC - QE	65%
CC - 1π	20%
CC - coherent π	1%
CC - multi π's	3%
NC - 1π	7%
NC - N π	7%

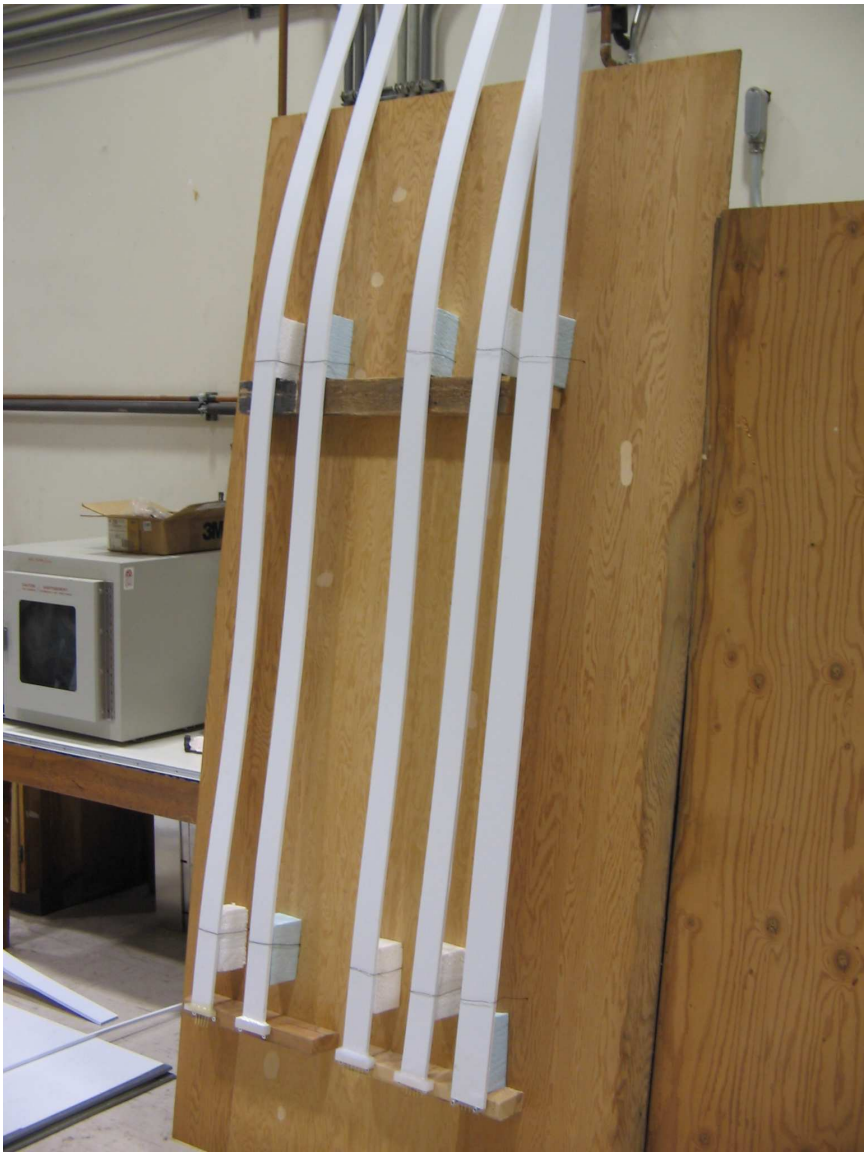

Figure A.1: First series of passive sealing tests using endcaps glued to Matraplast panels by mean of RTVs and epoxies.

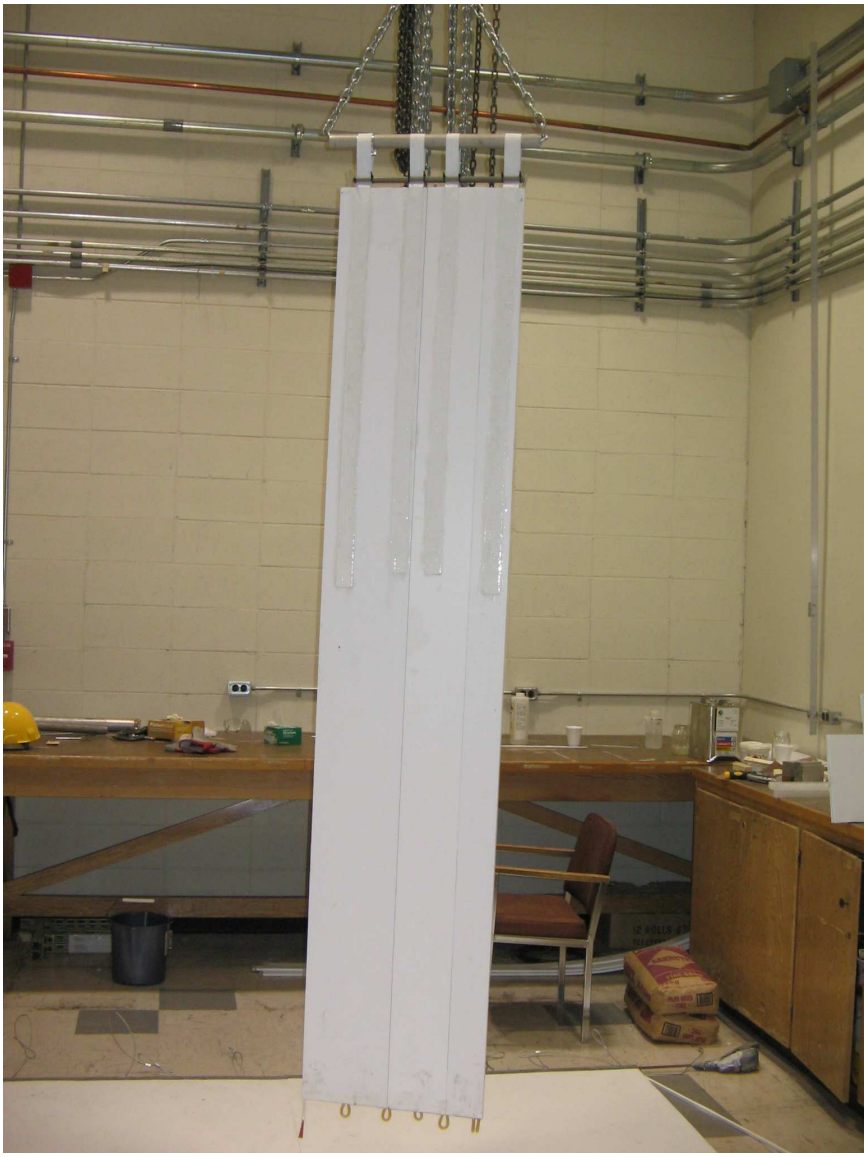

Figure A.2: Prototype B is a fifty-cell wide and three-layer thick passive module. All the 7 individual pieces forming the module are connected together by plastic tubes such that the panel fills as a whole when water is introduced. An unfortunate leak in between adjacent pieces caused major problems and consequently, the panel could not be filled completely with water. This prototype made more obvious the various problems arising from having a module made of many pieces.

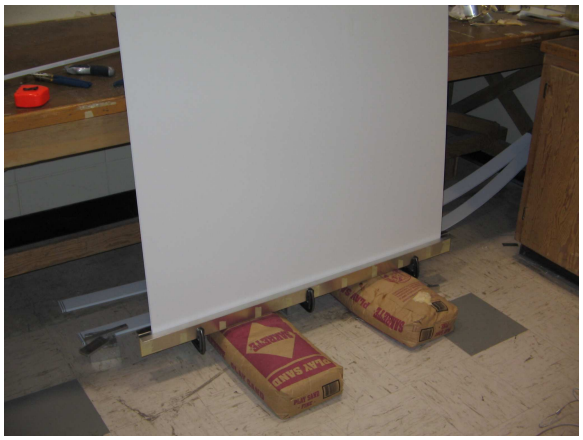

Figure A.3: 1-cm thick aluminum mould used to seal both ends of prototype C. This prototype consisted of a single complete Matraplast panel.

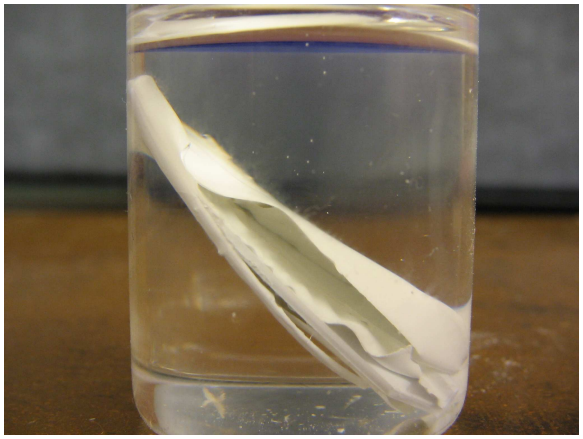

Figure A.4: Three coats of paint peeling off the plastic surface at a temperature of 35°C. The primer used in this case was Krylon.

Appendix B

Using the Spectrophotometer

B.1 Integrating Sphere Connection Procedure

Here is the procedure to be followed to insert the integrating hemisphere in the spectrophotometer for reflectance measurements. This is a simple procedure, but it may be quite obscure as it is not described anywhere in the user guide. I thought it would be pertinent to document it officially here.

- In the main opening of the spectrophotometer, where the samples are inserted, remove the two plastic sample holders and replace them by the integrating sphere. The side of the sphere where the mirrors are must face left, that is, where the incident light is coming from within the machine. The sphere must also be plugged in using the obvious connector attached to it.

- Open the actual machine removing the screws on the left and right, making sure the power is off (or at least the UV light is!).

- Inside the spectrophotometer, on the main vertical board on your right, unplug the small 2-pin red connector called P210 and replace it by the white J210 connector found inside.

- Still inside the spectrophotometer, take off the plastic protector located in the middle back of the machine. Inside of it, you will find some scary large blue and gray capacitors as well as another vertical board.

- On this vertical board, remove the small 2-pin red connector located at the bottom right of the board (P110) and replace it by the white connector J110.

- Put back the plastic protector and close the spectrophotometer. Obviously, to go back to a machine measuring transmittance rather than reflectance, the previous steps must be followed in reverse.

When looking at the different modes of the spectrophotometer, we see "ABS", "%T", "CONC" and "λ CAL". To take % reflectance measurements, once the sphere has been plugged in, just use "%T".

B.2 More About the Spectrophotometer

The spectrophotometer may not always be *user friendly*. Here are some tricks I picked up along the way.

- Sometimes, when taking a series of measurements, the machine will stop for no apparent reason in the middle of a computation. The program used to take the measurements works *way* faster than the spectrophotometer itself. To solve this, between each command sent to the spectrophotometer, the computer counts from 0 to 1,000,000 simply to mark time and allow the spectrophotometer to keep up. This number may be changed directly in the program, however, it happens that sometimes the machine just won't follow for no apparent reason. A good reboot (for the spectrophotometer) very often seems to solve the problem.

- If the spectrophotometer has not been used for some time (more than a month or so), you may encounter problems trying to take measurements. The spectrophotometer will not listen to the computer (although it actually "sees" it) and you won't be able to take any measurements. The solution is simple: just let the machine run for an hour or two, without trying to do anything useful with it. It should work just fine after that.

Good Luck!

Bibliography

[1] Pauli, Wolfgang, *Letter of Dec. 4 to the "Dear radioactive ladies and gentlemen"* (Lise Meitner et al., 1930).

[2] Akhmedov, Evgeny, *"Neutrino Physics", Lectures given at the Trieste Summer School in Particle Physics* (hep-ph/0001264, 1999).

[3] Z. Maki, M. Nakagawa, and S. Sakata, *Remarks on the Unified Model of Elementary Particles* (Prog. Theor. Phys. 28, 870, 1962).

[4] Fleurot, Fabrice, *Oscillation Probability Calculation; http://nu.phys.laurentian.ca/∼fleurot/oscillations* (Retrieved on June 15$^{\text{th}}$, 2006).

[5] M. Fukugita, G-C. Liu and N. Sugiyama, *Limits on Neutrino Mass from Cosmic Structure Formation* (Phys. Rev. Lett. 84, 1082-1085, 2000).

[6] Y. Fukuda *et al.*, *Evidence for Oscillation of Atmospheric Neutrinos* (Phys. Rev. Lett. 81, 1562-1567, 1998).

[7] Wikipedia, *www.wikipedia.org: Super-Kamiokande* (Retrieved on March 15$^{\text{th}}$, 2006).

[8] Y. Ashie *et al.*, *Measurement of Atmospheric Neutrino Oscillation Parameters by Super-Kamiokande I* (Phys. Rev. Lett. D71 112005, 2005).

[9] Y. Ashie *et al.*, *Evidence for an Oscillatory Signature in Atmospheric Neutrino Oscillations* (Phys. Rev. Lett. PRL93 101801, 2004).

[10] Q.R. Ahmad *et al.*, *Measurement of Charged-Current Interactions produced by ^8B Solar Neutrinos at the Sudbury Neutrino Observatory* (Phys. Rev. Lett. 87, 2001).

[11] Q.R. Ahmad *et al.*, *Direct Evidence for Neutrino Flavor Transformation from Neutral-Current Interactions in the Sudbury Neutrino Observatory* (Phys. Rev. Lett. 89, 2002).

[12] T. Araki *et al.*, *Measurement of Neutrino Oscillation with KamLAND: Evidence of Spectral Distortion* (Phys. Rev. Lett. PRL94 081801, 2005).

[13] N. Tagg *et al.*, *First MINOS Results from the NuMI Beam* (arXiv:hep-ex/0605058, 2006).

[14] T2K Collaboration, *Neutrino Oscillation at JHF* (Letter of Intent, 2003).

[15] Shiozawa, Masato, *Hyper-Kamiokande Project* (JHF-Kamioka ν workshop, 2001).

[16] T2K Collaboration, *T2K ND280 Conceptual Design Report* (T2K Internal Document, 2005).

[17] T2K ND280 TPC Group, *T2K TPC Feasibility Report* (T2K Internal Document, 2004).

[18] Oser, Scott, *The T2K Tracker : Fine-Grained Detectors* (NSERC Review, 2005).

[19] Yen, Stanley, *Oxygen to Carbon Ratio Analysis for Various Passive and Active Water Detector for T2K* (T2K Internal Report, April 2$^{\text{nd}}$, 2006).

[20] Henderson, Robert, *FGD Design* (T2K Internal Report, April 25$^{\text{th}}$, 2006).

[21] P. Border *et al.*, *A Large Liquid Scintillator Detector for a Long Baseline Neutrino Oscillation Experiment* (Nuclear Instruments and Methods in Physics Research A 463, p194-204, 2001).

[22] Oser, Scott, *Design and Performance Issues for Single- vs. Double-ended Readout of the Plastic FGD Layers (v1.0)* (T2K Internal Document, 2005).

[23] Eljen Company, *http://www.apace-science.com/eljen/ej-520.htm* (Retrieved on May 15$^{\text{th}}$, 2006).

[24] Nakahara, Hiroko *Contributions to the Development of a Water-Based Neutrino Detector for the T2K Project* (Bachelor's Degree Thesis, 2006).

[25] Yen, Stanley, *Report on Light Yield of Different Sizes of Wavelength Shifting Fiber* (T2K Internal Report, March 13$^{\text{th}}$, 2006).

[26] Choudhary, Brajesh C. *et al.*, *A Study in Scintillators, Fibre, Glues and Aging* (DETECTOR R&D at CALTECH, 1998).

[27] Oser, Scott M., *Neutrino Physics : A Selective Overview* (Lake Louise Winter Institute, 2006).